UNIVERSITA' DEGLI STUDI DI PADOVA

Dipartimento di Ingegneria Industriale DII

Corso di Laurea Magistrale in Ingegneria dei Materiali

ADDITIVE MANUFACTURING OF SiOC COMPOSITES AND INVESTIGATION OF THEIR ELECTROCHEMICAL BEHAVIOUR FOR ENERGY STORAGE APPLICATION

Relatore: Prof. Paolo Colombo
Correlatori: Dr. Gurpreet Singh,
Dr. Giorgia Franchin

Laureando: Federico Toigo

Anno Accademico 2018/2019

Abstract

This thesis illustrates the production of ceramic matrix composite (CMC) electrodes, based on SiOC with three different types of carbon sources as fillers, starting from a commercial preceramic polymer, H44, 3D-printed with a Direct Ink Writing technology (DIW). The electrodes are designed with a net-shape made of three layers, in which the filaments are separated from each other in three different lengths.

The electrodes produced have been applied to lithium-ion half-cells, in order to replace the graphitic electrodes used industrially in batteries, nowadays.

The aim of this research is to achieve high specific capacities, during cycling, using these 3D-printed electrodes in half-cells, investigating the electrochemical properties of the ceramic materials.

First of all, this study is focused on finding the proper mix of elements to combine in order to achieve an easy printing: materials with different amount of fillers have been produced and an estimative analysis on the rheological properties has then been conduced.

After that, the pyrolysis process has taken place with the conversion of the polymer into ceramic (SiOC). The kinetic of the process has been based on the several treatments reported in literature, in order to obtain the final shape as much as possible unvaried and the inorganic material without crystallin phases in the microstructure, which would have compromised the specific capacity results due to the low electrical conductivity.

The 3D printed ceramic material obtained has been characterized by several analysis in order to evaluate the chemical microstructure, ensuring the preparation of the ink was correct, as well as the thermal treatment, and also comparing the different materials prepared: thermogravimetry analysis (TGA) has first been performed to determine the ceramic yield of the polymer transformation, followed by Fourier transform infrared spectroscopy (FTIR) and X-ray diffraction (XRD) which allow to determine the bond created in the final structure and the present crystalline phases; moreover Raman Spectroscopy (RMN) has been done to analyse the carbon phases present in the material.

A scanning electron microscopy (SEM) has followed to analyse the physical structure after the pyrolysis treatment: a dimensional analysis has been reported to investigate the deformation of the net-shape electrodes, which are differentiated on the base of the filler used.

The research is also focused on the assembly of lithium-ion half-cells in a coin cell system, where the electrodes produced are allocated, determining the specific capacity and the efficiency of cyclability for certain material opportunely selected in order to have an overall view on the performance achievable with these innovative electrodes.

Riassunto

Questa tesi illustra la produzione di elettrodi compositi a matrice ceramica, realizzati in SiOC e con tre differenti filler di carbonio, a partire da un polimero preceramico commerciale, H44, stampato con la tecnologia *Direct Ink Writing* (DIW). Gli elettrodi sono progettati con una forma *net-shape* a tre strati e i filamenti del materiale stampato sono spaziati da tre differenti lunghezze.

Gli elettrodi prodotti sono poi inseriti in semicelle agli ioni di litio, realizzati per sostituire quelli ora utilizzati a livello industriale nelle batterie, costituiti da grafite.

Lo scopo di questa ricerca è quello di ottenere un'elevata capacità specifica durante il processo ciclico di carica e scarica, usando gli elettrodi 3D, studiando così le proprietà elettrochimiche del materiale ceramico.

In un primo momento lo studio si è focalizzato nel trovare le giuste quantità di elementi da combinare per realizzare l'inchiostro ed avere un efficace processo di stampa: sono stati prodotti materiali con diversi quantitativi di filler ed è stata fatta un'analisi estimativa sulle proprietà reologiche.

Successivamente è stato condotto il trattamento termico di pirolisi che ha portato alla trasformazione del polimero in materiale ceramico (SiOC).

La cinetica del processo è stata controllata sulla base di innumerevoli trattamenti già riportati in letteratura, in modo da ottenere degli elettrodi con forma il più possibile invariata rispetto a quella iniziale e un materiale inorganico senza fasi cristalline nella microstruttura, che avrebbe compromesso i risultati in termini di capacità specifica, oltre ad una bassa conducibilità elettrica.

Il materiale così ottenuto è stato caratterizzato con diverse analisi in modo da determinare la microstruttura chimica, assicurandosi della corretta preparazione dell'inchiostro, così come del trattamento termico, paragonando i diversi materiali prodotti: un'analisi termogravimetrica (TGA) è stata condotta per stabilire la resa ceramica del polimero trasformato, seguita da una spettroscopia infrarosso (FTIR) e diffrazione ai raggi X (XRD) che ha permesso di determinare i legami creati nella microstruttura finale e la presenza di fasi cristalline; inoltre una spettroscopia Raman (RMN) è stata eseguita per analizzare in dettaglio la fase di carbonio presente nel materiale.

E' seguita una spettroscopia elettronica a scansione (SEM) in modo da analizzare la struttura fisica dopo il trattamento di pirolisi: un'analisi dimensionale è stata riportata per studiare la deformazione avvenuta, che si è differenziata in base al filler utilizzato.

La ricerca si è focalizzata poi nell'assemblaggio di semicelle agli ioni di litio, dove gli elettrodi sono stati collocati, e si è stabilita la capacità specifica, l'efficienza e la ciclabilità, tramite un'analisi galvanostatica (GCD), per determinati materiali, selezionati opportunamente per avere un quadro generale sulle performance ottenibili da questi elettrodi.

Summary

Introduction

Energy is necessary in everyday life and the demand is exponentially increasing due to the continue development in technology: high storage energy accumulators, with high efficiency, are the most promising due to the growing interest in portable devices.

One of the most challenging fields in research is the study on alternative energy sources, due to the high pollution generated by the combustion of traditional fossil fuels, which are still the most used energy sources thanks to their high energy/weight ratio and long-life operation.

The solar and wind energy are surely promising substitutes as renewable and sustainable energy suppliers but, at the same time, they need high capacity accumulators to store the energy produced.

This research thesis has the purpose to study the materials and the manufacturing process to realize a new generation of electrodes that could be used in future batteries, which should be designed completely differently from the electrical storage devices used nowadays. These innovative electrodes are produced by taking advantage of the versatility and availability of preceramic polymers to manufacture complex 3D-shaped structures, by using direct ink writing, as an additive manufacturing (AM) technology, and exploiting their behaviour to produce self-standing ceramic electrodes. In this way it should be possible to demonstrate how these electrodes could be produced, avoiding typical manufacturing processes, diminishing the material wastes at the least , saving costs and in particular saving weight: the new generation energy devices could be shaped as the final object, with the outer cage as electrode, filled with the already known solid electrolytes.

The samples are then electrochemically characterized in half cells for batteries. In this study, polysiloxane has been used in combination with three different types of carbon fillers to achieve high capacity and high electrical conductivity due to the combination of properties achievable in a homogenous ceramic matrix composite structure (CMC), that otherwise could not be obtained with traditional ceramics.

Chapter n.1
Silicon based 3D-printed Electrodes starting from Preceramic Polymers

This chapter is here proposed to understand which kind of polymeric material is used in this research, the techniques used to obtain complex shaped items, as well as the thermal treatment processes to convert the polymer into ceramic and the most used applications, in particular energy storage devices, such as lithium-ion batteries.

1.1 Introduction to Preceramic Polymers

Preceramic polymers play an important role in the production of polymers derived ceramics (PDCs): their characteristics, such as rheology, reactivity, ceramic yield and cross-linking are the main variables for the manufacturing process of these materials, and in particular they influence the starting phase of the manufacture, that is the shaping process. The choice of this material has also repercussions in the final characteristics, both chemical and physical properties, of the PDCs materials.[1]

One of the main advantages in using organosilicon polymers is the easy way of processing these materials: they can be shaped with the most common processes used for polymers such as extrusion, resin transfer moulding (RTM), foaming, coatings with and without solvents, polymer infiltration pyrolysis (PIP), spinning and injection moulding. These types of processes allow to get products of complex shape or net-shape matrixes, and at the same time to obtain objects that are not easily achievable in other ways, typical of the ceramic production.

On the other hand, the possibility of modifying the side groups of the molecule backbones of polymers precursors, allows to reach a wide variety of final products, with different properties useful in various applications: their high thermo-chemical stability, combined with high young modulus, hardness, oxidation resistance, have made them perfect solutions in different fields. The main drawbacks of these materials are associated with the low mechanical strength caused by the cracks formed due to the shrinkage and gas evolution during pyrolysis, but these are avoidable by producing low dimensional objects, or by adequately controlling the thermal treatment.[2]

Once formed, in fact, the material is ready to be converted into ceramic, by removing all the organic compounds present in the chemical structure, achieving an inorganic material. Usually the most common way to convert the PDCs is a high thermal treatment, called pyrolysis, in controlled atmosphere, but the conversion could also be obtained in a non-thermal process using ion irradiation, if thin-coatings are produced.[1]

In any case these conversions require low temperatures thermal treatments compared to the traditional processes of ceramics.

1.1 History of preceramic polymers

In the middle years of the last century, in the ceramic community there was an upcoming interest in synthetizing new types of non-oxide ceramic materials starting from molecular precursors.

The first transformation of organosilicon compounds in ceramic material application was developed by Verbeek, Mansmann and Winter in 1970's, who explained the conversion of polymers into ceramic creating SiC/Si_3N_4 ceramic fibers to be used in high temperature applications. Before that time, there were some synthesis of ceramic materials from precursors (SiC) as testified by Fritz (Fritz,1956), and Yajima later (Yajima,1975), who produced high thermal stability ceramic fibers.

After the first practical conversion, there was a double line of thoughts. On the one hand, the community developed new precursors and on the other hand new ways to apply them: researchers studied the conversion treatment to transform polymers into ceramics and the microstructures obtained from the pyrolysis products. The main purpose of this process was dedicated to the production of fibers, coatings, bulk or porous components, even with complex shapes. From the late 1970s to the 1990s there was an increasing interest in synthetizing new preceramic polymers such as poly (organosilazanes) (Yajima, 1978), polysilanes (Miller,1989), polycarbosilanes (Boury,1990) and polysiloxanes (Corriu,1996): the synthesis route was not only developed for the binary preceramic polymers, but also for the ternary or quaternary materials. It was also possible to introduce other elements such as micro- or nano- fillers to obtain the desired properties like electrical conductivity, piezoresistivity or magnetical behaviour, or even to avoid defects that could occur with the release of gas during the thermal conversion treatment or because of the shrinkage.

Among all the glasses, the siliconoxycarbide glass had a huge development because of its low production cost and it was well characterized in its synthesis and properties by Renlund (Renlund, 1991) and Zhang & Pantano (Zhang, 1990), who developed the sol-gel synthesis route.[1]

1.2 Structure of Preceramic Polymers

Preceramic polymers are a class of hybrid organic-inorganic materials consisting of inorganic Si-based polymeric chains and organic functional groups attached to the sides. The molecular structure of the preceramic polymer determines the properties of the final ceramic material.

A simple generic representation of preceramic polymer used for the production of PDCs is presented in fig.1 where the polymer backbone is shown. It consists of Si atoms, bounded to X atoms, which determine the class of the preceramic polymer, as well as to R^1 and R^2 usually representing an aromatic, hydrogen (H) or aliphatic group (alkyl, aryl, etc.) that gives the organic characteristics to the material. The X group is of utmost importance because it determines the final structure of the ceramic material; The R groups are fundamental for the initial phases of the process, indeed they determine the rheology, solubility and stability properties of the preceramic polymer, biasing the process of shaping the material before the heat treatment (after which they decompose and volatilize). The nature and the amount of these groups are also important to control the carbon content in the final material and it was discovered that a big amount of carbon content leads to low mechanical properties and the loss of high thermal properties typical of PDCs; on the other hand, it discourages the crystallization during the heat treatment, enhancing the electrical conductivity property.

$$\left[\underset{R^2}{\overset{R^1}{\mathrm{Si}}} - X \right]_n$$

Figure 1.1 *preceramic polymer structure*

Modifying the X variable, it is possible to obtain different types of polymer ceramic precursors, as shown in the following table:

Table 1.1 *preceramic polymers class achievable with a specific X group*

Chemical Element	Group	Polymer Class
Si	Si	Poly(organosilanes)
C	CH_2	Poly(organocarbosilanes)
N	NH N=C=N	Polysilazanes Poly(organosilylcarbodiimides)
B	B	Poly(organoborosilanes)
O	O	Polysiloxanes, Polysilsesquioxanes

The preceramic polymer backbone could be composed of one or more of these groups creating hybrid polymers.

All these types of preceramic polymers and the combination between them are presented in the following panel:

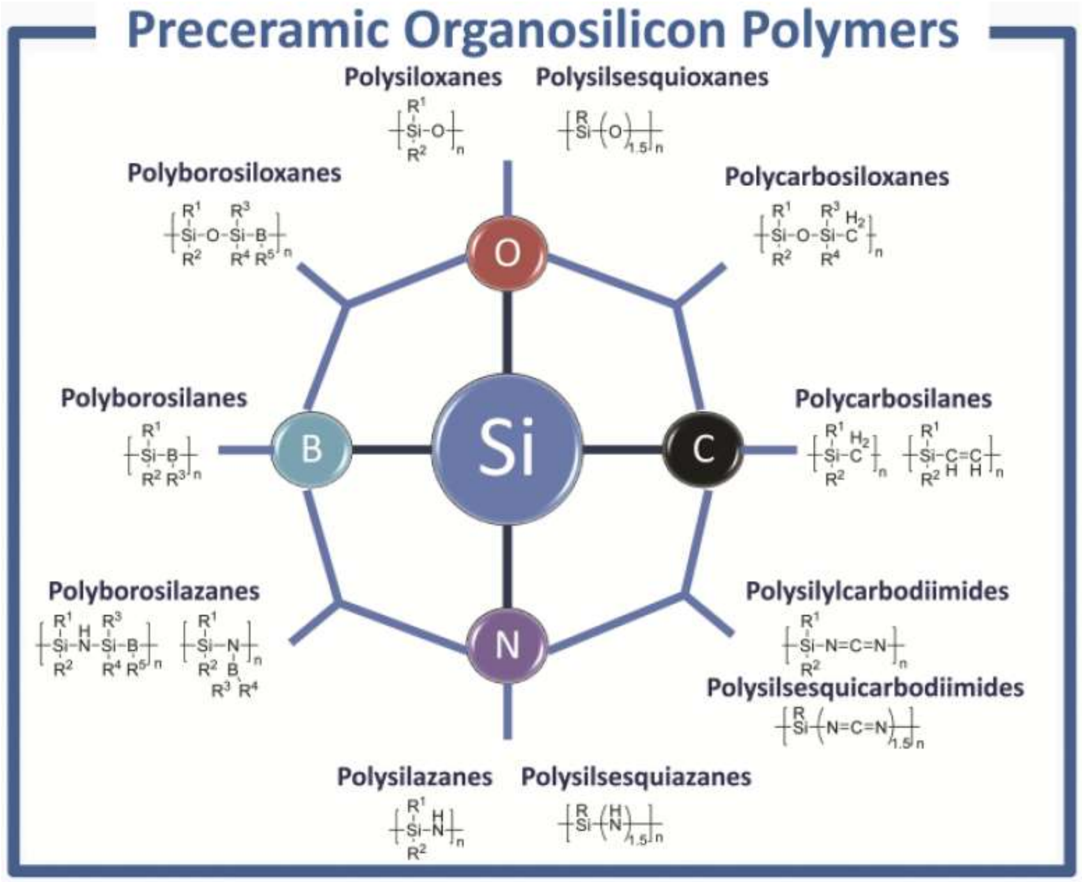

Figure 1.2 *schematic presentation of Preceramic Organosilicon Polymers achievable with different element of the periodic table*[1]

The selection of the polymer is of great importance to achieve the best properties required by the application and the handlings needed by manufacturing processes at the lowest achievable cost.

Before selecting the right polymer for a specific process, it is important to consider some aspects such as: chemical durability, toxicity, thermal stability and reactivity with the atmosphere.

For these reasons, the most useful and studied PDCs are the silicones such as polisilazanes, policarbodiimides, but especially poliorganosiloxanes which are one of the most interesting materials because of their low cost and good thermal stability up to 1200°C.

1.2.1 Introduction to Polysiloxanes

Polysiloxanes, a type of silicones, are one of the most technologically advanced preceramic polymers. They are characterized by excellent chemical-physical and electrical properties and low cost (the lowest compared to all the Si based materials) and for this reason they have been studied, up to now, to be used in a lot of applications, and not only to obtain final ceramic materials. [3]

The main advantage is the thermo-chemical stability, which allows these materials to be applied in a wide variety of applications.[4]

Their structure is formed by consequent silicon–oxygen bounds (Si-O), which give the inorganic characteristics due to the well-known siloxane bond, with the organic groups attached to the silicon, as shown in the following figure: [1]

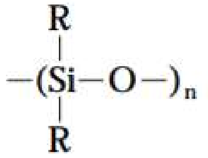

$$-(\overset{\displaystyle R}{\underset{\displaystyle R}{Si}}-O-)_n$$

Figure 1.3 chemical *structure of polysiloxanes*

The opportunity to change the -R organic group allows to have a wide variety of different structures. The first siloxane was obtained in 1872 by Landeburg and during the 20th century, especially after 1940s, when there was a particular interest for silicones in the industries, with an expanding research in the development of new polysiloxanes, particularly stimulated in finding well defined macromolecular architectures, as mentioned above in §1.1.

The units are connected to each other forming high molecular weight molecules and their functionality is expressed based of the number of R units attached to the silicon atoms: the monofunctional units are typical as final units in polysiloxane molecules because the Si atom is attached to three organic units forming a $SiR_3O_{1/2}$ structure; the difunctional molecules have a structure like SiR_2O, such as dimethylsiloxy $Si(CH_3)_2O$; the trifunctional units have a structure such as $SiRO_{3/2}$, typical of branching, cage (3D structure) and ladder structures (2D structure).[5] Also the quadrifunctional moieties can be formed as SiO_2.

The structure of the preceramic polymers generally acquires a disordered arrangement, marked by a random network, a ladder structure or an oligomeric cage structure (3D) and the ceramic final properties are not determined by replacing the functional organic group bonded to the silicon, but also based on the degree of polymerization and the control of the structure itself.[6]

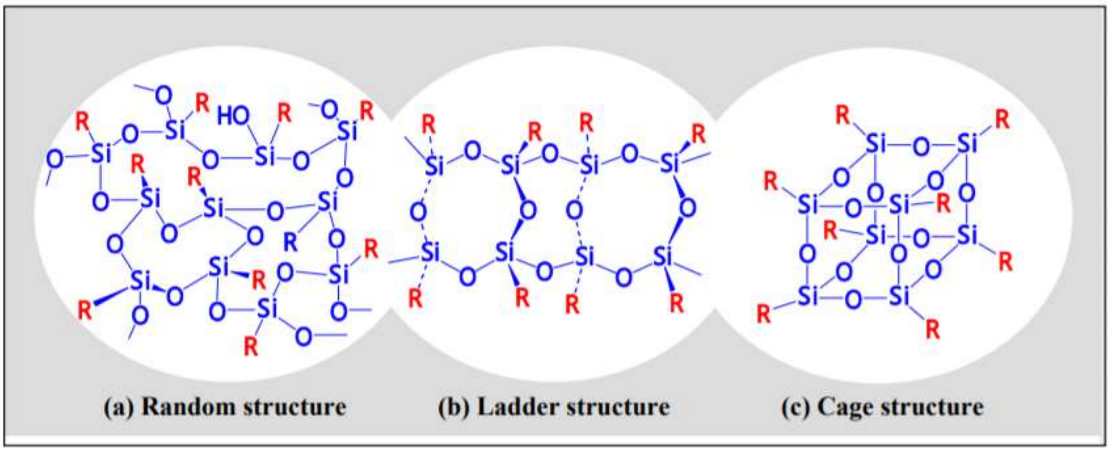
(a) Random structure (b) Ladder structure (c) Cage structure

Figure 1.2 *illustration of the typical microstructure of preceramic polymers (www.konishi-chem.co.jp)*

Moreover, these materials show high thermal stability (over 350°C), oxygen permeability, which is a negative aspect in the printing process because they absorb air producing bubbles (for this reason the ink would need a defoaming process before printing as it is shown further on), low surface energy, which allows to have good printability, and high biocompatibility, making them a good choice for use in medical applications.[7]

1.3 Ceramic Matrix Composite (CMC)

A composite material has a structure in which two or more distinct phases are embedded in a continuous matrix. Depending on the type of filler used, there are different categories that satisfy this type of material such as Metal Matrix Composite (MMC), polymer matrix composites (PMC) and ceramics matrix composites (CMC).

Ceramic Matrix Composite (CMC) could be obtained starting from polymer matrix composites, using preceramic polymers as the matrix material.

CMC is both a subcategory of ceramics and of composites.

In each case the filler is added to achieve higher structural and functional properties: the combination of mechanical, electrical and thermal properties achieved with these materials is unique. The main reason for adding filler in ceramic materials is to avoid brittle behaviours as shown by the monolithic materials. One of the main important parameters that influence the entire performance of the composite is the interface between the filler and the matrix.

In any case there are different kind of fillers that could be used to fulfil the matrix, as it is shown in the following picture:

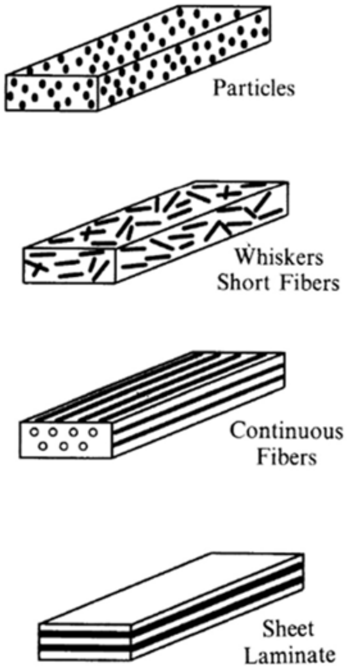

Figure 1.5 *Different types of ceramic reinforcement in ceramic matrix composites*
("Ceramix matrix composites" k. Chawla – Springer)

For this reason, Silicon oxycarbide has been recently studied by introducing fillers in order to enhance the properties of the neat polymers, without compromising the manufacturing processes, besides the total weight: the introduction of particles on the structure changes the morphology of the network, the chemical and physical properties of the ceramic matrix, improving the thermal, mechanical and electrical properties. [8]

The main manufacturing processes of this type of material are infiltration techniques, such as polymer infiltration and pyrolysis (PIP), chemical vapor infiltration (CVI), reactive melt infiltration (RMI), slurry infiltration, sol-gel infiltration ; or the additive manufacturing (AM) techniques, such as direct ink writing (DIW), hot pressing, tape casting, injection moulding, or extrusion.
If an infiltration technique is used, in order to avoid the porosity and fulfil the cracks generated during the pyrolysis process, it is important to re-infiltrate the material achieving a great density. [9]

1.4 Additive Manufacturing for Preceramic Polymers

The production of small and complex shape objects is difficult to achieve with the traditional subtracting manufacturing, but since the 1980s there has been an upcoming development in Solid Freedom Fabrication technologies (SFF) which develop the production of 3D printed shapes starting from Computer-Aided Design (CAD) projects.[10] The inability to produce products of complex shapes starting from the ceramic precursors is related to the nature of the material, in addition to the inability to process the ceramic materials after the forming procedure, due to their brittleness and hardness.[11]
Moreover these Additive Manufacturing techniques are surely avoiding the subsequent high thermal treatment, used in the traditional methods, because the material 3D printed does not need high temperatures to achieve a good homogeneity, which is necessary on the other hand, using powders. This is equivalent to avoiding high manufacturing costs and long processing, besides the waste of high quantity of material.
The ceramic materials started to be printed in the 1990s as reported by Marcus ed al. and Sachs et al. and the main three categories are classified according to the nature of the material printed: based on slurry, on powder and on bulk solid-basis.[11]

The AM techniques are divided into two categories: direct and indirect processes.
The former are characterized by a unique step process in which the material is deposited only in the place where the object has to be printed, immediately giving it the final properties; the indirect process is achieved in a multi-step process in which the material is deposited to print the component only after printing the necessary support to prop up the object. In this case the exceeding material need to be removed after the printing process.

The AM techniques developed so far are many, such as: stereolithography, laminated object manufacturing, binder jetting, selective laser sintering, fused deposition modelling, robocasting (direct ink writing), etc. The materials used to be printed could be whether present as slurries, liquids, powders or filaments.
In this work only two of them are presented and in particular a short explanation is dedicated to stereolithography, which is the oldest invented (mid 1980s), and the other is direct ink writing, which is the one used in this research.

1.4.1 Stereolithography (SLA):

Stereolithography is the first additive manufacturing process invented. The products are obtained by the UV-laser curing of a photosensitive liquid polymer containing additives like photo-initiator, absorbers, dispersing agents, but generally also micro/nanosized ceramic particles, such as silica (SiO_2), alumina (Al_2O_3), zirconia (ZrO_2) and silicon-carbide (SiC) (added for enhancing the mechanical properties and avoid shrinkages). The resin is in this way polymerized at a precise point focused by the laser and replicating the layer by layer structure typical of the AM methods. Then the printed element needs to be debinded and successively pyrolyzed, obtaining fully dense structures. The material to be printed must have the proper viscosity (around 3Pa·s) in addition to a suitable light absorption to obtain the desired curing depth (30-100μm). If the volume fraction of the particles is high, their segregation and the high index diffraction ratio achieved between ceramic particles and resin would not allow to print easily. On the other hand, this technique grants to reach high quality surface products compared to the other methods, even if the process is dramatically slow due to the low curing depth achievable.[11] SLA has seen several applications in different fields such as the production of moulds,[12] dental and biomedical applications[13,14,15] and microcomponents[16].

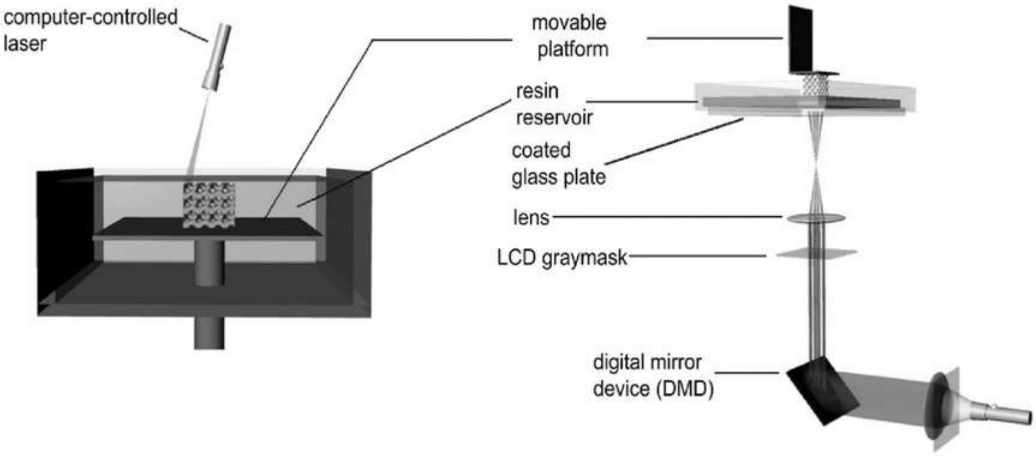

Figure 1.6 *Stereolithography in Bottom up (left) and top down (right) configuration* [17]

1.4.2 Direct ink writing (Robocasting)

This method is a free-form direct additive manufacturing technology in which a slurry ink is deposited on a surface, directly extruded as a filament from a syringe, connected to a compression pump. The syringe is placed in a mechanical arm which moves according to the CAD model set, printing the 3D printed object layer by layer, with a nozzle with a diameter between 0.1-1mm. The materials must have some prerequisites to be printed: first of all it must have a pseudoplastic behaviour (generally it is also a Bingham fluid) which reduces its viscosity increasing the pressure (and so applying a shear rate), allowing the extrusion process, but at the same time it needs to have a good retention shape after the extrusion, avoiding any collapse and maintaining the initial printing shape without any deformation. The rheology of the ink is important and for this reason, indeed the production of the material must be considered to gain a gel behaviour. The presence of the solvent is important because generally it volatizes just after the extrusion process, allowing to gain the initial gel consistency of the ink, and possibly converting the pseudoplastic behaviour into dilatant. [10]
Nowadays DIW is used is several applications such as the production of biomedical scaffolds[18], sensors[19], glass scaffolds for bone difects[20], drug delivery devices[21] and so on.

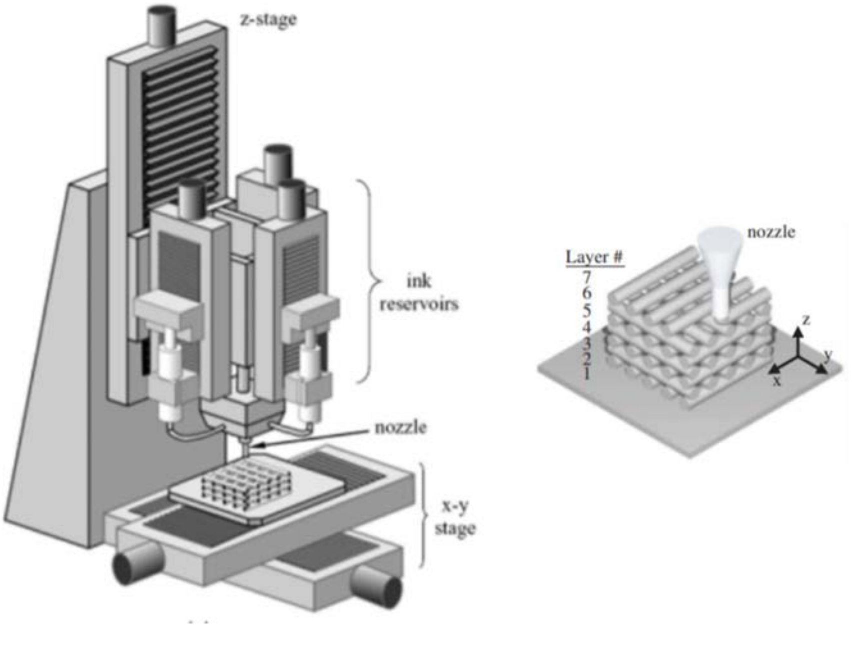

Figure 1.7 *left: Direct Ink Writing apparatus; right: an example of sample produced layer by layer*[22]

1.5 Thermal Treatment – Polymer to Ceramics conversion

Preceramic polymers, once shaped, need to be thermal treated in order to transform them into inorganic ceramics, as a result of the polymer-to-ceramics route:

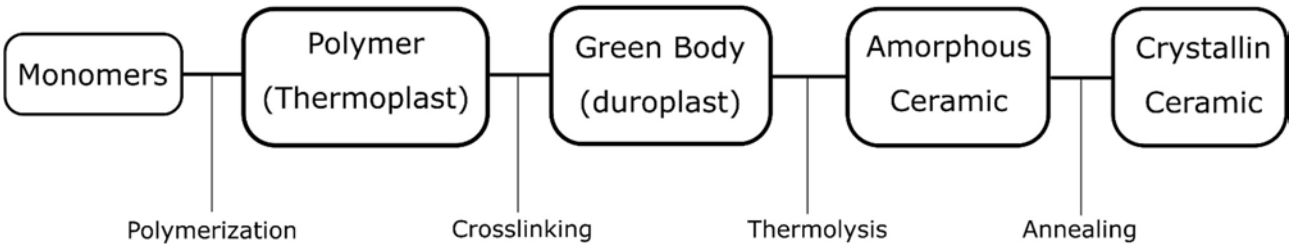

Figure 1.8 *Schematic presentation of the steps achievable starting from the monomer precursors through the polymer-to-ceramic conversion*

The heat treatment is divided into two steps:

1) The shaped material is heat treated at a moderate temperature (100-400°C) to promote the cross-linking process;

2) The ceramic transformation takes part in a controlled atmosphere and the crosslinked preceramic polymer is converted into an amorphous non-oxide ceramic material (because of the organic moieties decomposition) starting from 800°C. The typical set temperature is included between 1000 to 1400°C.
   Depending on the temperature chosen it is possible to reach different microstructures, chemical phases, and porosities on the final product.

In order to achieve a proper conversion of the preceramic polymers, removing the organic moieties attached to the molecular backbone (Si-O), they should respect the following prerequisites:

- high molecular weight to avoid the volatilization of functionalized components;
- proper rheological property to maintain the shape obtained during the shaping process;
- latent reactivity to achieve the crosslinking process, avoiding the depolymerization reactions;
- presence of rings and cages in the chemical backbone to avoid the volatilization due to the splitting of the structure.[1]

The thermal treatment is useful to achieve an amorphous ceramic structure concerning covalent strong bonds that ensure a good thermal stability, avoiding crystallization up to high temperatures. Indeed, above 1200°C the precipitation of β-SiC nanocrystals occurs.

$$SiO_2 + C_{free} \rightarrow SiC + 2CO \qquad (1.1)$$

Moreover, the thermolysis process is a well-controlled technique that allows the production of high purity ceramics with homogeneous chemical structures and with the desired morphology.

The crosslinking process is important because it allows the material to be converted into thermoset material, avoiding in this way the collapse of the shape.

In polyorganosiloxanes the cross-linking process could be promoted in different ways such as condensation, transition metal catalysed addition or free-radical initiation and hydrosilization.

In any case, the cross-link is controlled by the process parameters such as the temperature, the time in contact with the cross-linker, the type and quantity of the cross-linker: it could react only as catalyser and then volatilize or, on the other hand, react with the backbone and remain in the chemical structure with a vulcanization process (high temperature vulcanization or room temperature vulcanization).

The cross-linking process could also occur physically between the monomers of the preceramic polymer, but in this case the bonds created would be weak compared to the chemical crosslinking, in fact the forces created are secondary-forces. This mode is mainly used when the amount of filler is very high, allowing the shape to be maintain without the introduction of any chemical reagent.

The ceramization process and the volatilization of organic moieties (mineralization) begin at 600°C and is brought up to 1000-1400°C (the upper temperature is set according to the organic groups of the preceramic polymer used as shown in the following figure). In the first part of the process, up to 1000°C, the reactions involve the gas formation, which arises from the inside part of the material, leaving a structure with high porosity.[23] Over that temperature the material starts to condense reaching fully dense structures at 1000°C. One of the drawbacks of the pyrolysis treatment is the high shrinkage reached on the final material: to avoid this disadvantage inert fillers are usually introduced, which contrast the compressive strength created by the evaporation and cooling treatment, in addition to conducing low heating rates, assuring the near bulk material formation. In other researches it has been emphasized the use of active filler, instead of inert, with expansion properties at high temperatures, introduced for the same purposes.

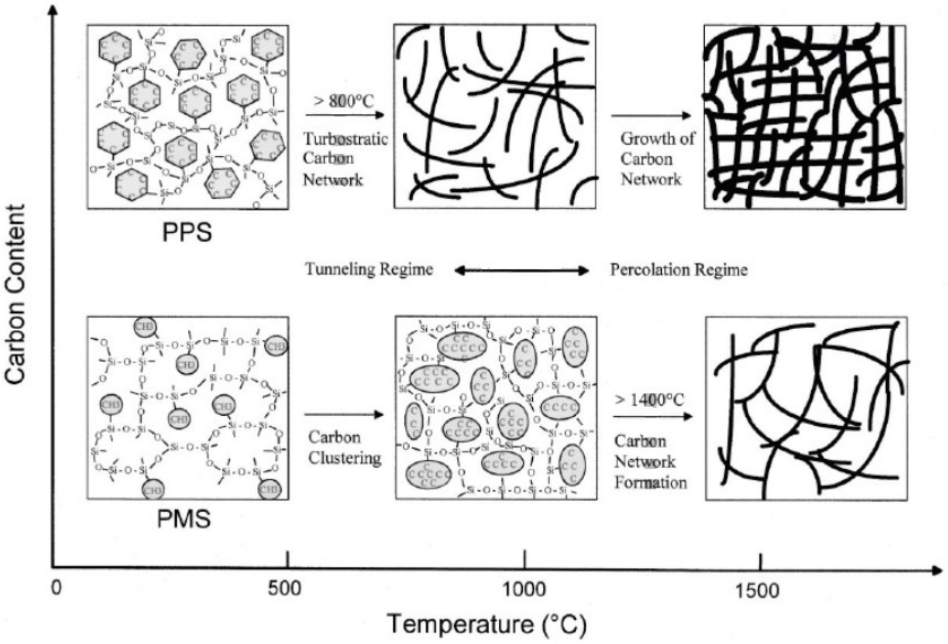

Figure 1.9 *illustration of the different microstructures achievable with Polymethyliloxane (PMS) and Polyphenylsiloxane (PPS) at different pyrolysis temperatures* [24]

Polysiloxanes resins are pyrolized up to 1200°C [25] in order to obtain amorphous silicon oxycarbide networks (SiCO) composed of Si-C, Si-O and amorphous carbon phase (the turbostratic carbon network). For this reason, it is important to conduce the process in an inert atmosphere (argon or nitrogen) in order to avoid any carbon loss. The quantity of the free carbon depends on the types of functional groups attached to the backbone of Si-O,in fact it is well known that higher amounts of phenyl groups produce a structure with higher carbon content in comparison with high methyl groups. Moreover, as shown in the previous picture, Polyphenylsiloxanes (PPS) achieve the turbostratic carbon network at lower temperatures compared to Polymethylsiloxanes (PMS).

From 400°C to 600°C Si-O, Si-C and Si-H bonds are redistributed by decreasing the ceramic yield. At upper temperatures (depending on the material) the structure cleavage of Si-C and C-H bonds take place, converting the material into an amorphous inorganic ceramic with the gas production of CH_4 (emitted and produced starting from CH_3, as well as from the cleavage of Si-C) and H_2 (from the cleavage of C-H). Thanks to this last process it is also possible to find residual free carbon, as mentioned before, which makes the glass appear black. The growth of free carbon involves the nucleation of clusters with several layers of graphene and the formation of turbostratic carbon, creating a carbon network all over the SiOC matrix. At temperatures above 1200°C, the matrix is devitrificated with the combination of C with Si, producing local β-SiC nanocrystals, which gain a

spheroidal shape at 1400°C. At this temperature the nucleation of SiO_2 and the crystallization as cristobalite take place (especially for materials with high carbon content), so far inhibited by the presence of the graphitic carbon (otherwise it should be at 1200°C). The presence of free carbon is expected up to 1400°C (1at%). The kinetic of the process is particularly related to the precursors used. The turbostratic carbon has a sp_2 hybridization and is particularly important in electrical applications because of its high electrical conductivity. The sp_3 hybridization is, on the other hand, correlated to the carbon bond with the silicon and does not participate to the electrical conductivity of the material.[26] In order to increase the carbon content, the material could also be subjected to an HF attack which could remove the SiO_2 phase from the material, leaving behind a C-based porous structure.[24,27] The final structure is indeed composed of SiOC (Si bonded to C and O) and disordered carbon. Generally it is possible to see two types of amorphous SiOC in the structure, one of each has a higher content of carbon and is allocated near the carbon free phase.[28]
Moreover, if the carbon source is introduced as filler, to enhance the carbon content and achieve higher electrical conductivity, it is possible to match this phase by means of an XRD analysis which shows the peaks concerning the crystalline carbon introduced, as shown further.[1]

1.6 Silicon Oxycarbide Glasses - SiOC

Silicon Oxicarbide are glasses in which the amorphous network structure is made up of oxygen and carbon bonded to silicon: it is possible to find carbon in both the amorphous network forms and as elemental carbon.

Its chemical structure is formed by a tetrahedral network in which the silicon is bonded both to oxygen, which is two coordinated, and carbon, which is four coordinated, forming a structure with higher mechanical and thermal resistance compared to silica (SiO_4), where silicon is bonded only with oxygen. Indeed, the strong bonds between carbon and silicon prevent the volatilization of the hydrocarbon molecules.
The chemical formula of this material is $[SiC_xO_{4-x}]$ where x=1,2,3.
This material is not easily achievable from melting because of the oxidation of carbon, and for this reason it is generally produced starting from preceramic polymers of with sol-gel precursors.

The chemical structure of the material before heating has Hydrogen terminal-bonds (-CH, $-CH_2$, $-CH_3$) and polyaromatic carbon groups (like methyl, phenyl), as shown before.

During the pyrolysis the organic compounds decompose, and two or three phases are formed on the base of the precursors and the heat temperature reached: amorphous SiOC, graphitic carbon and at high temperature β-SiC.

The final microstructure obtained, before the crystallization, can be described as $SiC_xO_{2(1-x)} + yC_{free.}$

The chemical properties of the final material are variable and depend on the behaviour of the organic compounds with temperature, in addition to the interaction with the inorganic component and with the processing atmosphere. In this way it is possible to create infinite materials by also changing the nature of the organic functionalities attached to the backbone or simply modifying the heat treatment (temperature, time and rate).

Moreover, it has been noticed in previous works that the introduction of Carbon into the material structure increases the annealing point of the glass. The shape and the quantity of carbon determine the main property of the final material as the electrical conductivity.[25]

In order to promote the electrical conduction is important to discourage the formation of SiC that cause the free carbon loss.

The final porosity of the material, pyrolyzed at 1000°C is expected to be between 200-500nm , but with a treatment at a higher temperature, the matrix assumes a redistribution of the molecules, achieving pores of 20-50nm at 1200° and obtaining a dense material at 1400°C, with the presence of SiC which encourages the formation of a dense bulk.

The silicon oxycarbide achievable from the conversion of the polymer into ceramic could have different properties, as seen so far, on the base of the precursors and the heat treatment conduced. For this reason, this type of materials has a wide range of application.

1.8 Applications

Nowadays, Preceramic Polymers are widespread in the market because of their versatility. They are really different from each other, since they can be produced in different ways and with different precursors. These determine the final properties of the material such as fusibility, thermal stability, chemical reactivity and for this reason they could be used in different fields. The nanodomains and their intergrowth, as well as the organic compounds attached to the silicon atoms in the backbone are the main factor that influences the solubility, the reactivity of the polymer and the final mechanical, electrical and chemical properties.

Surely the production of preceramic polymers ensures the achievement of pure and homogenous ceramic products thanks to the high purity synthesis and the homogenous elements in the precursor compounds.

Their main attitude is high thermal resistance that prevents creep, low oxidation, high thermal shock resistance.

The most typical and oldest application of these materials is the production of fibers (the first attempt was in 1970's with Verbeek, Winter and Mansmann who produced small-diameter Si_3N_4/SiC fibers) or ceramic matrices for fiber-reinforced composites: the progress of the manufacturing process over the years allows to reach a minimum amount of oxygen contamination (from 15% to 0.5%), enhancing the thermal stability without diminishing the mechanical performances (σ_s=2.6-3.3GPa). Moreover, the introduction into the backbone of elements such as N or B allows to produce fibers that remain amorphous up to 1700°C in an inert atmosphere and with an oxidation and creep resistance better than SiC-based fibers.

The Preceramic Polymers are also fitted to make high porous components that allow the filtration, separation or absorption of gasses, even as thermal protection, thanks to the capability to be foamed during the production process, obtaining different types of porosity.

The Ceramic-Matrix composite is another well-known use of preceramic polymers because of the aided shaping process (CVI and melt infiltration) of these materials that allow to obtain also parts of complex shape with low residual porosity, as already seen in §1.3 and §1.4. With this process it has been possible to create brakes for high performance motorsport, achieving a high friction coefficient (>0,5), also at high temperature conditions, and low wear compared with the traditional metal breaks. They could also be used in more technical fields as testified by NASA in the repair kits for space shuttle.[29]

Moreover, the presence of nanoscale compounds and graphite sheets introduced with the fillers allows to achieve properties such as piezoresistivity, semiconduction and photoluminescence, that other materials could not obtain. For this reason, they could be used in electric manufacturing as insulator for semiconductor components or for the production of glass fibers and silicon chips.

A recent application in electronic is presented by the micro electromechanical systems (MEMS).

In any case they could be applied not only to obtain ceramic materials, but they are also used as polymers for sealants, lubricants for bearings, thermal insulation for engine components, in cosmetical products, thanks to their low reactivity and high biocompatibility, or even in food industries.

Moreover, they could be used thanks to their adhesive properties, in chemical industries for the manufacture of glues, paints and adhesive foams.

In other cases they can be used as electrodes because of the high capacity of SiOC, as already testified by the literature and in this thesis proposed in a new way.

1.9 Energy Storage Devices

Nowadays, energy storage devices are designed in order to find a good substitute to fossil fuel energies.

There are different types of electrochemical devices that deal with this topic such as supercapacitors, batteries and fuel cells. Both of these devices store energy due to the mechanisms and reactions that occur in the boundary phase between electrodes and electrolyte.

Whichever they are, the diffusion of the electrons and the ions is the same in them: the electrons are conducted in the external electrical system while the ions are moving inside the electrolyte.

The main difference is the way of storing and converting energy: batteries and fuel cells are units that store chemical energy exclusively with redox reaction and convert it into electrical energy, the former are closed devices that use the elements already set in the device, while the latter are open devices that need to be fed continuously with fuel and an oxidizing reagent to continue the electrochemical reactions; the supercapacitors were initially used only to store energy electrostatically, thanks to the electrical double layer formation on the electrodes, but nowadays they use other types of materials for the electrodes, such as metal oxides, which store energy also thanks to the electrochemical reactions (pseudo-capacitors).

Lithium-ion batteries are the promising storage device to have long-time energy suppliers, while supercapacitors are used in order to have high power release.[30]

This research has been especially focused on batteries, where the 3D printed electrodes are tested.

The main advantage of using the 3D printed electrodes is due to the time saving during the process of the battery production, thanks to the self-standing properties of these samples, which avoid using the same material in powder to produce electrodes with the traditional method, wasting also other types of materials used as support and binder, such as copper, carbon black (CB) and polyvinylidene difluoride (PVDF), saving additional costs, as shown below.

The final goal of this research should be to achieve results comparable with the traditional graphite electrodes used industrially today to assemble these types of devices.

In order to understand better the properties and the operation principles of these devices a detailed analysis on the thermodynamics principles is suggested as follows.

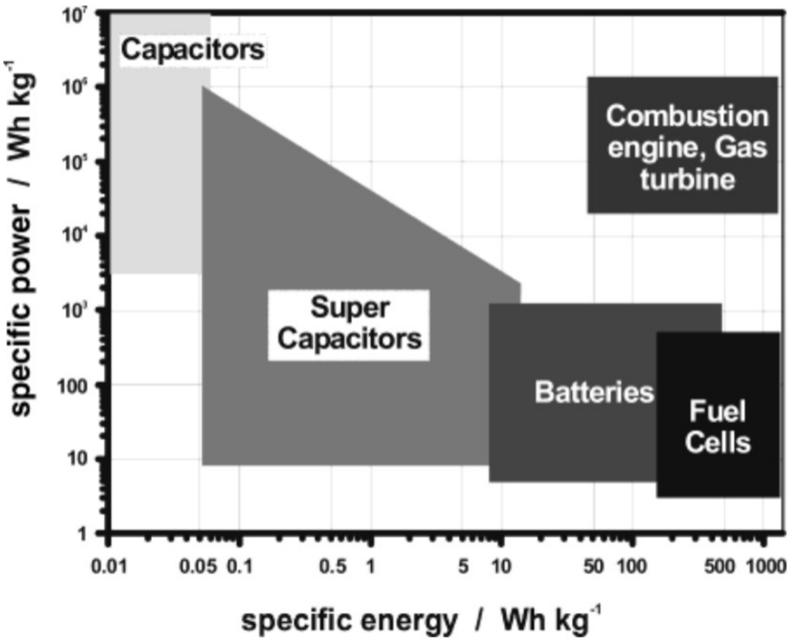

Figure 1.10 *Different types of energy storage devices in base of the specific energy or specific power needed for the particular application* [31]

1.9.1 Thermodynamics principles

The electrochemical reactions follow the thermodynamics and kinetics equations that describe the chemical reactions, for this reason the electrical chemical principles are here reported, then related to the electrochemical behaviour.

The amount of free energy, or better the energy available from the chemical reaction into the cell, convertible into electrical energy and in active work, is described by the Gibbs equation:

$$\Delta G = \Delta H - T\Delta S \qquad (1.2)$$

Where ΔH is the enthalpy, T is the temperature and ΔS is the entropy of the system.

From the electrical point of view the free energy could be described with the following formula:

$$\Delta G = -nFE \qquad (1.3)$$

Where in this case *ΔG* is the electrical active work (expressed in Joule), *n* is the number of moles of electrons flowing on the circuit due to the chemical reaction, *F* is the Faraday constant [u.m. Coulomb/mole] and *E* is the potential of the cell. In this way *nF* is the number of charges flowing.

The negative sign determines the spontaneity of the reaction: in a galvanic cell (a device that converts the chemical energy into electrical energy, such as the cell during discharging) the potential of the cell (*E*) is positive so the reaction proceeds spontaneously, while in the electrolytic cell (a device that converts the electrical energy into chemical energy, such as the cell during charging) the potential is negative and the reaction needs an external force to take place.

This equation can also be related to the standard state (25°C and unit activity):

$$\Delta G^o = -nFE^o \qquad (1.4)$$

For a chemical equation it is also possible to relate the free energy, in the isothermal condition, with the equilibrium constant (*K*):

$$\Delta G = RT\ln(K) \qquad (1.5)$$

Where *R* is the gas constant (*R = 8.314 J mol-1 K-1*) and *K* the equilibrium constant. Considering the following chemical reaction:

$$bB + cC \leftrightarrow dD + eE \qquad (1.6)$$

The equilibrium constant is described as:

$$K = \frac{a_B^b \cdot a_C^c}{a_D^d \cdot a_E^e} \qquad (1.7)$$

If *K>1* the reaction moves the equilibrium in favour of the products;
if *K<1* the reaction moves the equilibrium in favour of the reagents.

Also in this case it is possible to relate the equation to the standard condition:

$$\Delta G^o = -RT\ln(K) \qquad (1.8)$$

Matching the chemical and the electrical equation it is possible to connect the chemical and the electrical field in the standard condition:

$$-RT\ln(K) = -nFE^o \qquad (1.9)$$

In this way, it is possible to relate the potential of the cell to the equilibrium constant, derived from the chemical considerations, thanks to the Nerst equation:

$$E^o = \frac{RT}{nF} \cdot \ln(K) = -\frac{\Delta G}{nF} \qquad (1.10)$$

This equation determines the electromotoric force ($emf = E^o$) of the reaction.

Similarly, in a non-standard condition, or better when the concentration of the reagents deviates from the standard condition, the isothermal free energy could be determined by the Van't Hoff equation:

$$\Delta G = \Delta G^o - RT\ln(K) \qquad (1.11)$$

And in the same way, by substituting the free energy (ΔG) and the free energy in standard conditions (ΔG^o) with the electrical definition, it is possible to obtain the Nerst equation in non-standard conditions:

$$-nFE = -nFE^o - RT\ln(K) \qquad (1.12)$$

$$E = E^o - \frac{RT}{nF} \cdot \ln(K) \qquad (1.13)$$

Thus, it is possible to determine the potential of the cell in non-standard conditions.

During the charging and discharging processes, the concentration of the reactants is not stable and for this reason the equilibrium constant changes, varying the potential of the cell and, for example, it is possible to notice that during the discharge the K increases, decreasing the potential of the cell.

1.10 Batteries, an overview

Batteries are devices that convert chemical energy into electrical energy.
They are composed of two electrodes, one positive and one negative, separated from each other by an electrolyte solution, which must be both electrical insulator and ionically conductive.
The electrolyte must have different electrode potentials in order to have the energy conversion and supply electrical current, once the circuit is closed.
The reactions that occur in the batteries are redox reactions and in particular, during discharge, an oxidation reaction, also called anodic reaction, occurs on the negative electrode (the anode), with release of electrons, while a reduction reaction, also called cathodic reaction, occurs at the positive electrode (the cathode), where electrons are collected. The reactions are inverted during the charging process and the negative electrode becomes a cathode, while the positive electrode an anode, even if, by convention, the negative electrode is always called anode and the positive cathode, avoiding in this way any misunderstanding.

The higher the difference between the potential of the two electrodes, the easier is the progress of the reactions.

Mainly, there are two types of batteries called primary and secondary systems:

1) Primary systems (Galvanic cells): they are devices in which the reactants are limited and as soon as the electrodes are consumed it is not possible to restore new energy and they need to be discharged.
   The most important category of these batteries is presented by cells with zinc anodes in which the well-known alkaline and zinc-carbon cells take part.
   Another important category of primary batteries is presented by the lithium anode cells in which lithium is used as pure element due to its low potential (-3,05V vs SHE) that allows to reach high voltages, more than 3V, and high specific energies of 600Wh/kg, achievable also thanks to the light weight of the lithium element[…];

2) Secondary systems: they are batteries in which it is possible to have multiple cycles thanks to their behaviour to be recharged, besides supplying energy, thus converting electrical energy into chemical energy.
   An example of this type of system is presented by the most used batteries on the market such as the lead-acid batteries which can supply energy densities of 30-40Wh/kg, small values due to the high weight of lead.
   Lithium-ion batteries are instead the most promising energy accumulator used nowadays due to their high energy density of 150-180Wh/kg.

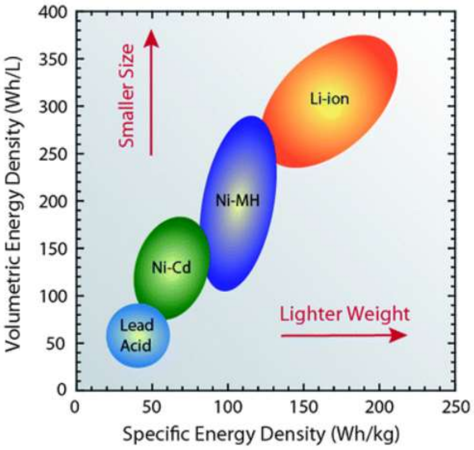

Figure 1.11 *Comparison of Li-ion batteries with other commercial rechargeable batteries used nowadays (www.epectec.com)*

In order to determine the potential of a battery, it is necessary to determine the electrode potential of the individual electrodes. This parameter must be related to a standard electrode and for this reason all the potentials are defined considering the standard hydrogen element, as reported in the following table:

Table 1.2 *Standard electrode potentials vs standard hydrogen electrode (SHE)*

Reaction	E^0, V (SHE)	Reaction	E^0, V (SHE)
$Li^+ + e^- \rightleftarrows Li$	−3.045	$HgO + H_2O + 2e^- \rightleftarrows Hg + 2OH^-$	0.098
$K^+ + e^- \rightleftarrows K$	−2.935	$Sn^{4+} + 2e^- \rightleftarrows Sn^{2+}$	0.154
$Ca^{2+} + 2e^- \rightleftarrows Ca$	−2.866	$Cu^{2+} + e^- \rightleftarrows Cu^+$	0.153
$Na^+ + e^- \rightleftarrows Na$	−2.714	$AgCl + e^- \rightleftarrows Ag + Cl^-$	0.2224
$Mg^{2+} + 2e^- \rightleftarrows Mg$	−2.363	$Hg_2Cl_2 + 2e^- \rightleftarrows 2Hg + 2Cl^-$	0.2676
$Al^{3+} + 3e^- \rightleftarrows Al$	−1.662	$Cu^{2+} + 2e^- \rightleftarrows Cu$	0.337
$Ti^{2+} + e^- \rightleftarrows 2e^- \rightleftarrows Ti$	−1.628	$Fe(CN)_6{}^{3-} + e^- \rightleftarrows e(CN)_6{}^{4-}$	0.36
$Zn(OH)_2 + 2e^- \rightleftarrows Zn + 2OH^-$	−1.245	$Cu^+ + e^- \rightleftarrows Cu$	0.521
$Mn^{2+} + 2e^- \rightleftarrows Mn$	−1.180	$I_2 + 2e^- \rightleftarrows 2I^-$	0.536
$2H_2O + 2e^- \rightleftarrows H_2 + 2OH^-$	−0.822	$O_2 + 2H^+ + 2e^- \rightleftarrows H_2O_2$	0.682
$Zn^{2+} + 2e^- \rightleftarrows Zn$	−0.764	$Fe^{3+} + e^- \rightleftarrows Fe^{2+}$	0.771
$S + 2e^- \rightleftarrows S^{2-}$	−0.48	$Br_2 + 2e^- \rightleftarrows 2Br^-$	1.065
$Fe^{2+} + 2e^- \rightleftarrows Fe$	−0.441	$O_2 + 4H^+ + 4e^- \rightleftarrows 2H_2O$	1.229
$Cd^{2+} + 2e^- \rightleftarrows Cd$	−0.403	$Cl_2 + 2e^- \rightleftarrows 2Cl^-$	1.358
$Ni^{2+} + 2e^- \rightleftarrows Ni$	−0.250	$PbO_2 + 4H^+ + e^- \rightleftarrows Pb^{2+} + 2H_2O$	1.455
$Sn^{2+} + 2e^- \rightleftarrows Sn$	−0.136	$Ce^{4+} + e^- \rightleftarrows Ce^{3+}$	1.61
$2H^+ + 2e^- \rightleftarrows H_2$	0.0000	$F_2 + 2e^- \rightleftarrows 2F^-$	1.87

In this way, each element has a standard potential (E^o) related the redox nature of the material, described by the Nerst equation mentioned in §1.9.1: all the elements that have negative potential could be a good candidate as anodes because of their attitude to be oxidized during discharging and on the other hand the materials with positive potential could be used as cathodes.

The total potential of the battery is defined as the difference between the cathode (positive potential) and the anode (negative potential) and it is always positive:

$$U = V^+ - V^- \tag{1.14}$$

From the previous table it is possible to see how pure Lithium is largely electronegative (-3.05V) and for this reason it has been used for a long time as anode electrode in lithium batteries (primary system).

The greater is the difference between the potential of the electrodes and the easier the reaction is because the electromotoric force (*emf*) increases. Also sodium is particularly electronegative (-2.71V) and for its lower cost, compared to lithium, it is widely used as anode, even if the capacity achievable is lower.

The battery could also be considered as made of two half cells, each including one electrode, where a single chemical reaction takes place.

In the experimental analysis, the active electrode materials to be analysed are set in half cells to level out the analysis comparing the results obtained with the scientific society. In these cases the reference electrode is always Lithium or Sodium, used as anode, while the cathode is the active material to be analysed: in case of graphite or silicon materials, they are cathodes in half cells, but when applied in full-cells, they covert they behaviour into anodes because the electrode materials paired have higher potential, as seen further.

[…] The pure lithium electrodes were used as anodes because of its high specific charge of 3862Ah/kg, achieving in this way high capacity. Indeed, the main advantage is related to the high energy/weight ratio, also called energy density, due to the presence of the lithium ions that have the highest achievable energy density for naturally produced ions, because of the low weight that also encourages the production of lightweight devices.

A cathode material combined with pure lithium anodes is generally manganese dioxide, which allows to reach potentials greater than 3V, or iron sulfide which are both used instead of the alkaline batteries due to the similar potential of 1.5V, generally applied in devices such as photography cameras.

The first lithium batteries were produced in 1912 by G.N.Lewis, but they were particularly dangerous because of the high reactivity of Lithium. Moreover this type of batteries could not be used as rechargeable devices just because of the dendritic precipitation of lithium that occurs on the cathode during charging, which could penetrate the separator, besides the high volume variations due to the intercalation, inducing shortcuts and overheating with possible fires or explosions.

Because of their high instability and sensibility even in environments with little moisture, lithium anodes could not be used with aqueous electrolytes and for this reason they were combined with an organic solvent.

The critical behaviour of lithium anodes led during the 1970s to an intensive development of lithium batteries that could be recharged, achieving high voltage potentials anyway. The first lithium ion batteries still used lithium as negative electrode, but they still had safety problems. For this reason, during the 1980s lithium intercalated compounds were developed such as the most used cobalt oxide lithium ($LiCoO_2$), besides manganese oxide (LMO), nickel manganese cobalt oxide (NCM), nickel cobalt aluminium oxide (NCA) and iron phosphate (LFP) to be used as cathodes. Lithium ions, if intercalated in such metal oxide achieve a stable and quiet condition.

This new generation of batteries was developed from 1991 by Sony, thanks to the study directed by the physicist J.B. Goodenough, which allows to reach a higher operating voltage (3.8V), compared to the rechargeable batteries (secondary systems) produced since that period, with high energy density

up to 150Wh/kg and cyclability over one hundred cycles: this battery is made of $LiCoO_2$ cathode, which has a specific capacity of 137Ah/kg and 0.8V (vs SHE), combined with a graphite anode, merged in an organic electrolyte of carbonates and hexafluorophosphate ($LiPF_6$).
Moreover, the lithium atoms have a low radium dimension compared to other elements and this allows to have a high intercalation and deintercalation of the ions in the active material of the electrode, favouring a high cyclability.

The following diagram presents how Li/$LiCoO_2$ has an operating voltage of 3.9V, while Li/graphite has the lowest operating voltage of 0.1V. Thus, $LiCoO_2$ is used as cathode material while graphite as anode material, with a potential similar to pure lithium.

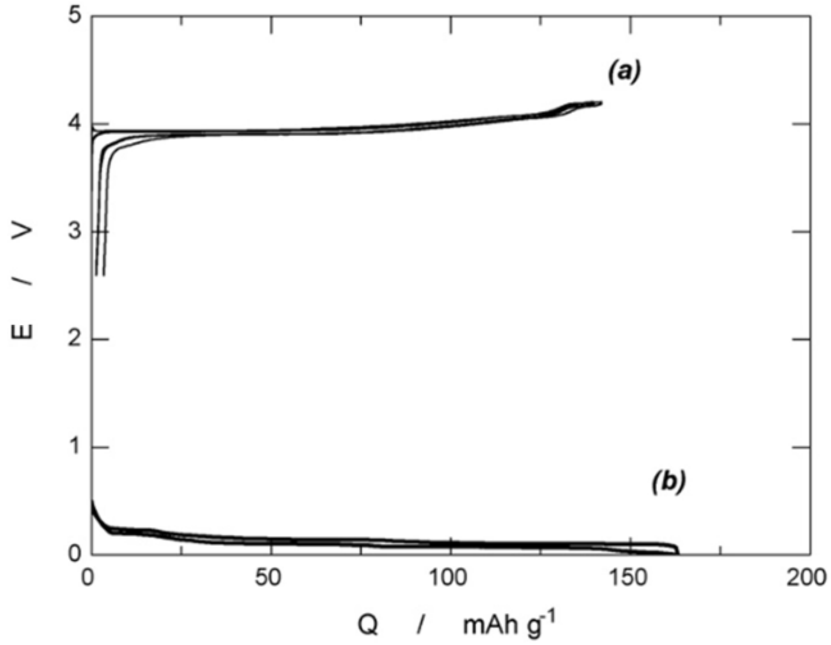

Figure 1.12 Charge/Discharge Plot of (a) Li/LiCoO2 and (b) Li/graphite half-cells. The combination of the two gives a cell.

At first, lithium ion batteries had low energy compared to the nickel cadmium batteries, but they have been developed to reach today a huge availability on the market in various applications such as smartphones and laptops, hybrid and electric vehicles, stationary energy storage systems to be combined with renewable energy collectors, such as solar panels or wind turbines.
Compared to the Ni-Mh (Nichel-Hydride metal) rechargeable batteries, also lithium batteries have no memory effect and the auto-discharging is only decreasing to 5% monthly.
Also lithium ion batteries do not contain any traces of cadmium and for this reason they should be better for the environmental impact, since cadmium is toxic, especially if the cathode is made of LMO, and because cobalt present in the others is toxic.[32]

Safety is one of the main problems of these devices, which must adopt electrical circuit breakers, also known as CID (current interrupt devices), in order to avoid any battery overload or any shortcut that could generate fire and explosions. This kind of systems is activated also when heat conduces the battery to overtemperatures. In order to avoid these problems, nowadays batteries with inflammable resistance electrolyte made of polymer or doped glass are studied. Another drawback of these batteries is their natural degradation, regardless of the use of the device: generally, 20% of the battery is lost during the first year of life, considering an average temperature of 25°C. For this reason, batteries need to work in a proper temperature and voltage window in order to achieve the best performance in safety conditions.

The recent application of lithium-ion batteries in cars, favoured by the capability to assemble a large serial number of cells, providing high capacity and power (compared to the other batteries in use), has forced the development of these strict safety tests.
The temperature range accepted for this purpose is between -20 to 50ºC during charging and 0-45ºC during discharging, while the potential range is usually between 1.5 to 2.7V.[33]

1.10.1 How Lithium Ion Batteries work

Lithium ion batteries work thanks to the intercalation and deintercalation process of lithium ions that happen in the electrodes, embedded in the electrolyte, in these devices.
Considering a typical $LiCoO_2$/graphite battery and applying an external force as a potential, the Li atoms escape from $LiCoO_2$, becoming single ions, thus losing their external electron, which flows on the electrical circuit that connects the two electrodes.
When that potential is stopped, the lithium ions are automatically encouraged to gain the lowest energy setup, returning to the metal oxide, engaging its previously lost electron.

The electrodes must have a microstructure that easily absorbs the lithium ions dissolved on the electrolyte, which separates the two electrodes.
For this purpose, graphite is largely used as anode, in fact the structure of this material, which has a low strength bonding between the hexagonal layers due to the Van Der Waals bonding, allows an easy absorption of lithium ions. For this reason, the specific capacity of these batteries reaches high values around 370mAh/g. If multivalence ions were used instead of lithium, they could have a higher charge capacity, but at the same time they would have less mobility, causing a limited absorption of the element in the solid electrode, thus giving less efficiency.

The electrolyte has a dual role in the lithium-ion batteries:

- avoid the conduction of electrons;
- supply the lithium ion to the anode as much as possible, guarantying high capacity values.

For this reason, the commonly used electrolyte is a solution of lithium such as lithium hexafluorophosfate in lithium carbonate and dimethylcarbonate.

During the ion conduction in charging, the electrons, the losses from the cathodes, reach the anode passing through the external electrical circuit, joining the intercalated lithium ions.

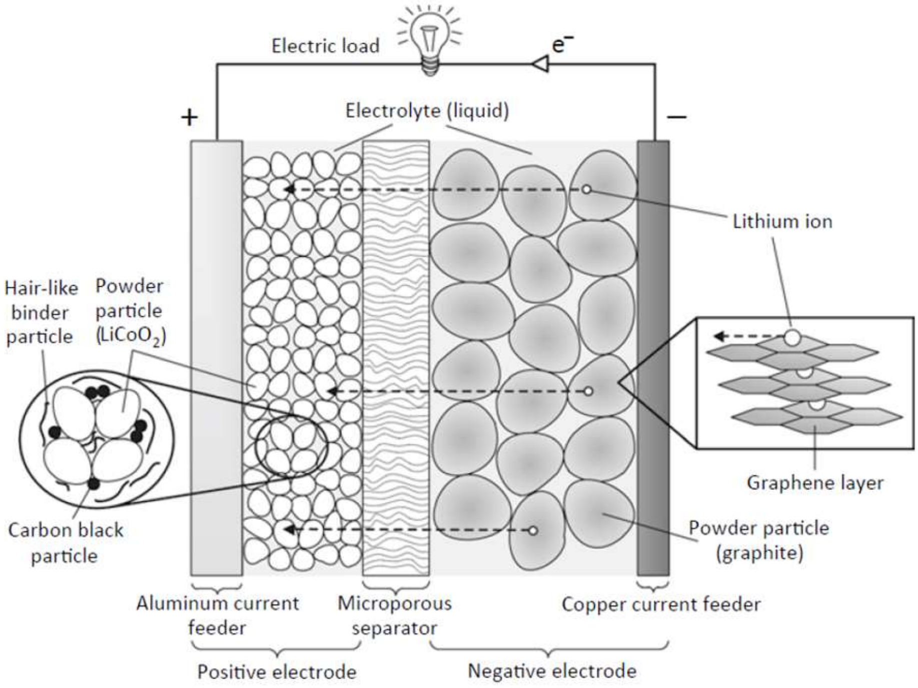

Figure1.13 A lithium ion battery illustrate during discharging [32]

The ions, deintercalated from the cathode, during the charging process, are only 50% of the available amount, in fact higher diffusions could promote the collapse of the electrode with the release of oxygen, causing critical conditions.

By the way, during lithiation, when the anode is saturated with lithium ions, the battery is completely charged.

Considering a typical $LiCoO_2$/graphite battery, dismissing the potential applied, the lithium ions are encouraged to return to the anode, completing the process of delithiation from the anode. The discharging processes are thus described by the following reaction:

- At the cathode: reduction/intercalation

$$2Li_{0.5}CoO_2 + Li^+ + e^- \rightarrow 2LiCoO_2 \qquad (1.14)$$

- At the anode: oxidation/deintercalation

$$LiC_6 \rightarrow\ Li^+ + e^- + 6C \qquad (1.15)$$

Thus, every Lithium ion is hosted by six carbon atoms.
During the charging process the reaction is opposite to those described.

In order to avoid any contact between the two electrode that would involve shortcuts, and to avoid any transmission of electrons through the electrolyte, a glass separator is set between them.
This item is also important to inhibit any heat of the electrolyte which could favour its evaporation, with related critical conditions.

The electrodes described here are not only used in lithium ion batteries, but the study in these devices has led to the search for new materials to be used as cathodes and anodes, gaining high energy and power densities and, at the same time, achieving the best performance reducing manufacturing costs. For example, alternative materials used in producing cathodes are:

Table 1.3 Cathode materials for battery

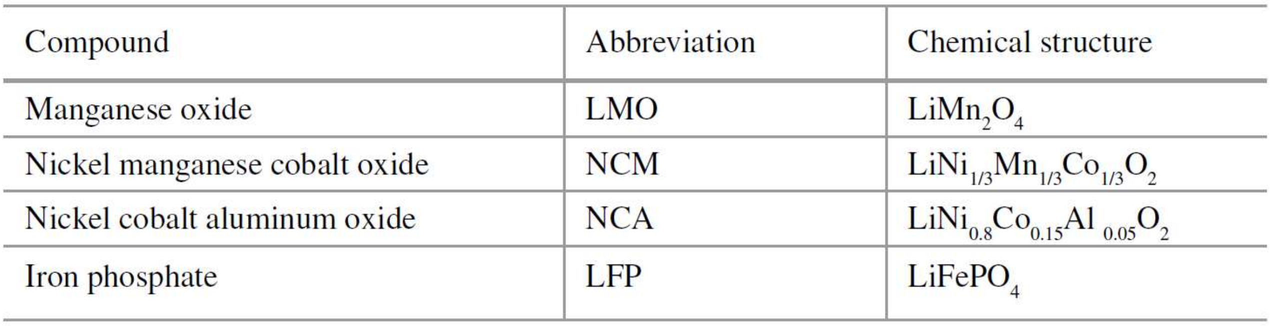

Compound	Abbreviation	Chemical structure
Manganese oxide	LMO	$LiMn_2O_4$
Nickel manganese cobalt oxide	NCM	$LiNi_{1/3}Mn_{1/3}Co_{1/3}O_2$
Nickel cobalt aluminum oxide	NCA	$LiNi_{0.8}Co_{0.15}Al_{0.05}O_2$
Iron phosphate	LFP	$LiFePO_4$

The choice of the material used for the production of the different part of the battery as the electrodes, is decided on base of the abundance in the earth crust and the price.
For example, by looking at following periodic table, it is possible to understand why an element like manganese is commonly used as transition metal in cathodes due to its cost, lower than cobalt.

In the second period table, the equivalent volumetric and gravimetric capacity of the elements is reported, even though the electrodes are not generally produced by a pure element, but in alloys.

(a) Availability

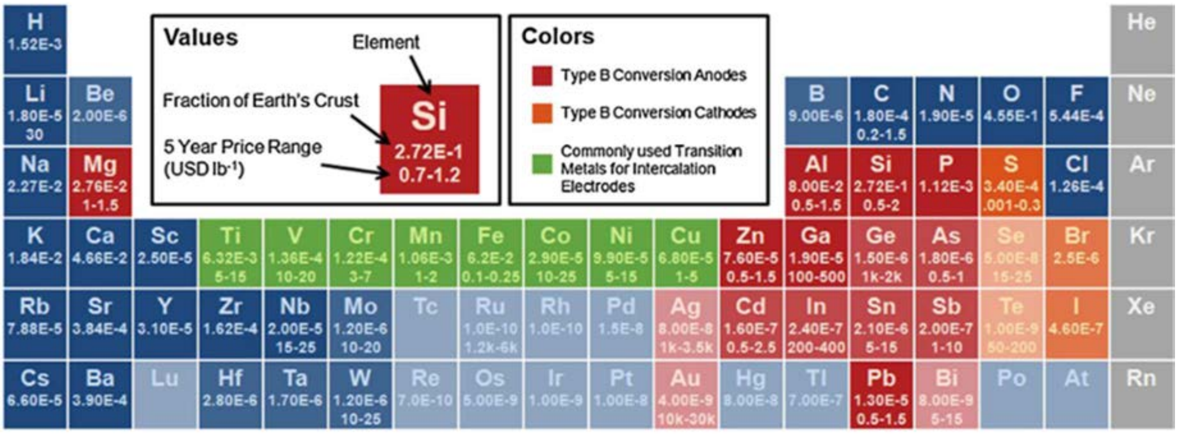

(b) Charge Capacity

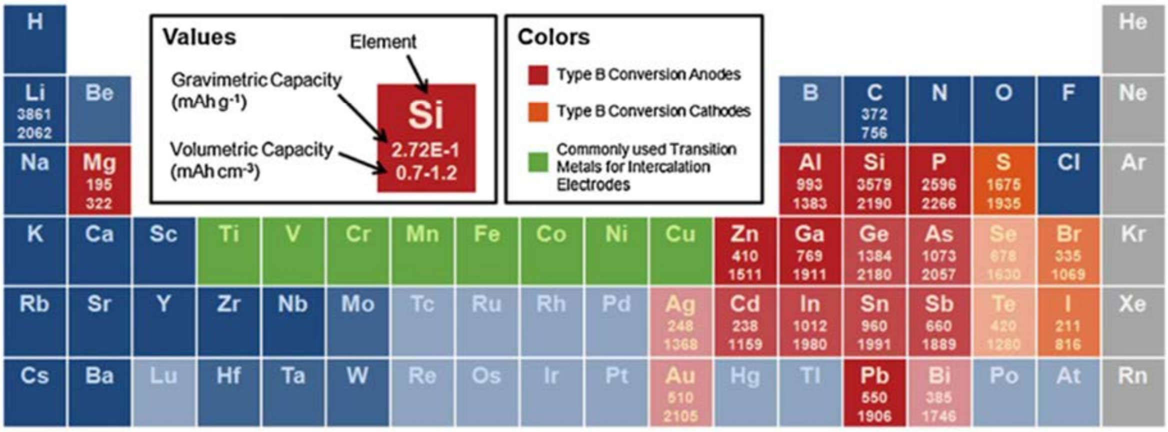

Figure 1.14 *in the (a) periodic table are shown the availability of the elements, while in the (b) is given the specific charge capacity for the elements that may host Lithium ions.*[34]

One of the main characteristics that the electrodes should have is the high potential difference related to the anode used, besides high ion-capacity and electrical conductivity. On the other hand, it is also reasonable to consider other parameters and characteristics such as the rate capability, which is usually inversely proportional to the capacity, and cyclability.

For the production of anodes, graphite has been considered as the best material due to its low standard reduction potential (approximately 0.2V), but at the same time other elements, such as silicon (Si), have low potential and very high specific capacity, which means high energy densities.

For this reason, there has been an intense research on anode materials with the development of lithium-metal alloys such as lithium-silicon (Li-Si) and lithium- tin (Li-Sn): lithium-silicon alloys are indeed one of the most suitable materials, gaining specific capacity values of 4200Ah/kg compared to the 372Ah/g of the graphite. On the other hand, the high volume expansion of these materials (300%), after a few cycles, would not allow the production of these batteries that would work for a short time, because of the degradation of the anode electrode.

For this reason, nowadays there is an upcoming research on silicon based materials such as the silicon/carbon composites to be applied as anodes in lithium ion batteries, which show, in their traditional production specific capacity values of 800Ah/kg, with high cyclability.

Chapter n.2

Electrode Preparation and Material Characterization

This chapter explains the experimental process of producing the 3D printed electrodes, followed by the thermal treatment conduced to convert polymer into ceramic material, and finally all the physical, structural-chemical, rheological and thermal characterization.

The first part is focused on the ink preparation of the preceramic polymer Polymethylphenyl-silsesquioxane (H44 resin), with a molecular weight of 2100g/mol, filled with different type of carbon sources in order to achieve high electrical conductivity; after that, a short explanation on the printing phase with some considerations on the rheological properties follows; once the 3D printed specimens are cured adequately, the thermal treatment is carried on thus the TGA/DSC analysis is the best solution to understand the thermal decomposition and the reactions that occur during this step.

The electrodes are ready to be set on electrical storage devices like batteries and supercapacitors, but some more analysis are needed in order to characterize the surface of the samples (scanning electron microscopy - SEM) and ensure the success of the thermal treatment, testing the material with X-Ray diffraction (XRD), Raman Spectroscopy (Raman), Fourier-transform infrared spectroscopy (FTIR).

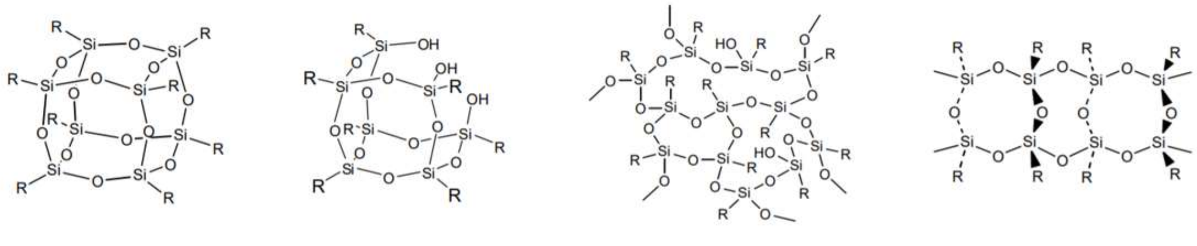

Figure 2.1 Representation *of the microstructure of preceramic polymers*

2.1 Ink Design

The choice of H44 for the production of these electrodes is based on the main advantages of polymer derived ceramics (PDCs) such as the homogeneity achievable compared to the traditional ceramics, besides the easy processability and shapeability that allow to obtain complex structures.

The particular choice of polysilesquioxane is due to the low cost of this type of preceramic polymer, the low reactivity with air and moisture that allow to easily handle them, the commercially availability, the high solubility in organic solvents, the fast curing adding crosslinkers, the final chemical structure, after the thermal treatment, that develops the production of SiOC material and free carbon (high amount of carbon because of the presence especially of phenyl groups), which is particularly recommended for the final application of this research due to the high specific capacity of SiOC and the electrical conductivity of the free-carbon.

The choice of adding carbon filler to the preceramic polymer is done to achieve higher electrical conductivity that should encourage the lithium ion penetration in higher surface area of the sample during the charging process in batteries.

In order to verify if the type of carbon filler is affecting the results, three types of carbon source are considered:

- Carbon fibers: diameter of 7.5 μm and an average length of ≈100 μm, produced by Ferrari Carbon srl, Milano, Italy;

- Graphite powder: Timrex KS 25 with a particle size range between 5-25 μm with a surface area of 8.6 m^2/g, produced by Imerys Graphite & Carbon Switzerland ltd, Bodio, Switzerland;

- Carbon Nanoplatelets: Nano25 with a surface area of 172.08 m^2/g, produced by Asbury Carbons, New Jersey, USA.

The first step of the research is to find the best amount of ink elements in order to achieve the proper viscosity to extrude the mixture and print the specimens.

The preceramic polymer Silres H44 used is a powder (produced by Waker Chemie AG, München, Germany) and it needs to be dissolved in a solvent to obtain the silicon. The solvent selected for this purpose is Isopropyl alcohol (commonly called isopropanol, 2-propanol, IPA) because of the high solubility of polymethylphenylsilequioxane (H44) and high vapour pressure, that allows to have an high evaporation rate of the alcohol, performing the best rheology properties of the solution and curing the specimens for less time before the heat treatment.

In order to achieve the proper viscosity range to extrude the ink, a catalyst needs to be added in the solution: triethylamine is selected for this purpose, bounding the side groups [$-OH$] and [$-OC_2H_5$] of the backbone (Si-O).

After several attempts the best percentage of constituents is defined as follows, without adding the carbon filler for now:

Table 2.1 *Basic element of the material, chemical formula and relative amount (without filler)*

COMPONENT	***CHEMICAL FORMULA***	***AMOUNT (%)***
Polymethylphenyl-silsesquioxane (H44) – PDC	$[(C_6H_5)_{0.62}(CH_3)_{0.31}(OR)_{0.07}SiO_{1.5}]_n$ with R=[$-OH$] , [$-OC_2H_5$] and n=20	86
Isopropanol – Solvent	C_3H_8O	13
Triethylamine – Catalyst	$(C_2H_5)_3N$	1

The ink is prepared through the following steps:

- Weigh the plastic cup (reference);
- Add H44 (5.36g) and Isopropanol (0.08g) with the equivalent ratio 86.8/13.2;
- Mix the H44 and Isopropanol for 10minutes in a Thinky Are-250 planetary mixer at 1000rpm, till the preceramic polymer is completely dissolved in the solvent;
- Weigh the cup with the solution to determine the amount of isopropanol evaporated and subsequently add the amount of alcohol needed to reach the fixed threshold (0.8g);

- Add the triethylamine catalyst (0.08g) to activate the polymer chains bonds, supporting the increase of viscosity and encouraging the pseudoplastic behaviour of the solution.
- Mix for 2-3 minutes at 1000rpm to homogenize the mixture;
- Put the ink in a syringe and defoam the ink for 7minutes at 200rpm in order to avoid the voids in the final samples: in this way all the air trapped in the solution is collected below the piston.

The catalyst needs to be added just before the printing process, otherwise the increase of viscosity, due to the bonding growth, does not allow the extruding process of the ink, not even at high pressure.

The main important behaviour for the ink to be printed with DIW is the viscoelastic response of the solution that allows the resin to flow through the nozzle when a pressure is applied thanks to the shear stress created, followed by a shape retention when the mixture is extruded. In this way it is possible to deposit a stable filament on the surface of the printing plate avoiding any collapse of the structure, by printing layer by layer.

In order to achieve the proper printing performances, the ink has to be formulated with the appropriate viscosity, otherwise it flows as a liquid if this parameter is too low, involving structural collapse, or on the other hand, it does not extrude if the viscosity is too high.

One of the main purposes of the research is to understand the electrochemical behaviour of the material in base of the amount of carbon filler added to the ink.
For this reason, the mixtures are filled with different quantities up to the extruding process is achievable: the viscosity of the ink increases proportionally to the amount of filler and the solution needs to be diluted with more solvent (isopropanol). The quantity of filler, depending on the nozzle diameter of extrusion (inversely proportional) and on the type of carbon source (graphite, carbon fibers, nanoplatelets), is upper limited, over which the ink is not able to be printed because of the clogs created due to the amassment of solid particles on the exit, which are not allowing the solution to flow over.

Graphite filler shows the highest amount addable to print the electrodes with a diameter of 250μm. It is added with a maximum quantity of 54.54% of the entire ink (not considering the ceramic yield of H44 yet, otherwise it should be higher and exactly 65.6%).

For this reason it makes sense to estimate the isopropanol trend, in base of the amount of graphite filler added into H44, as reported in the following plot.

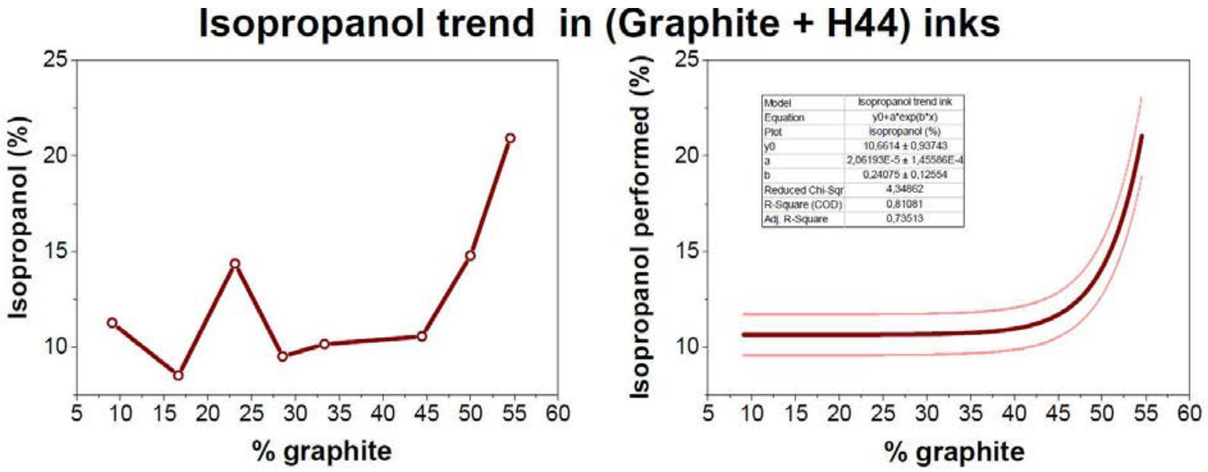

Figure 2.2 *left: solvent amount in base of the graphite material added as filler; right: interpolation of the results using an exponential function*

On the left side is reported the experimental percentage of isopropanol added in the ink, while on the right side the solvent amount is estimated with an exponential trend.

As expected the amount of isopropanol increases proportionally with the amount of graphite because the filler absorbs much of the solvent.

Actually, there is not an exact amount of solvent to add in order to have the proper viscosity to print the ink, but there is a range of values acceptable. For this reason, a deviation of 10% from the estimated value is considered adequate for an easy printing.

The amount of isopropanol % in the other types of carbon sources, carbon fibers and carbon nanoplatelets, is not estimated because the maximum amount of filler is less compared to the maximum carbon graphite: the evaluation does not have enough data to predict the behaviour because of the minor diversity on the amount of isopropanol between the inks prepared.

The maximum amount of carbon fibers added in the ink is 28.5%, while the maximum amount of carbon nanoplatelets is 33.3%.

Considering the ceramic yield of H44, after the heat treatment, which is determined as 63.0%, with a TGA analysis for the heat treatment conduced, the final theoretical maximum amount of carbon filler is higher compared to the amount previously declared, and in particular:

- Graphite: 65.6%
- Carbon Fibers: 38.3%
- Carbon Nanoplatelets: 44.2%

The other inks prepared in order to print the electrodes have a carbon filler content below the amount just mentioned, and in particular:

Table 2.2 *inks prepared considering different amount of fillers (percentage related to the H44 added)*

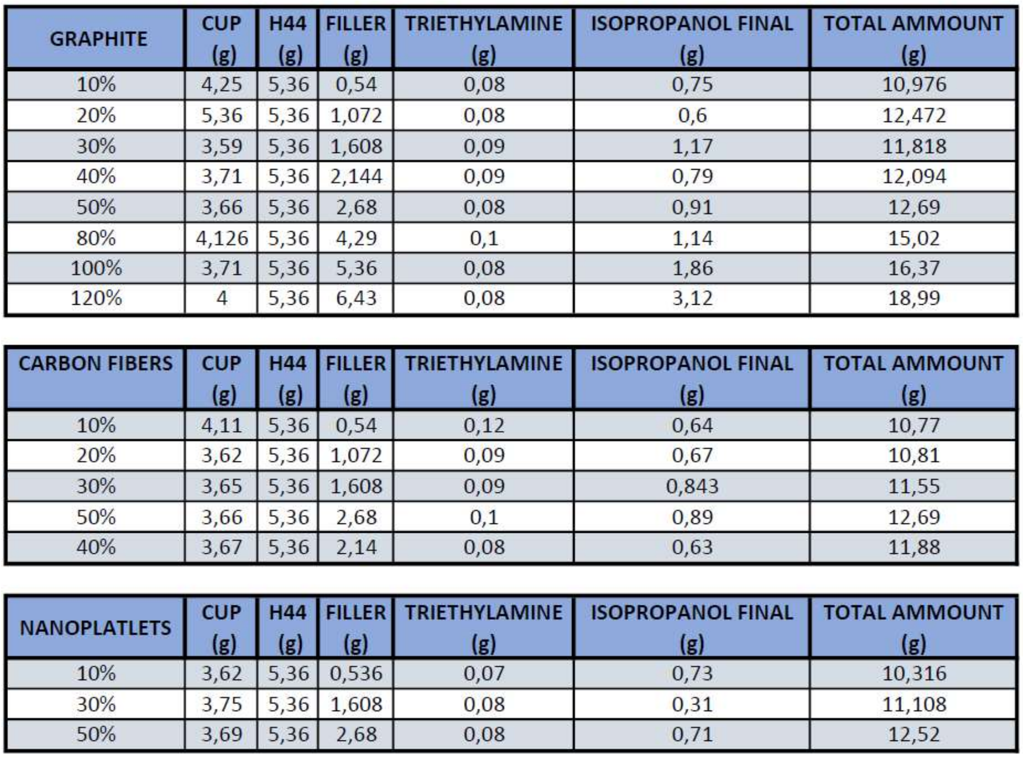

GRAPHITE	CUP (g)	H44 (g)	FILLER (g)	TRIETHYLAMINE (g)	ISOPROPANOL FINAL (g)	TOTAL AMMOUNT (g)
10%	4,25	5,36	0,54	0,08	0,75	10,976
20%	5,36	5,36	1,072	0,08	0,6	12,472
30%	3,59	5,36	1,608	0,09	1,17	11,818
40%	3,71	5,36	2,144	0,09	0,79	12,094
50%	3,66	5,36	2,68	0,08	0,91	12,69
80%	4,126	5,36	4,29	0,1	1,14	15,02
100%	3,71	5,36	5,36	0,08	1,86	16,37
120%	4	5,36	6,43	0,08	3,12	18,99

CARBON FIBERS	CUP (g)	H44 (g)	FILLER (g)	TRIETHYLAMINE (g)	ISOPROPANOL FINAL (g)	TOTAL AMMOUNT (g)
10%	4,11	5,36	0,54	0,12	0,64	10,77
20%	3,62	5,36	1,072	0,09	0,67	10,81
30%	3,65	5,36	1,608	0,09	0,843	11,55
50%	3,66	5,36	2,68	0,1	0,89	12,69
40%	3,67	5,36	2,14	0,08	0,63	11,88

NANOPLATLETS	CUP (g)	H44 (g)	FILLER (g)	TRIETHYLAMINE (g)	ISOPROPANOL FINAL (g)	TOTAL AMMOUNT (g)
10%	3,62	5,36	0,536	0,07	0,73	10,316
30%	3,75	5,36	1,608	0,08	0,31	11,108
50%	3,69	5,36	2,68	0,08	0,71	12,52

The amount of filler % is related to the H44 added.

The following chart shows the equivalent amount of filler compared to the H44 added, as shown in the previous table, but it's more convenient to consider it in relation to the total weight of the ink or consider also the ceramic yield of the preceramic polymer after the heat treatment:

Table 2.3 *Amount of fillers related to the H44 quantity, to the total ink weight and to the total ink weight considering also the ceramic yield*

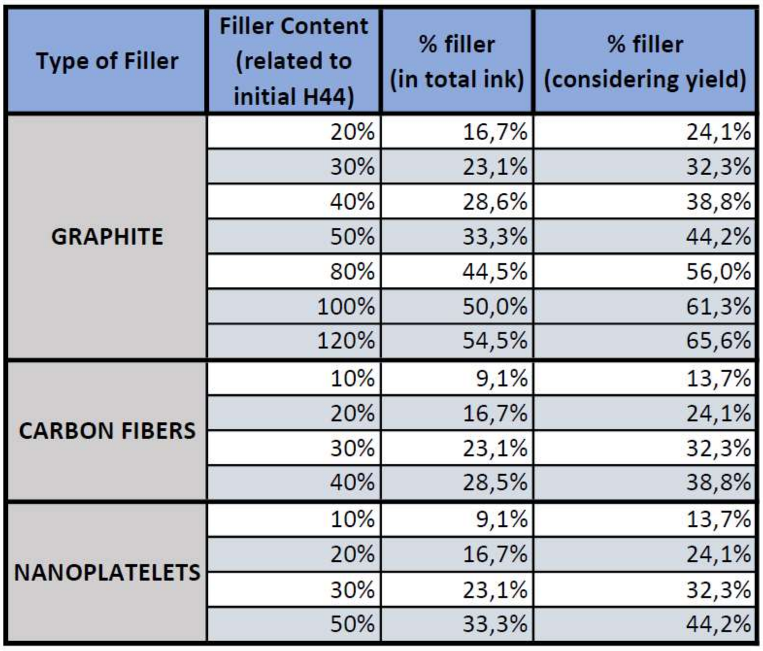

Type of Filler	Filler Content (related to initial H44)	% filler (in total ink)	% filler (considering yield)
GRAPHITE	20%	16,7%	24,1%
	30%	23,1%	32,3%
	40%	28,6%	38,8%
	50%	33,3%	44,2%
	80%	44,5%	56,0%
	100%	50,0%	61,3%
	120%	54,5%	65,6%
CARBON FIBERS	10%	9,1%	13,7%
	20%	16,7%	24,1%
	30%	23,1%	32,3%
	40%	28,5%	38,8%
NANOPLATELETS	10%	9,1%	13,7%
	20%	16,7%	24,1%
	30%	23,1%	32,3%
	50%	33,3%	44,2%

The viscosity of the material to be printed is one of the fundamental parameters to monitor in order to have a high efficiency of printing. This is well monitored in base of the amount of filler and solvent, as explained above, but also the time of printing is fundamental, because of the catalyst added which encourages the bounds between the polymeric chains, enhancing the viscosity.
For this reason it is important to print the ink with the proper rheology and to produce the electrodes as fast as possible (within 30minutes).

2.1.1 Rheometer Analysis - Viscosity

In order to verify the pseudoplastic behaviour of the ink and have an idea of the rheology of this material, without any filler, a rotational rheometer test is conduced to study its flow and deformation.

Figure 2.3 *Advance Rheometer AR2000*

The preceramic polymer and the solvent are mixed together in the proper amount of 5.36g H44 and 0.8g Isopropanol, as described above. The solution would be ready to be added with the crosslinker and to print the electrodes, even without any filler.

The ink is in this way analysed with an Advance Rheometer AR2000 set with a room temperature (25°C), printing parameter, using a cone-plate system of 40mm diameter and 2°angle, with a isopropanol trap in order to avoid any solvent evaporation during the analysis, maintaining the same initial condition as much as possible.

The choice of the type of system is important in base of the material analysed: using a cone plate assembly is possible to apply a uniform shear rate all over the sample, while a plate system is the best choice in case of materials with big particles, as it permits them to accommodate easier.

Only angles below 4° are allowed, over which tanα could not be approximated with α and the velocity profile could not be predictable. Moreover, smaller angles are allowing to reach higher shear rates. In this research a 2° is selected. A gap of 500μm is set.

On the other hand, the diameter of the plate should be designated in base of the shear stress achievable, indeed the dimension is inversely proportional to this parameter, gaining more sensitivity with large geometries, particularly suitable for low viscosity materials.
Generally diameter between 2 to 6 cm are allowed, and in this case a 4cm is selected because of its versatility and proper for medium viscosities, as the ink used.

In order to avoid any evaporation of the solvent, a trap cover is set upon the system, avoiding any loss of isopropanol from the ink analysed because of the saturation of the vapour in the free space, as illustrated in the following picture, thanks to the solvent arranged over the well.

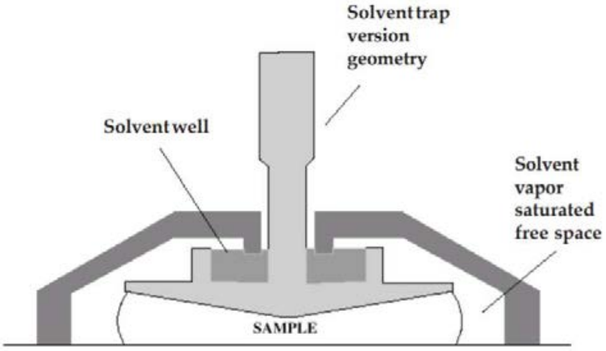

Figure 2.4 *Solvent trap and geometries illustrated*
(www.mse.iastate.edu)

Viscosimeters determine the viscosity under restricted limitations, but rheometers can operate in wider conditions, determining yield stress, viscoelasticity, stress relaxation behaviour and other properties of non-Newtonian fluids. In this research these properties are not investigated because they are beyond the aim of the work; the study is focused in particular to determine the viscosity over the shear stress to understand the material behaviour during the printing, when a pressure is applied to extrude the filament, and to monitor the shear stress over the shear rate which is proving the pseudoplastic behaviour of the ink produced, as expected.
The measurement is taken with a shear rate control which is the best solution to simulate operation of flowing through tubes, like in the 3D printing process over the nozzle.
In this way the system gives the shear stress and from the relation shear stress/ shear rate is possible to calculate the viscosity instantaneously.

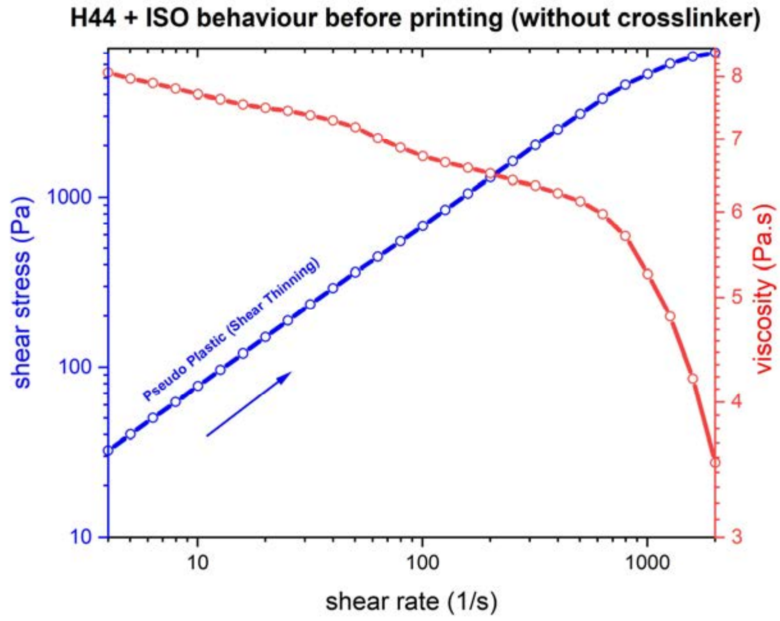

Figure 2.5 Results *of the rheometer analysis in a log-log plot where is possible to observe the pseudoplastic behaviour of the ink (without filler)*

The results of this analysis are explained in a log-log plot where it is possible to observe the non-Newtonian behaviour due to the change of viscosity when a different shear rate is considered (associated with a change of rotational speed): the viscosity of the material decreases with the increase of shear rate.

Moreover, the shear stress increases with an increase of shear rate but at the same time the angular coefficient, which is the dynamic viscosity, decreases.

The decrease of viscosity on higher shear rate is explained with the thixotropic structure of this material in which the polymeric filamentary molecules are originally disposed in a chaotic and random arrangement and when stressed they align in the same direction, slide over each other, achieving a behaviour similar to liquid materials.

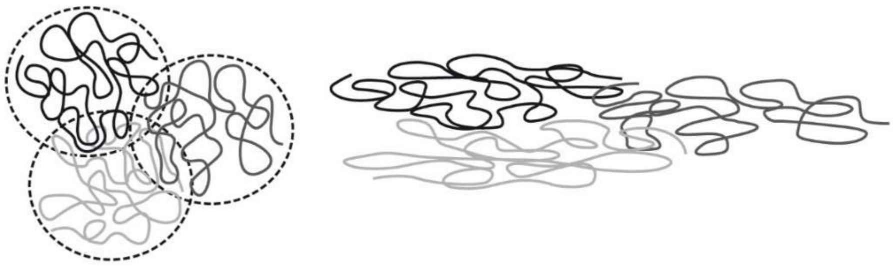

Figure 2.6 *Filamentary polymeric molecules in a quiet condition (left) and then stretched and aligned in the direction of the strength (right)*
(https://wiki.anton-paar.com)

This phenomenon has hysteresis, indeed when the ink is extruded, the filament does not collapse over its own weight because the stress is not applied, and the chains agglomerate over each other again, guaranteeing the shape retention. This phenomenon is also encouraged by the easily solvent evaporation increasing the viscosity of the material and avoiding any deformation.

In this plot, it is also possible to see how the ink is not able to have any deformation below a certain yield stress and this explains its Bingham behaviour. In this way the material does not flow over the nozzle as soon as a pressure is applied, but it needs a certain amount of stress before it begins to be extruded.

Adding the catalyst, this phenomenon is expected to be more pronounced because of the bounds created between the chains. For this reason, it is not possible to have a great evaluation of the exact rheology of the ink during the printing process, also because there are other parameters which are affecting these properties such as the diameter and shape of the nozzle, which is related to the surface tension and the capillarity of the material. On the other hand, this analysis proves the expectation on the rheology of this material especially because in this way it is possible to reach the same viscosity by adding also the filler.

Moreover, adding carbon powders it is expected to increase the pseudoplastic behaviour because of the micromechanics phenomenon which arises due to the interactions between the particles that allow to increase the temperature locally, decreasing the viscosity at high shear rate.

It is interesting to compare the viscosity of this resin with products of daily use to have an easy and immediate perception of its behaviour:

Table 2.4 *Comparison of the ink viscosity analysed with different materials of daily use (www.vp-scientific.com)*

Material	**Viscosity [Pa·s] (at room temperature)**
Water	0.001
Milk	0.003
Castrol Oil	1
H44+ISOPROPANOL	***8***
Honey	10
Chocolate	25
Ketchup	50
Mustard	70

The viscosity obtained for the material tested begins from 8Pa·s and decreases till 3.6 Pa·s at a shear rate of 2000 1/s. This results are similar to the trend of viscosity reached with another type of commercial preceramic polymer, polymethylsilsesquioxane (MK), dissolved in isopropyl alcohol, catalysed with DabcoT12N, and filled with MK fine powder and graphene oxide (GO) studied in a previous work published as "Direct Ink Writing of micrometric SiOC ceramic structures using a preceramic polymer" by Giovanni Pierin, Chiara Grotta, Paolo Colombo and Cecilia Mattevi, Elsevier 2016: in this research a [IPA/MK(40/60)](70%)+crMK(30%)+0.05%GO has shown a starting viscosity around 7Pa·s and a decrease over shear rate a little bit more evident than the material now tested. Also in that case, the material was used to produce specimens printed with DIW.

2.2 Direct Ink Writing

The samples are produced with an additive manufacturing technique thanks to the polymeric behaviour of the material used, before the heat treatment. In this way it is possible to gain high complexity shapes, with high homogeneity and low quantity of pores, which are impossible to reach manufacturing with the traditional methods, starting directly from the ceramic materials.

Direct ink writing (DIW) is selected as the most suitable process for this purpose, especially because in this research it allows to reach 3D printed samples of preceramic polymer and carbon additives with a high homogeneity of the filler in the polymer matrix. In this way it is possible to assure a good electrical conductivity all over the sample, which is fundamental to achieve high ion absorption.

The presence of carbon content, which has a high light absorption, also precludes other additive manufacturing techniques as stereolithography, which would not allow the reticulation of the layers because of the inability of the polymer to crosslink under light irradiation.

On the other hand DIW is preferred, compared to powder bed-based printing because of the inability to produce dense products caused by the low flow rate of the powders, besides the high amount of waste, because of the not bonded particles.

The electrodes to be tested are thought to have a simple net-shape design with a different distance between the filament in order to study if the structural shape is affecting the electrochemical results. Three different shapes are analysed with the ratio interspace/(interspace + filament) of 50%, 70%, 80%.

Considering the same perimeter length of the specimens, the samples with a structural shape of 50% are heavier than the others, while the 80% are the lightest.

The samples are designed with three layers in order to have light electrodes, but at the same time they retain a structural strength, essential to handle the samples, which give them the self-standing performance. Thus, they differ from the traditional electrodes which are produced starting from the same material in powder, but applied on a copper plate, without any stiffness property.
Three layers are also chosen in order to allow the electrode to be set in button cell, which has a limited depth dedicated to this item.

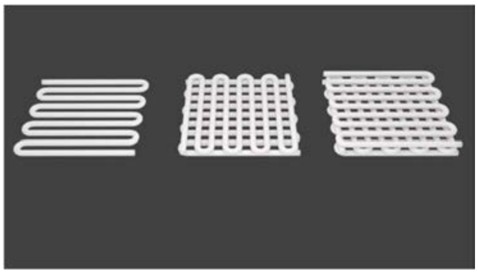

Figure 2.7 *Design of the electrodes prepared: the three layers are illustrated*

The project of the samples is drawn on Blender, an open source software in which it is possible to create the .stl file. The samples have a square base shape, three layers with a side dimension of 14.5mm. Then Simplify3D is used for slicing the pattern and produce the. gcode to set on Wasproject, Massa Lombarda, IT.

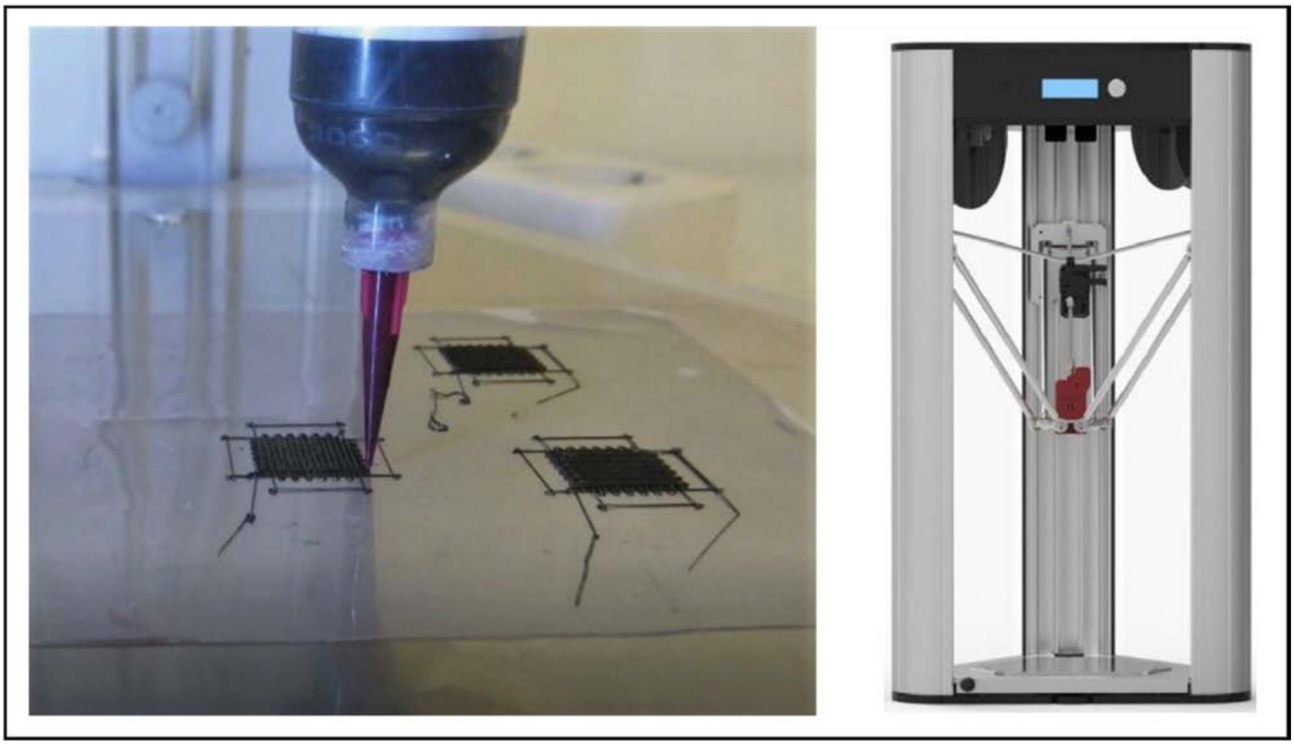

Figure 2.8 *Printing process of the electrodes (left) and Wasproject DIW printer (right)*

The nozzle used on this research to extrude the ink in the DIW printer has a diameter of 250µm. The size is chosen in order to have the smallest filament diameter, considering that a size smaller than this would not allow to extrude the material because of the solid filler added, which would clog the ink in the nozzle during printing.

The smallest diameter is the favourite to produce light specimens: it promotes light weight batteries, create a larger surface area, which would encourage the lithium absorption in lithium-ion battery devices.

Once the ink is prepared, it is injected into a syringe, after adding the catalyst element, then it is pushed into the extrusion tip with a piston of the proper dimensions. The syringe is then sealed and the solution is degassed in the planetary mixer at 200rpm for 7 minutes in order to avoid bubbles, which would interrupt the printing process, producing gaps on the printed specimens, compromising the final shape.

The syringe is then set on its holder on the 3D-printer and connected to the air pump, which would apply a pressure on the piston which is producing a shear stress in the ink, letting it flowing over the die, due to its pseudo-dilatant behaviour. Before printing, a 250µm nozzle is set and the z-axis zero position with an offset determined manually to let the filament being extruded without squeezing on the plate.

During the printing process two main parameters are constantly monitored:

- The pressure applied on the piston, and then to the ink;
- The velocity of the mechanical arm.

These two parameters are also correlated to each other and are set according to the rheology changings of the ink extruded. Actually, the pressure applied on the solution is directly proportional to the shear stress applied, which generates a shear strain on the material, with a decrease of viscosity: the ink is in this way encouraged to be extruded. At this point, it is possible that the filament produced does not retain its shape soon after the extrusion and the material flows too fast causing the collapse of the filament because of the gravity force; the collapse is avoided by the low gap between the tip nozzle and the printing plate. At the same time, low printing velocities allocate much more quantity of ink in a little space, if the viscosity is too low. For this reason, it is very important to find the best compromise between velocity and pressure in base of the viscosity of the solution.

The presence of the catalyst in the ink composition affects the rheology of the material over time, increasing the bonds between the polymer molecules and so increasing the viscosity.

Thus, during the printing process it is reasonable to decrease the velocity or increase the pressure applied to have a uniform extrusion.

The addition of filler, such as carbon sources in the ink composition also affects the parameters set during printing; actually the powder is not interested by the pseudoplastic behaviour of the polymer material: the graphite is in this way pushed to the exit of the nozzle and it could clog the extruder if the amount, related to the polymer, is too high. Only by adding more solvent, it is possible to avoid any impedance, because in such a way the filler is less condensed, but at the same time the viscosity could decrease so rapidly that it prevents any printing because the ink is too liquid

Thus, one of the main points of this research is finding the best percentage of components to easily ink writing, with the three types of carbon filler selected.

There are also differences in base of the carbon filler considered:

- Carbon fibers: are rotated and oriented in the same direction of the flow because of the shear stress applied, as demonstrated in previous works ("Direct ink writing of ceramic matrix composite structures" by Giorgia Franchin Larissa Wahl Paolo Colombo and "Optimization and Characterization of Preceramic Inks for Direct Ink Writing of Ceramic Matrix Composite Structures" by Giorgia Franchin, Halide Selin Maden , Larissa Wahl, Andrea Baliello , Marco Pasetto and Paolo Colombo). Their low surface area affects the maximum amount of filler achievable (38.8% considering the final composition) because during printing it is easy to clog the ink in the nozzle.

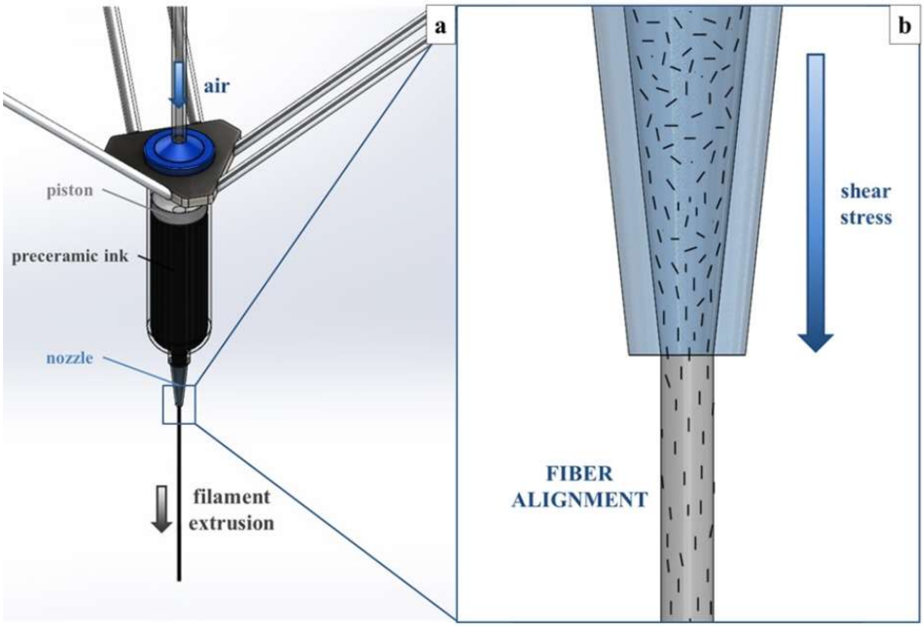

Figure 2.9 *Filament extrusion during printing (left) and alignment of the fibers due to the shear stress applied at the nozzle tip (right)* [9]

- Graphite: the maximum amount of graphite, with this size of nozzle, is in this case higher than carbon fibers because of the higher surface area of the powder (65.8% of the final composition);

- Carbon Nanoplatelets25: the highest specific area of the nanoplatelets is suggesting to have the highest amount of filler, but in this case, because of the nanoscale dimensions, which are precluding unique phenomenon, the maximum amount of filler reached is 44.2%, slightly higher than the carbon fibers and less than the graphite powder. Probably the nanoplatelets, as soon as added to the polymer + solvent solution, agglomerate together because of the attractive interaction forces, caused by their low mass, producing conglomerates unevenly dispersed in the ink, which facilitate the clog in the nozzle during printing.
  In order to prove this, specific tests should be done on the printed material, such as TEM with the aim of analysing the homogeneity of the filler, because SEM analysis is not enough powerful for this purpose, as it is possible to see further on.

As soon as the materials are printed, they are cured overnight in a flat surface, to avoid any deformation, letting them crosslink and dry to the point of being removed from the plastic substrate and then heat-treat.

2.3 Heat Treating Process – Pyrolysis

Once printed and cured, the specimens are ready to be pyrolyzed to convert the polymeric matrix of the H44 into a SiOC ceramic, obtaining a ceramic matrix composite (CMC).

The heat treatment on polymer derived ceramics is generally conduced at different temperatures in base of the final ceramic material desired.
The treatment is conduced over 1000°C in order to deteriorate the organic groups present in the side position of the main chain of the polymer's molecule such as $-CH_3$ (methyl) and $-C_6H_5$ (phenyl), gaining a SiOC glass structure. In rare cases, the thermal treatment is conduced with lower temperatures, from 800°C to 1000°C, when a pseudo-ceramic material is prepared because of the incomplete pyrolyzing process. In this case, the final structure achieved has a high macro-porosity (few microns to hundreds microns).[35]

Reaching a temperature beyond 1000°C the pores produced are bound to be closed, achieving an amorphous SiOC structure with higher density.
The heat treatment is conduced in an inert atmosphere in order to avoid any carbon loss, which would react with the oxygen flowing into the furnace: for this reason argon or nitrogen are generally used.
The pyrolysis process can be conduced at temperature above 1200°C, when the glass structure starts the phase-separation and crystallization, forming amorphous silica SiO_2, amorphous SiC and crystallin β-SiC, besides the production of graphitic carbon.[36,35]

The reaction of the crystallin formation of SiC is the following:

$$SiOC \rightarrow SiO_2 + x\ SiC\ (\beta) + y\ C(grap) \qquad (2.1)$$

The SiC formation is also stocked by the reaction between carbon and silica.

$$SiO_2 + 3C \rightarrow SiC(\beta) + 2CO\ (g) \qquad (2.2)$$

In this way, the carbon graphite produced inhibits the crystallization of silica.
Carbothermal reductions are achieved above 1500°C with decomposition of the glass structure.

One of the goals of this research is to reach an electrode made of SiOC matrix with a homogenous dispersed filler, a low shrinkage and high surface area, as well as high electrical conductivity.
For this purpose, the choice of the thermal treatment is of fundamental importance because the presence of silica and carbon silicon would decrease the electrical properties, but at the same time the carbon graphite can not be produced at temperatures below 1200°C.
Because of this a carbon filler is added to the matrix, in order to conduce a pyrolisis process at 1000°C, under nitrogen atmosphere, without giving up to the electrical conductivity, basic condition to apply the samples as electrodes. Moreover, above this temperature the initial formation of carbon clusters[37] is expected, which surely contributes, also if partially, to the final electrical conductivity, due to its less amount compared to the filler introduced in the structure.

First of all, the specimens need to be heat-treated to crosslink the polymeric matrix in order to avoid any collapse at high temperatures, which can be caused by the thermoplastic behaviour of H44.
During the night-time, the catalyst partially interacts with the material and the solvent evaporates,

however at room temperature it is not possible to conclude the cross-linking process, just because it needs higher temperature to be activated.

For this reason a crosslinking process is preceded at 300°C with a steady time of 3hours, then followed with a pyrolisis at 1000°C for 2 hours. All the process is conduced under flowing nitrogen (99.9%) with a heating rate of 1°C/min in order to avoid shape deformation with bending, achievable with higher rates, compromising the application of the samples as electrodes, expecially using carbon fibers as filler, because of the anysotropic thermal expansion. [9]

Table 2.5 *Parameters of the pyrolysis treatment conduced*

Heating rate: 1°C/min	**Temperature**	**Steady Time**
Crosslinking process	300°C	3hours
Pyrolisis process	1000°C	2hours

The process is conduced with a Tersid tube fornuce. The system is designed with an allumina (Al_2O_3) tube sorrounded by heating coils, insulated with a thermal insulator matrix and covered with an alluminum cage.

The tube is stocked with the samples and the two openings are hermetically closed with three gears each one, divided by two thermoresistents seals. This closing system is designed to achieve high vacuum condition (10^{-5}mbar) and is connected on one side to a vacuum tube system and a gas feeding, regulated with valves, and on the other side with an exaust gas exit device, allowing the forced gas flowing in the tube.

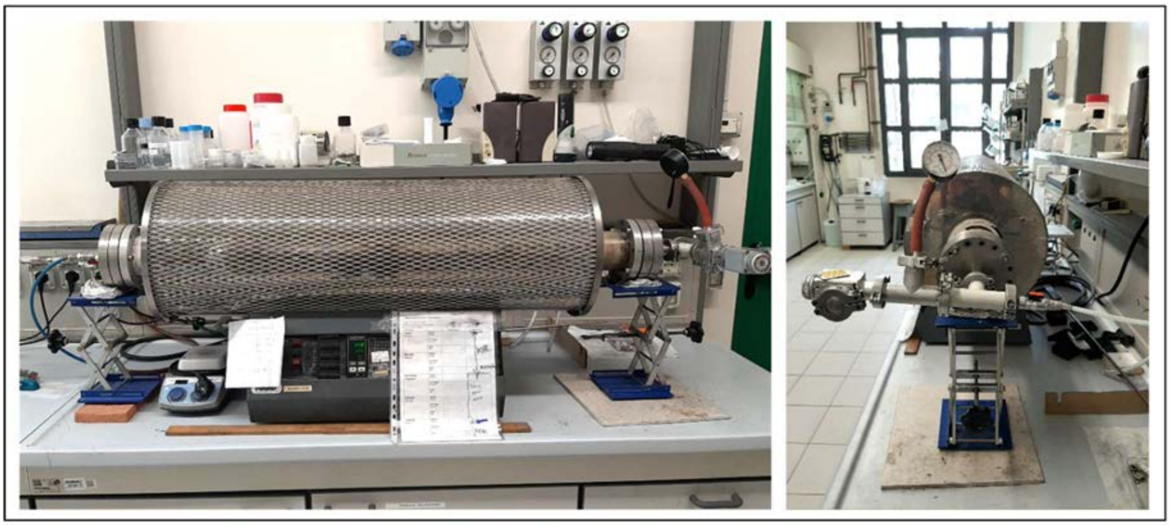

Figure 2.10 *Tersid tube furnace used for the pyrolysis treatment of the samples*

The samples are disposed on an allumina crucible, which has high thermal conductivity in order to have a uniform temperature all over the surface of the specimens, and set in the middle of the allumina tube (for a lenght of 20cm), where the temperature is more reliably uniform, as set on the heating program.

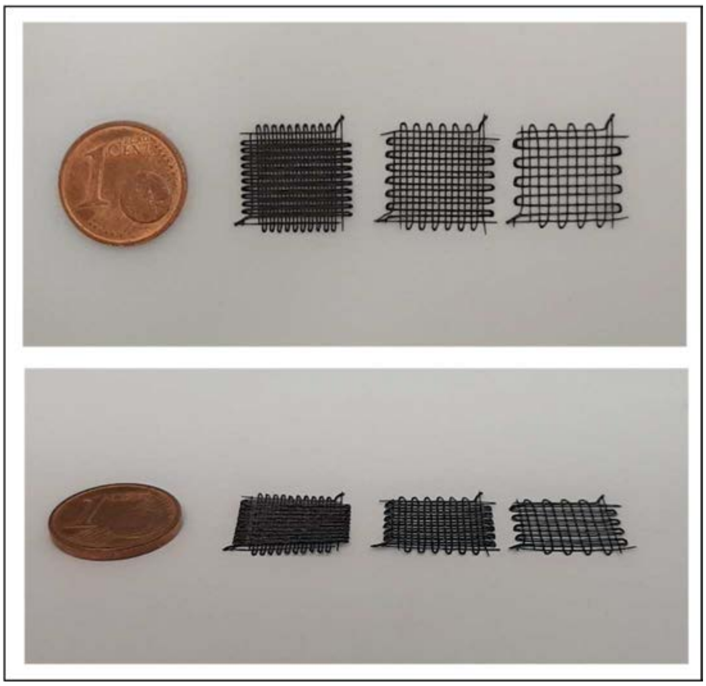

Figure 2.11 *Three different structures of electrodes produced*

The program is set as described above in the electronic system of the furnace and it keeps 21.7 hours to finish the treatment, plus the time to return at room temperature.

The material produced has to be characterized in order to understand whether the heat treatment conduced has proceed as expected.
For this reason several analysis are conduced, which are described subsequently.

2.3.1 Thermogravimetry Analysis - TGA

The first analysis conduced is a thermogravimentric analysis in which it is possible to monitor the weight of the material during the heat treatment. Its change is related to the chemical reaction and phase formation occuring over time, increasing the temperature.

Figure 2.12 *STA409 TGA analyser*

For this purpose a STA409 (Netzsch Geratebau GmbH, Selb, Germany) has been used, performing the analysis under nitrogen atmosphere, simulating the pyrolisis process in the tube furnace: starting from room temperature, heating directly up to 1000°C with a rate of 5°C/min. The crosslinking step at 300°C is not considered because the sample is powder and this experiment is not focused on determining the shape deformation and the structural collapse of the sample, but, on the other hand, it is intersting to analyse the reactions process which take place during the pyrolisis. The results for this reason could be slightly different from the real one, but in case they should be understimated, because the curing process occuring at 300°C should stabilize the structure, avoiding high weight losses. For this reasearch it is resonable to consider these approximations, just to have an idea of the thermal process.

The printed material, after overnight curing, is grindered to fine powder and placed in a 5mg allumina crugible, which is set on an analytical precision balance in the furnace device.

The three parameters for this analysis are:

- Time
- Temperature
- Weight of the sample

The temperature is set by the programmer controller over time, while the exit parameter collected is the weight of the sample.

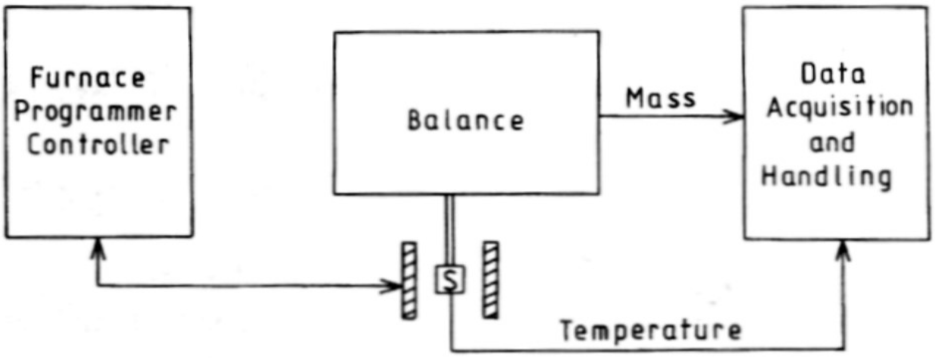

Figure 2.13 *Elements of a thermogravimetric device*
(www2.sci.u-szeged.hu)

In this way, it is possible to achieve a weight vs time/temperature plot, in which it is possible to understand when the weight changes occur.

The same plot can be derived over time/temperature, achieving a derivative thermogravimetry (DTG) plot where the peaks give the rate of mass lost. In this way the weight changes are more evident.

The first sample analyzed with TGA is pure H44, which gives the ceramic yield of this preceramic polymer:

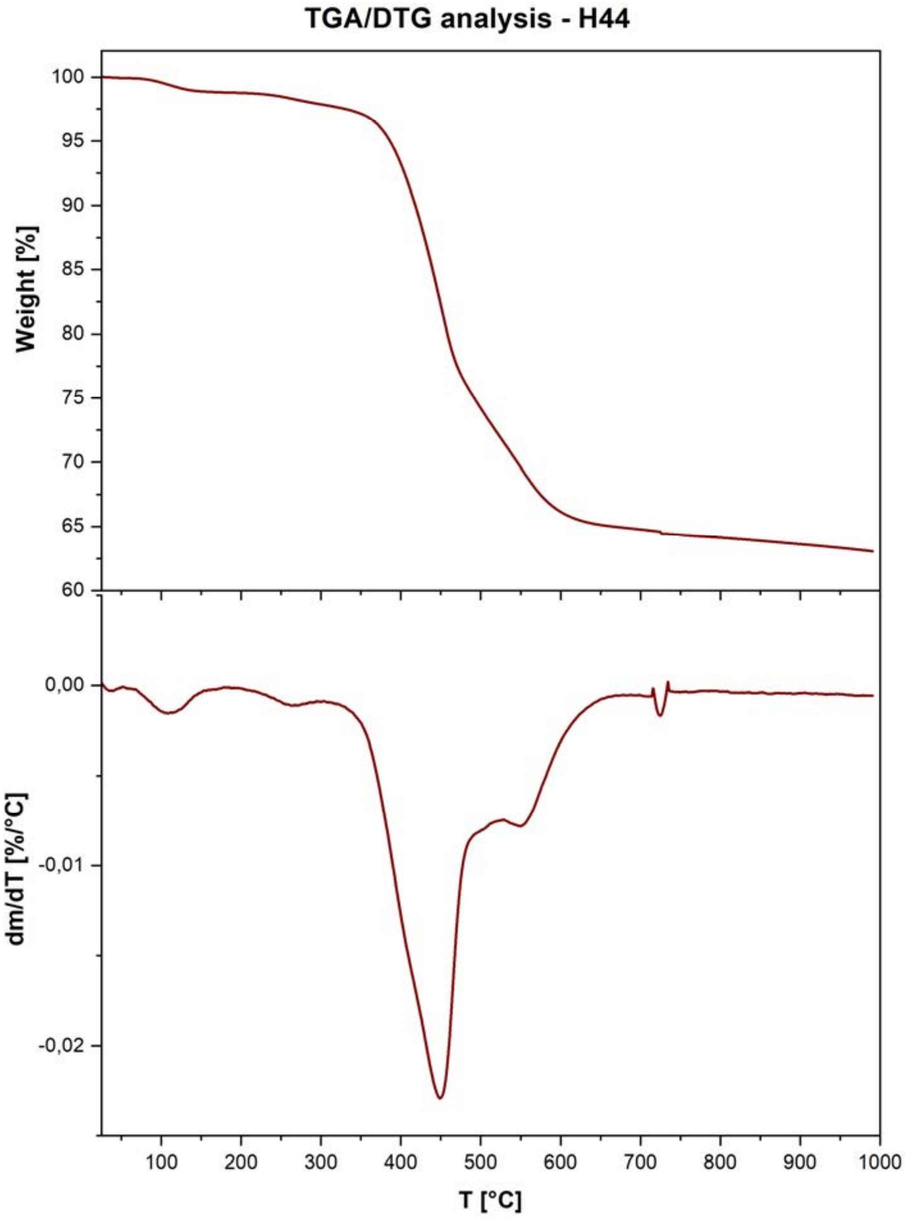

Figure 2.14 *TGA/DTG analysis of pure H44*

The ceramic yield of the H44 used is 63% which it is slightly lower to another preceramic polymer, which gives SiOC, such as Poly(methyl-siloxane) (MK) , that generally has values around 85%. The ceramic yield of these polymers is related to the molecular structure of the initial chains and this is also more evident with Poly(di-methyl siloxane) (PDMS) which has a linear structure and it has lower ceramic yield than the partial-ladder structures of silicons such as MK and H44.[23] The values obtained are also affected by the atmosphere condition, indeed using air instead of nitrogen the ceramic yield should decrease considerably because of the oxidation of carbon over 600°C.

The first weight loss up to 150°C is due to the remaining solvent traces and moisture present in the material. From that temperature to 300°C the small weight change is related to the crosslinking products such as water and alcohol, as well as to some possible sublimation of polymer entities[38].

The polymer-to-ceramic transformation is occurring starting from 400°C, where the mineralization process takes place, and it goes on till 900°C: in this range of temperature the cleavage and changing of the structure occurs as reported in literature, with the reorganization of several bonds such as the methyl and phenyl groups attached to the backbone of the H44 polymer ($Si-CH_3$, $Si-C_6H_5$), with partial decomposition, dehydrogenation and dehydrocarbonation.[23]

The weight loss at this step is around 32% of the total weight and this high loss is surely related to the large dimension of the aromatic groups present in the material.[38]

The first reactions are related to the Si-C cleavage: the dissociation energy of Si-C is different between methyl and phenyl groups and respectively 413kJ/mol and 473kJ/mol. These groups, spitted off the structure of the polymer react among them and with the Si-O backbone, in which not all the methyl and phenyl groups are already decomposed, producing hydrocarbons, graphite, hydrogens, and rearranging the structure, forming Si-C-Si bonds, as shown in the picture below, redistributing Si-C and Si-O bonds, and achieving the inorganic material as shown in the following picture. [37]

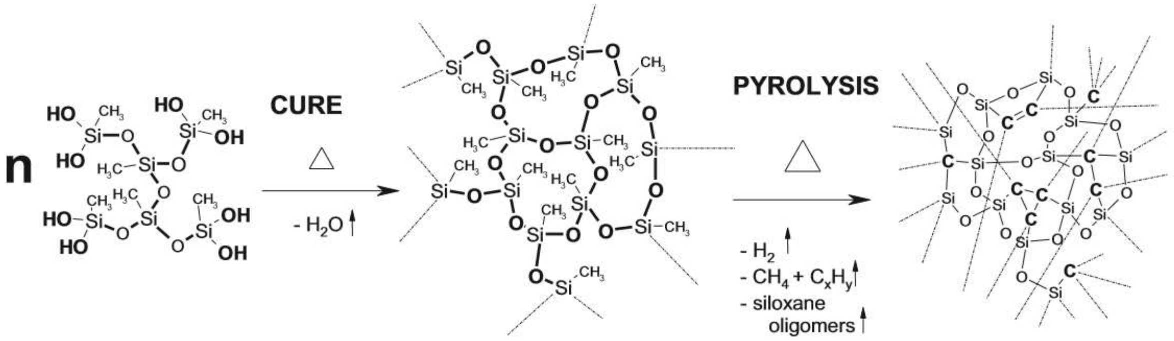

Figure 2.15 *microstructure of a PMS before and after the pyrolysis treatment, through the curing process*

As it can be seen from the DTG of H44, the pyrolysis process is divided into two steps, one with the peak at 450°C and the other one at 545°C: this is related to the different dissociation energy of $Si-CH_3$ and $Si-C_6H_5$, where the former occurs before the latter.

By the way, the weight loss is ascribed only to the carbon and hydrogen elements, while the silicon and oxygen are do not affect this parameters, indeed the Si-Si bonds are generated above 1500°C, as reported in previous works.[37]

Adding fillers to the preceramic polymer, the final ceramic yield expected is higher because of the carbon content added that should not react during the pyrolysis process.

In this research not all the compositions of ink prepared are investigated, but only some of them are taken into consideration

The materials with graphite filler show a trend as follows:

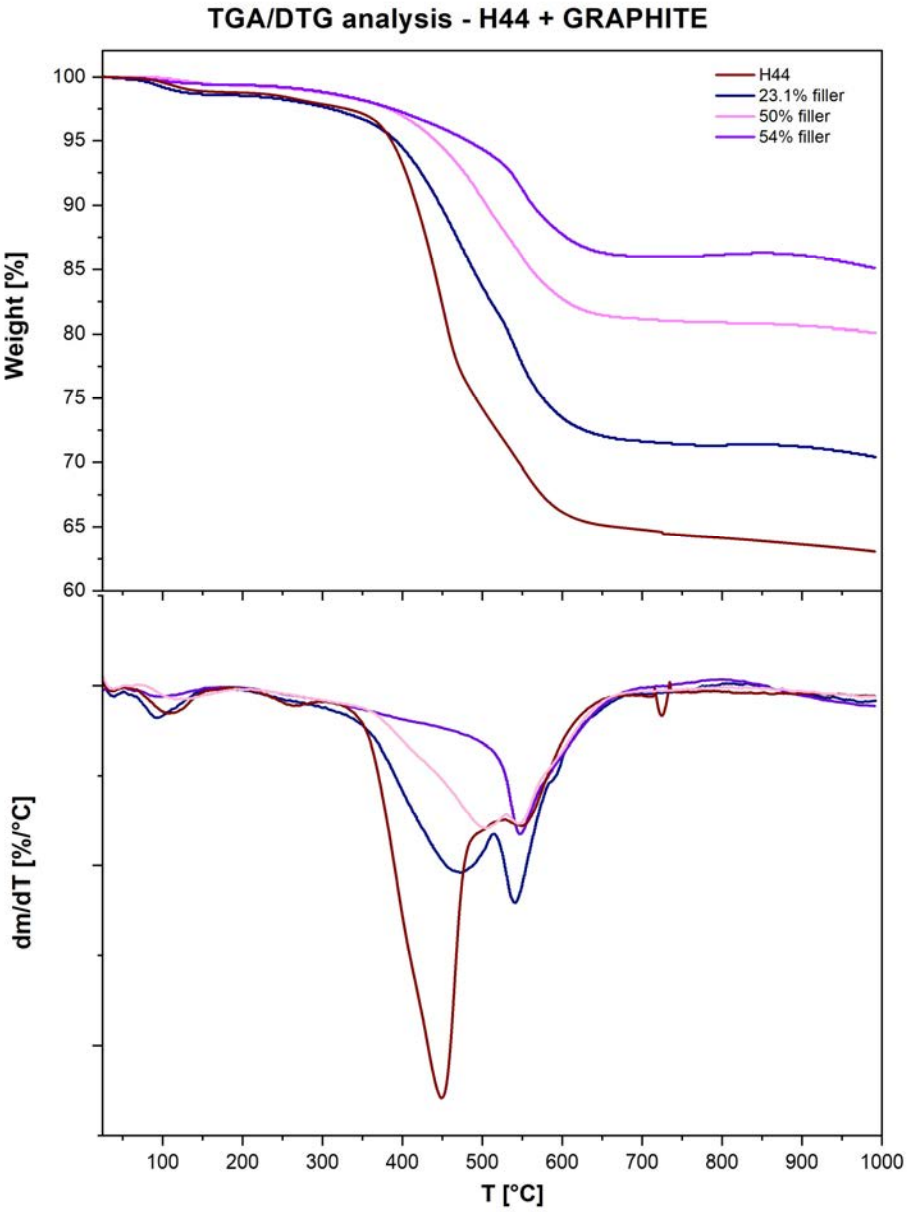

Figure 2.16 *TGA/DTG analysis of H44+graphite, different amount of filler*

As expected, the ceramic yield increases with the amount of filler and in particular:

Table 2.6 *Ceramic Yield of the preceramic polymer considering the graphite filler amount introduced in the composition*

	Initial Graphite content	Ceramic Yield	Theoretical Ceramic Yield
H44 + Graphite	23.1%	70.4%	71.5%
	50.0%	80.1%	81.5%
	54.5%	85.2%	83.2%

The results obtained differ less than 2% from the theoretical values calculated and for this reason the values could be considered acceptable. Ceramic yield beyond the theoretical values seems not acceptable but, it could be related to experimental error during the ink preparation, caused by an excessive addition of filler.

From the TGA curves it is possible to see how the initial process up to 350°C is similar among the different materials: during this range of temperature the siloxane condenses and the free water of the structure evaporates, moreover the curing compounds decay. The weight loss is less than 5%.
Moreover, adding graphite to the PDC, the pyrolysis process is delayed at a higher temperature and for certain compositions such as 23.1% and 50% of graphite, the process takes place in two phases, well defined in the DTG curve, while for higher amount of carbon powder (54.5%) the entire decomposition process is delayed at temperature around 545°C, where both the methyl and phenyl groups decompose. It is sure that they are eliminated from the backbone of the molecule because in the FTIR there are no more traces of those components after the heat treatment.
This means that by adding the graphite filler to the polymer material, the thermal stability of the final material increases because of the low interaction of the carbon filler during the thermal treatment and of the less amount of polymer in the total composition.
This suggests that the carbon added as filler could be considered unvaried during the pyrolysis process.

For the materials produced by blending the preceramic polymer with carbon fibers the TGA curves obtained are as follows:

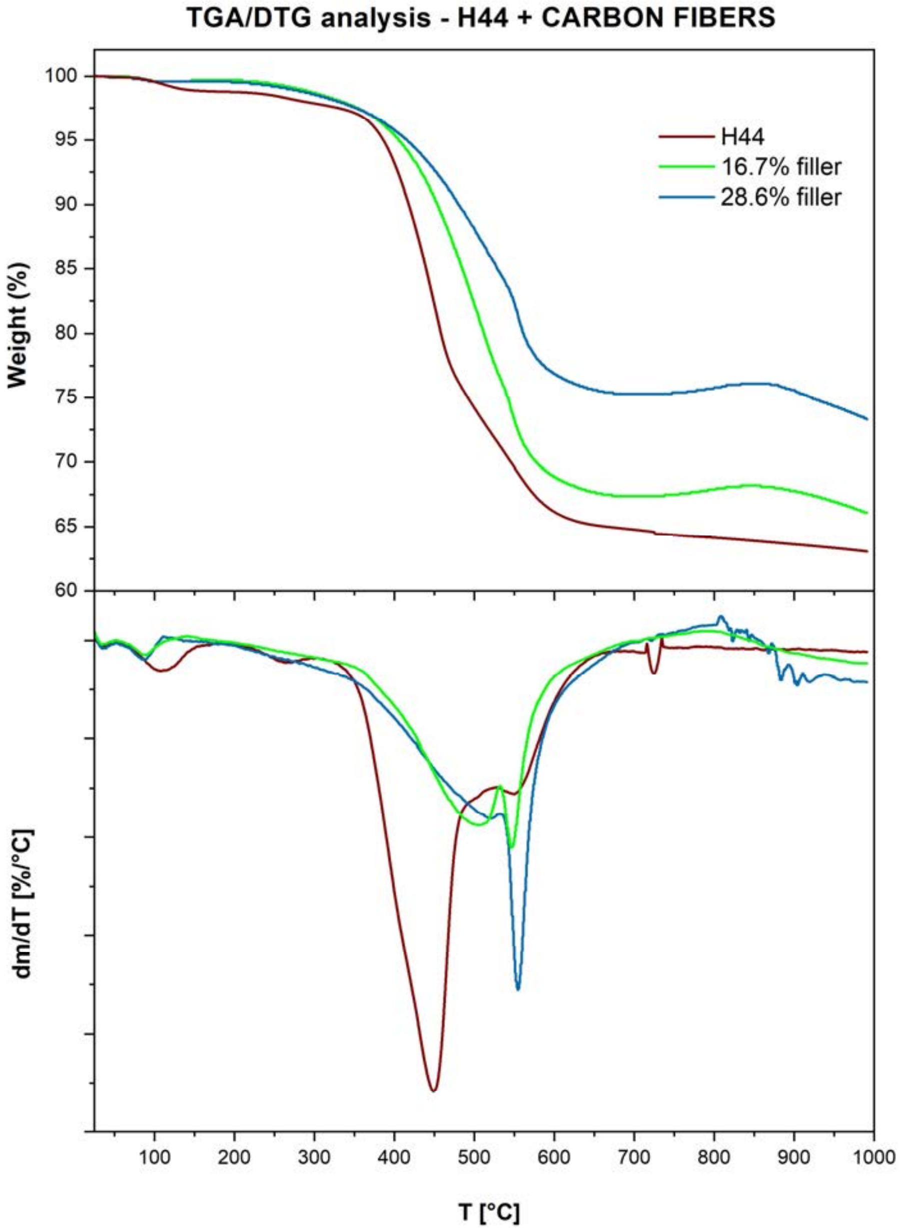

Figure 2.17 *TGA/DTG analysis of H44+carbon fibers, different amount of filler*

Table 2.7 *Ceramic Yield of the preceramic polymer considering the carbon fiber filler amount introduced in the composition*

	Initial C.Fibers content	**Ceramic Yield**	**Theoretical Ceramic Yield**
H44 + C.Fibers	16.7%	66.1%	69.16%
	28.6%	73.4%	73.5%

The results achieved in terms of ceramic yield are still acceptable because the deviation is less than 0.8% of the theoretical values calculated.

Also in this case, by adding the filler to the polymer, the heat treatment process remains unvaried compared to the pure H44 and the pyrolysis process is delayed at 550°C, approximately the same verified with the graphite powder, stabilizing the thermal treatment.

In this case, right from a low amount of filler such as 23.1%, the polymer-to-ceramic transformation occurs wholly at the temperature of 550°C.

In any case the amount of carbon fibers at the final process could be approximated to the initial theoretical quantity.

The same consideration could be defined for the material produced by mixing H44 with carbon nanoplatelets25:

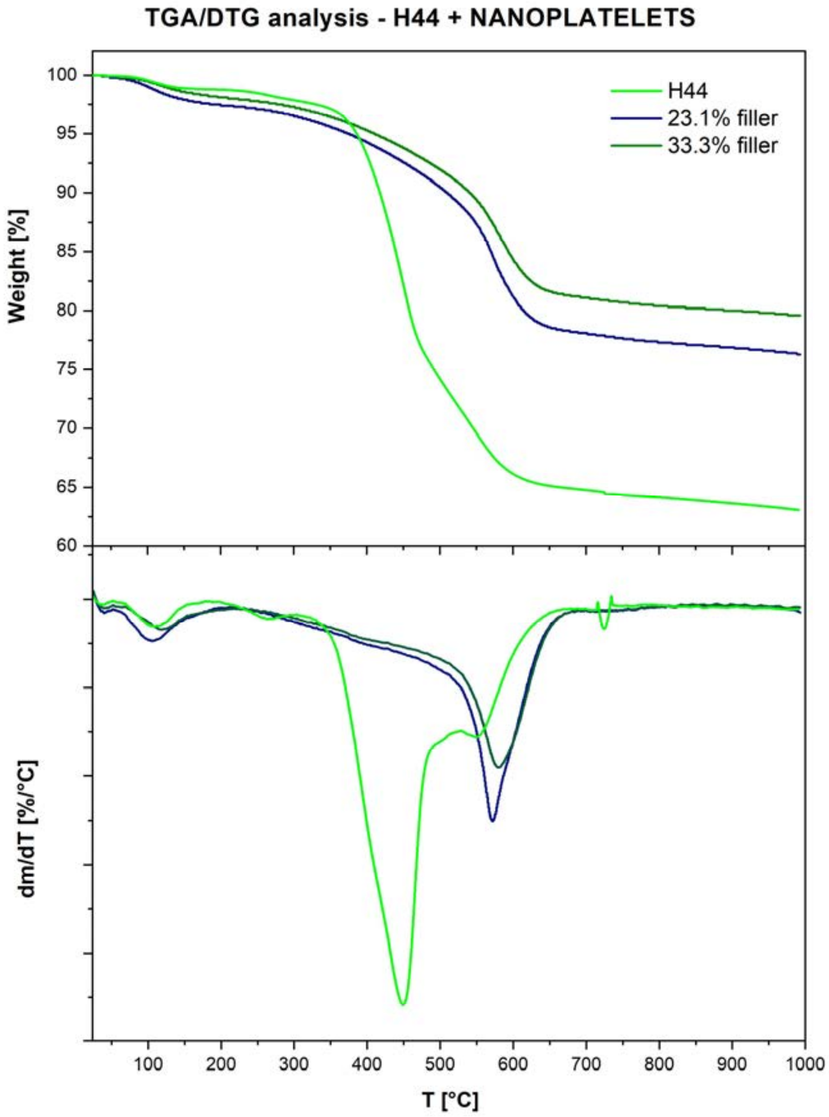

Figure 2.18 *TGA/DTG analysis of H44+carbon nanoplatelets, different amount of filler*

Table 2.8 *Ceramic Yield of the preceramic polymer considering the carbon nanoplatelets filler amount introduced in the composition*

	Initial C.Fibers content	Ceramic Yield	Theoretical Ceramic Yield
H44 + C.Nano25	23.1%	76.3%	72.3%
	33.3%	79.6%	75.2%

Also in this case, the results of ceramic yield are higher than expected and the trend of the TGA is similar to the materials produced with carbon graphite and carbon fibers as fillers.
In any case the materials expected after the pyrolysis process should have a complex network of amorphous SiO_2, Si-O-C structure and carbon uniformly dispersed, due to the presence of the filler and to the turbostratic carbon formed.[24]

In order to verify the presence of the graphitic carbon, combined between the cluster deriving from the polymer-to-ceramic conversion and the filler added, after the heat treatment, an XRD analysis is conduced. This also guarantees that the carbon does not oxidize during the pyrolysis, maintaining high electrical conductivity on the 3D printed electrodes.

2.3.2 X-Ray Diffraction - XRD analysis

This analysis is not generally interesting if polymers and glasses are investigated because of their amorphous structure which would not generate any peak on a X-Ray powder diffraction analysis, which is a useful technique to investigate the phase distribution in a crystalline material.
The SiOC material produced starting from H44 with the thermal treatment, reported above, is not expected to have any crystalline phase, except the carbon phase, due to the crystalline filler added to the polymer at the beginning, and in particular graphite and nanoparticles25.
From the literature, it is well known that only for thermal treatment above 1300°C other crystalline phases can be formed,[39] such as SiO_2 and SiC. For this reason, it is interesting to verify the prerequisites, otherwise any silica crystal in the structure would decrease the electrical conductivity of the SiOC, because of its intrinsic property, affecting the final goal of the research. Also silicon-carbide has to be avoided in the structure for the same reason.
Silicon-oxycarbide is preferred, instead of silica, also because of other properties, for example because of its higher glass transition, hardness and elastic modulus, as shown in the table 2.9.[39]

Table 2.9 *Properties of the Silicon Oxycarbide compared to Silica*

Properties	**SiOC**	**SiO_2**
Density (g/cm^3)	2.35	2.20
Thermal expansion coefficient (10^{-6}/K)	3.14	0.5
Vickers Hardness (GPa)	7.0-8.6	6.0-7.0
Elastic Modulus (GPa)	97.9	70
Glass transition temperature (°C)	1350	1190
Refractive Index	1.58	1.46
Dielectric constant	4.4	4
Electric Conductivity (/Ω·cm)	$4 \cdot 10^{-13}$	$\approx 10^{22}$

The base material, H44, is analysed before and after the heat treatment of pyrolysis at 1000°C.

In order to conduce the experiment, the material is prepared in powder, ground in a crucible, and disposed in a silica XRD holder, conveniently pressed and levelled.

The sample holder is than set on a Bruker D8 Advance Eco and the program is set to analyse the diffraction of the material between a range of 2θ = 10-80 with a scan speed of 1 step/sec and increments of 0.01, in "locked couple" scanning mode, in which the detector moves coupled to the X-ray source. The plots are then analysed with Jade XRD software in which it is possible to associate the peaks to know patterns of crystalline materials.

Figure 2.19 *Bruker D8 Advance Eco – Xray Powder Diffractometer*

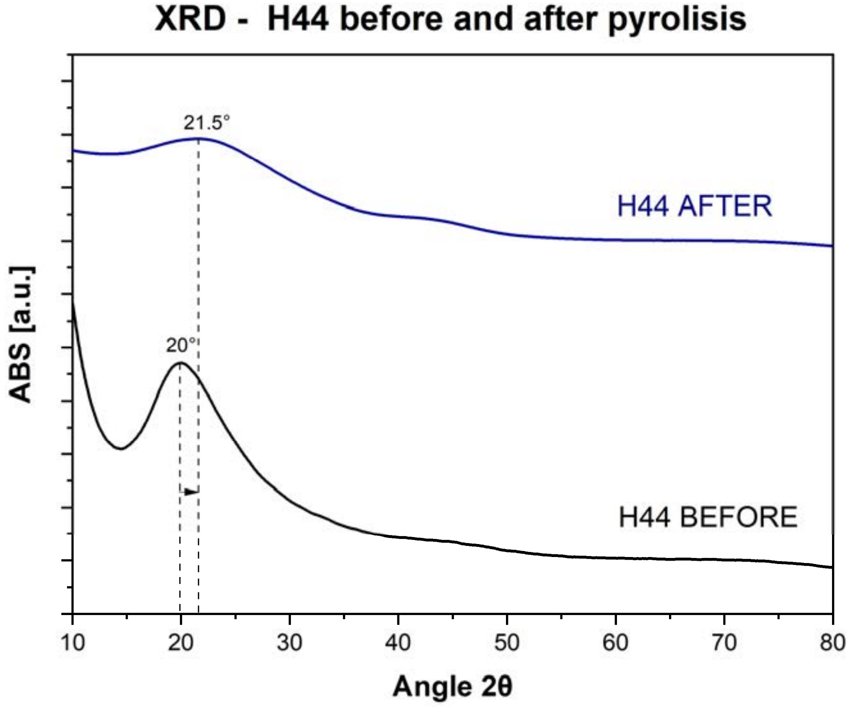

Figure 2.20 *XRD results for pure H44 before and after the pyrolysis*

As shown in the diagram, the raw material (H44) has a broad scattering peak at 20°C due the diffraction of the Si-O primary bonding in the amorphous structure of the polymer (SiO_2).

The initial decrease of intensity at low angles ($2\theta < 14°$) is attributed to the small, but sharp, peak that should be revealed around 8.78°, related to the SiO_2, but generally disposed at lower angles compared to preceramic polymers such as MK. That is due to the presence of phenyl groups, which increase the distance of the planes owing to their high obstruction.[38]

The same peak is found after the heat treatment, with a slight shift in the higher angles (21.5°C), with a lower intensity, proving a recombination of the bonds in the structure with the formation of free carbon, detached from the Si-O-C lattice, besides the decrease of the interplanar distance and an increase of the structural disorder.

The hint of peak at low angles disappears, as described in the literature.[38]

No other changes at higher angles are noticed.

Another interesting analysis has been conduced on the carbon sources in order to understand the intrinsic behaviour of the raw materials used, then evaluating the results on the final 3D printed material.

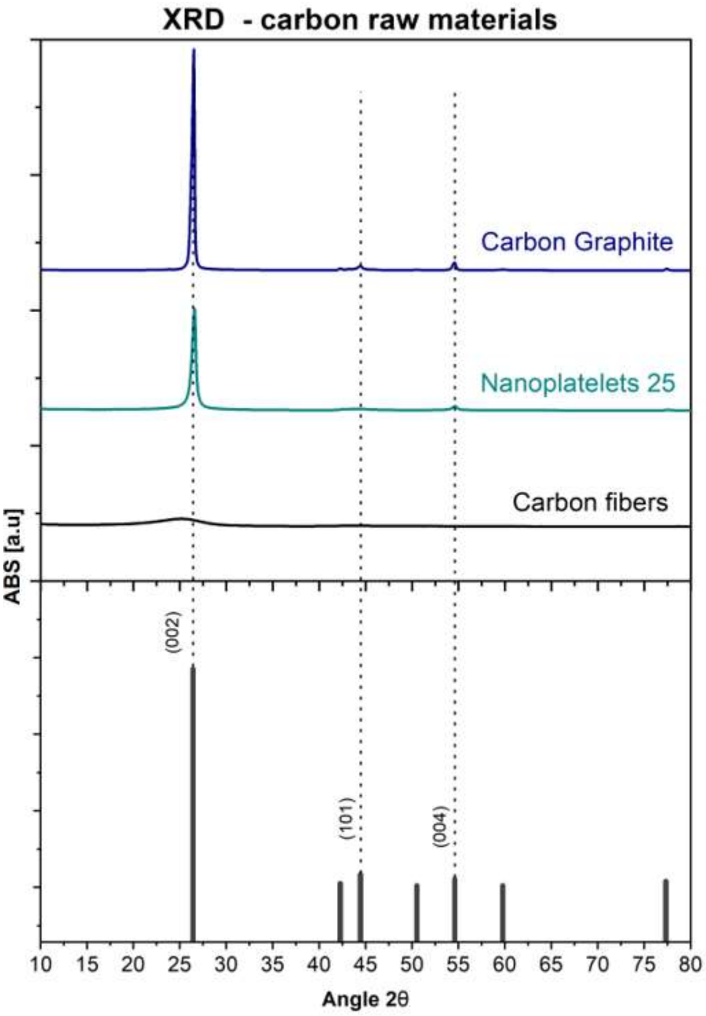

Figure 2.21 *XRD results of the carbon raw material used compared with graphite pattern (bottom)*

From the XRD plot of the three carbon sources, it is possible to understand that not all of them are crystalline and in particular the carbon fibers are showing an amorphous behaviour, as expected, due to the lack of narrow peaks as the others.

On the other hand, the nanoplatelets25 and the carbon graphite fillers show three distinct peaks at 26.4°, 44.4° and 54.5° which are the most preponderant peaks, characteristic of the graphite-2H pattern, which belongs to the hexagonal crystal system.

The nanoplatelets show a less intensive peak, compared to graphite powder, at 2θ=26° and this is ascribable to the nature of the filler: it is not uncommon to find less intensive and broader peaks with the equivalent nanosized material and this is well explainable with the Scherrer equation, where the Full Width at Half Maximum (FWHM) of the peak in inversely proportional to the size of the particles:

$$D = \frac{k \cdot \lambda}{d \cdot cos\theta} \tag{2.3}$$

Where *k* is the shape constant, λ is the wavelength, *d* is the FWHM and θ is the angle.

Anyway the determination of the dimension of the crystals is out of context for this study because it is already known from the datasheet.

Here are the XRD results of the pyrolyzed SiOC material, loaded with graphite in different quantities:

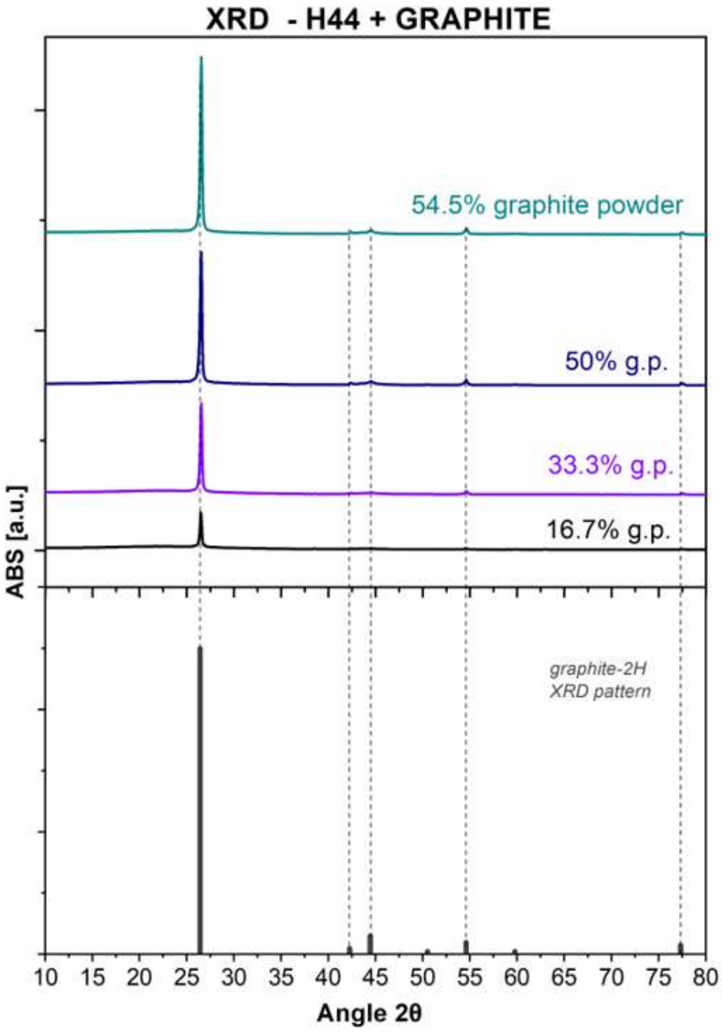

Figure 2.22 *XRD results for H44+graphite after pyrolysis with different amount of filler*

The trend of the curves is similar to the carbon raw material because the only crystalline phase is that, as expected. From the plot it is possible to see how the intensity of the main peak increases proportionally with the amount of filler added, due to the abundant quantity of this phase in the final material.

As expected, there are no peaks related to βSiC and SiO_2 crystalline, typical at higher pyrolysis temperatures, which have a pattern as follows:

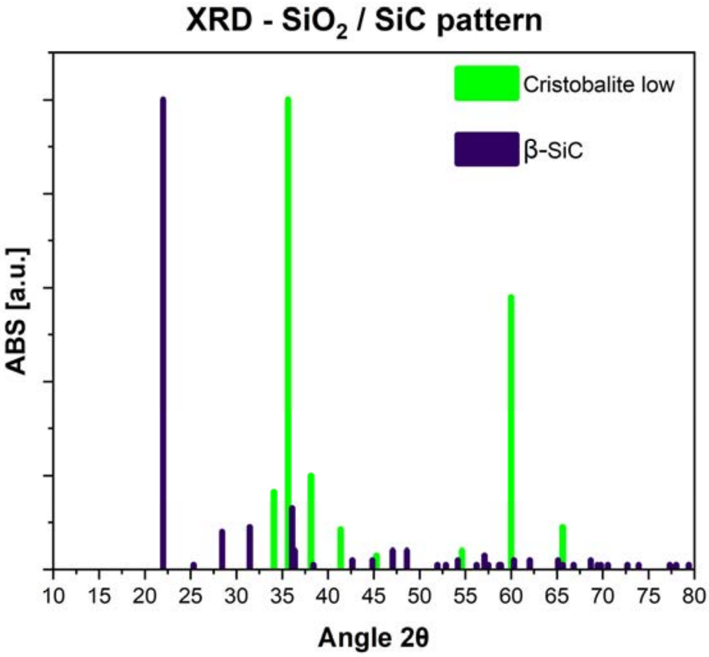

Figure 2.23 *Cristobalite (SiO_2) and βSiC XRD pattern achievable for higher temperature of pyrolysis*

The same analysis is conduced for the materials containing carbon fibers:

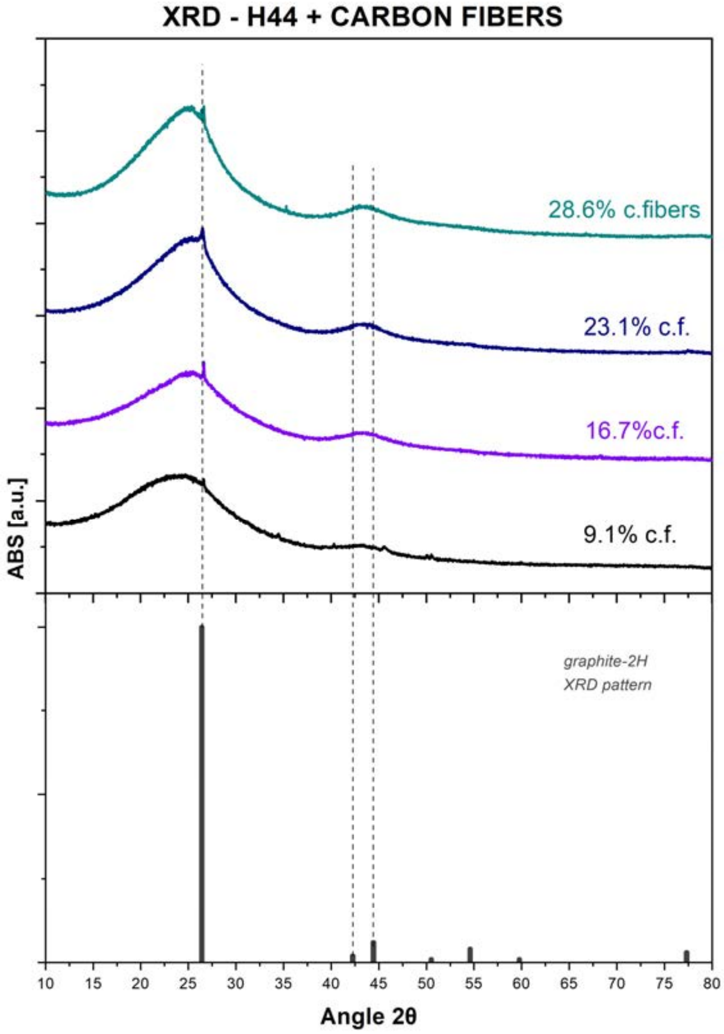

Figure 2.24 *XRD results for H44+carbon fibers after pyrolysis with different amount of filler*

In this case the peaks are similar to the SiOC plot obtained after the pyrolysis of H44, reported in fig.2.20, which proves the amorphous behaviour of the final material. This is due to the non-crystallinity of the carbon fibers used as filler, which do not affect the XRD analysis, if not for a slight hint of the peaks in conformity to the most important points of the graphite-2H pattern, respectively at 26°, 42.2° and 44.4°.

Also in this case, even if the peaks are broad, they seem to increase the intensity by adding more filler.

On the other hand, for the SiOC + carbon nanoplatelets the plot is similar to the SiOC + carbon graphite:

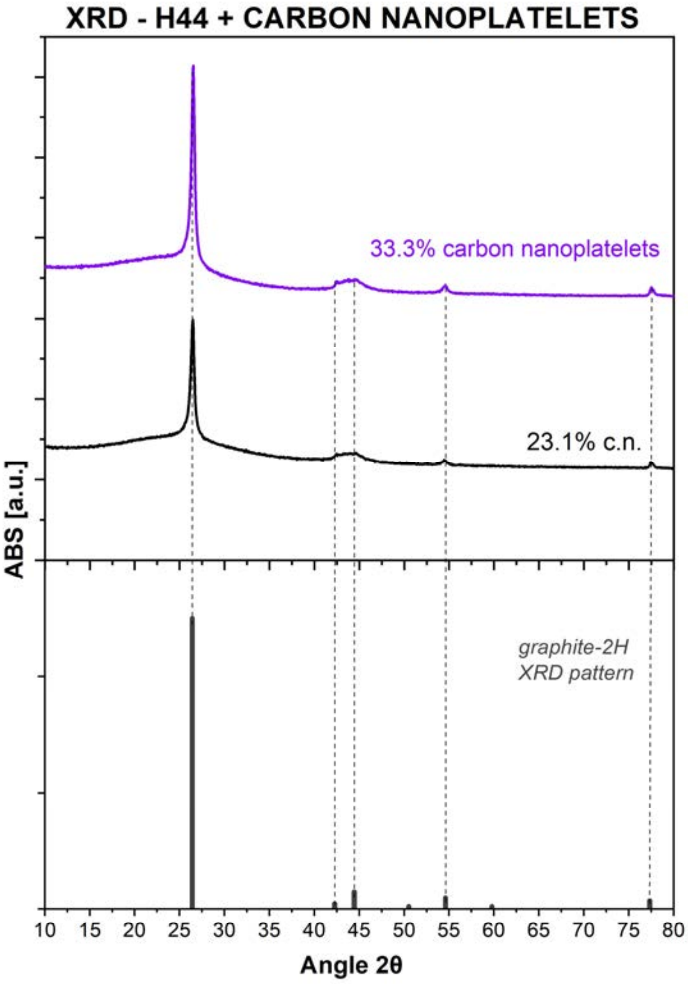

Figure 2.25 *XRD results for H44+carbon nanoplatelets after pyrolysis with different amount of filler*

All the peaks found are related to the graphite-2H pattern and also in this case, as in the others, the intensity of the main peak increases proportionally with the amount of filler added due to the major preponderance of this phase on the final material.

The amorphous SiO_2 is still attributed to the broad peak allocated from 15° to 30°, but its intensity is concealed by the greater crystalline peak at 26°.

In order to have an overview of the bonds created during the polymer-to-ceramic conversion throughout the heat treatment process and verify what already investigated with the thermogravimetric analysis, Fourier Transform Infrared spectroscopy (FTIR) and Raman Spectroscopy (RMN) are considered as the suitable analysis to conduce for this purpose.

The two experiments are both based on the detection of vibration of the bonds, associated to the energy transition of the molecules caused by the irradiation induced, but the operational modes of both analysis are complementary: FTIR detects the changing on the dipole moment between the atoms, while RMN is sensitive to the polarizability.

It's assumed that each molecule has its vibrational modes depending on the orientation of atoms and bonds, bonds order, mass of atoms and hydrogen bonds. The most important vibrational modes are: stretching (symmetric/asymmetric), bending, rocking and scissoring.

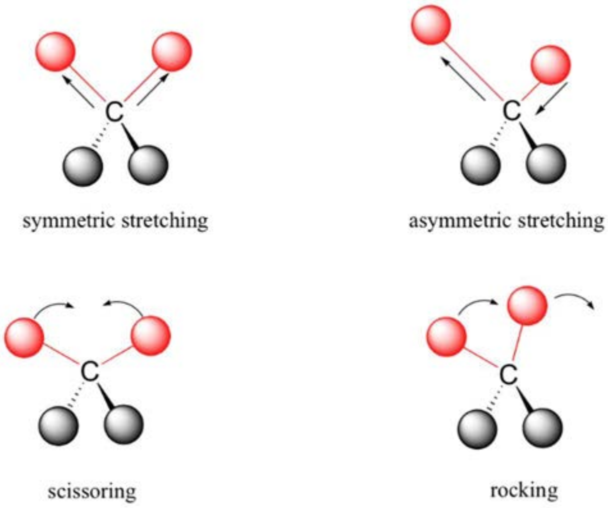

Figure 2.26 *types of molecular vibrations illustrated (https://chem.libretexts.org)*

Every molecule absorbs a particular frequency of the irradiation which implicates the vibrational mode, based on the constant force (*k*) and the reduced mass (*m*), as the following formula shows:

$$\nu = \frac{1}{2\pi}\sqrt{\frac{k}{m}} \tag{2.4}$$

where,

$$m = \frac{m_1 \cdot m_2}{m_1 + m_2} \tag{2.5}$$

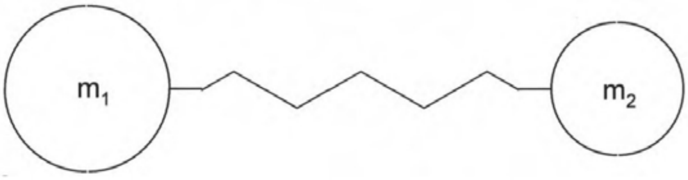

Figure 2.27 *Spring model for a diatomic molecule (http://web.uni-plovdiv.bg)*

Moreover, based on the exclusion rule, when a molecule has a centre of inversion no vibrational mode can be both Infrared and Raman active and, in particular, when a molecule is Infrared active for a particular normal mode surely it is not Raman active, but when it is not Infrared active, because the dipole moment is null, it should not necessarily be Raman active, but it might be. In this way it is possible to find different results between the two techniques and for this reason both are considered in this research.

2.3.3 Fourier Transform Infrared Spectroscopy - FTIR

In order to have a FTIR active molecule, it must show a change in the electric dipole moment when irradiated with an infrared light. In this way the plot, resulting from this analysis, shows only the absorbance/transmittance related to the polar and asymmetric vibration.
Generally FTIR is well performed in presence of organic materials, so it is particularly dedicated to polymers, rubbers and resins, where the covalent bonds are detected, even if not all the molecular structure can be determined, because of the possible C-H and C-C noise.
In this case it is interesting to understand if all the aromatic groups are sublimated during the pyrolysis process, achieving a completely inorganic material.

The experiment is conduced with a JASCO FT/IR-4200 spectrometer, set with a disk sample older in order to analyse the material in absorbance. The analysis is set, for all the samples, with an IR inspection between 450-5000cm^{-1} and a resolution of 4cm^{-1} in 64-scan acquisition mode.

Figure 2.28 *Jasco FT/IR 4200 spectrometer (left) and sample holder for KBr disks.*

The sample is prepared by mixing a small amount of the powder material to analyse (1mg approximately) with potassium bromide (KBr) dry powder (1:5 proportion approximately) with high purity. This salt is chosen for its high transmittance in the IR range (λ=700nm-1mm), not affecting the absorbing results.

The mixture is than arranged on the polished surface of a pellet (D), positioned in a bored cylinder (B/C), as shown in fig.2.29 (right).

The upper pellet (D) is than set in order to create a hermetic powder bed. Then, a plunger (A) is placed on it and the die is inserted in a hydraulic press.

The press is maintained at 5tons for 1min subsequently for two times.

The die is then opened, and the disk is ready to be analysed.

During this procedure it is important to mix the proper amount of salt with the active material in order to produce a fine disk, otherwise the signal deriving from the experiment would be saturated.

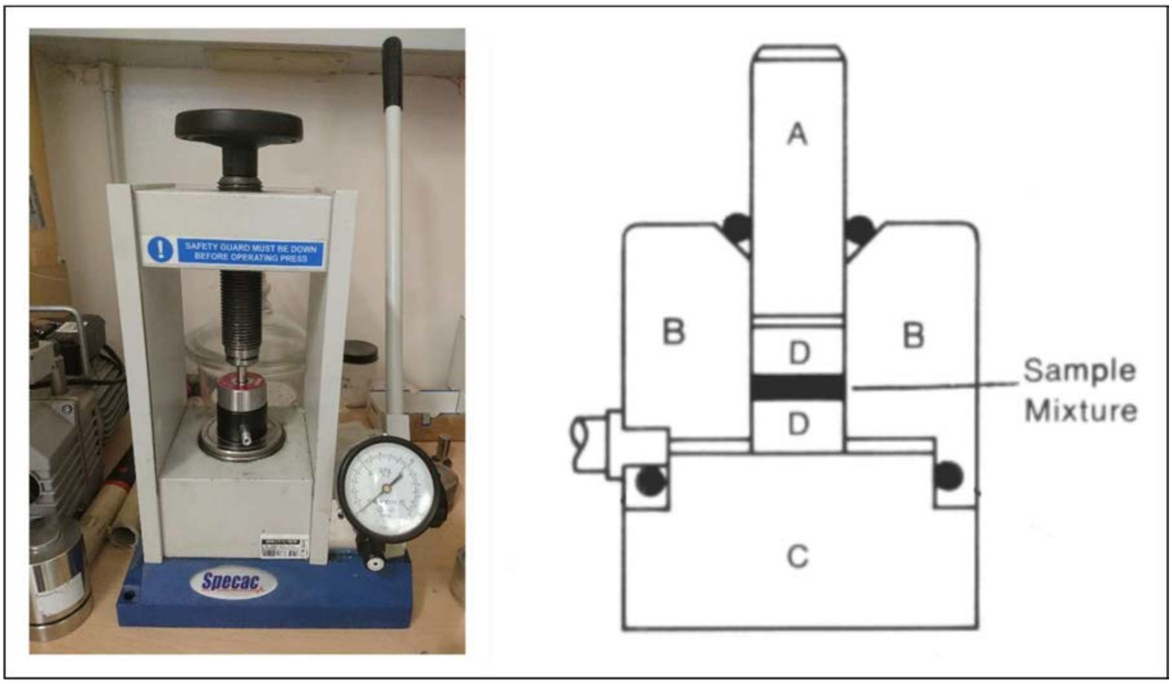

Figure 2.29 *Hydraulic press used for preparing the KBr disks (left) ; schematic KBr die (right) (https://depts.washington.edu)*

First, it is important to understand, as mentioned before with XRD, the developing of the raw material used. For this purpose, the FTIR of pure H44 is investigated, followed by the material printed, containing crosslinker and solvent (without any filler), and then pyrolyzed.
In this way it is possible to dynamically analyse the chemical structure of the material after its forming process and the heat treatment.

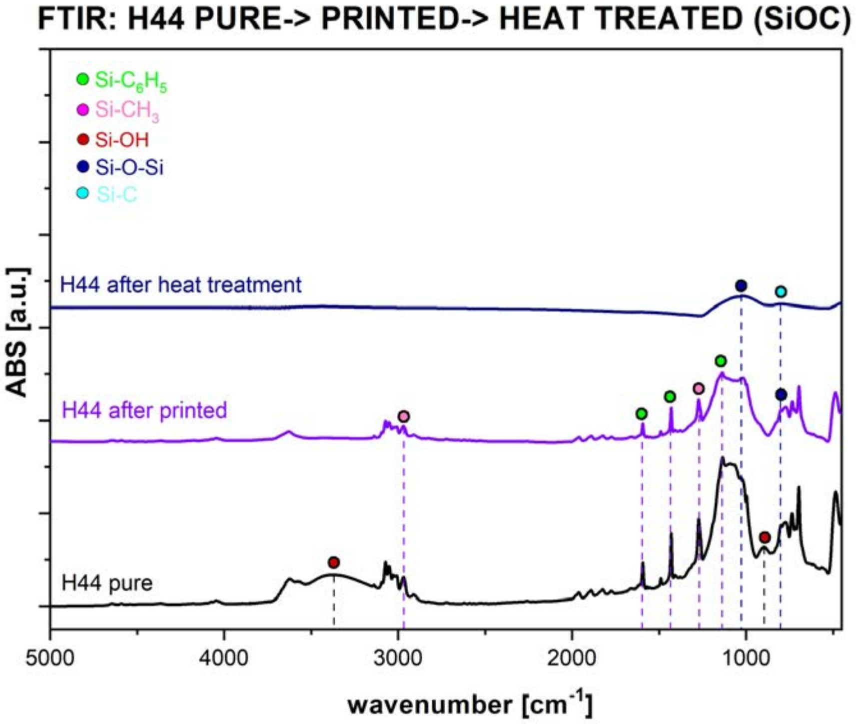

Figure 2.30 *FTIR results for H44 before printing, after printed; after pyrolyzed.*

The plot above shows the absorbance of the pure H44; the plot in the middle points out the absorbance of H44 with the addition of triethylamine (catalyst) and isopropanol (solvent); the plot on the top represents the absorbance of the material after the heat treatment.
As shown, the silicon - organic compounds bonds, methyl (CH_3) and phenyl (C_6H_5), respectively at 1273cm^{-1} /2978cm^{-1} and 1134cm^{-1}(bending)/1595-1431cm^{-1}(stretching), besides the Si-OH bond, which has a narrow peak at 900cm^{-1} and a broad one around 3400cm^{-1} (due to the absorbed moisture), both disappear after the heat treatment at 1000°C (2hours), proving the pyrolytic transformation in a completely inorganic material, as expected. [35,40,41]
The Si-OH bond seems it has even vanished after the 3D-printing of the material, probably for the addition of isopropanol and catalyst with a primary recombination of the bonds, especially with the methyl groups of the triethylamine, producing methane (gas), or bounding with oxygen evaporating as aqueous vapour.

In this way the Si-O-Si bonds are favourite and this is proved for the persistent peaks at 1025cm^{-1} (stretching) and 802cm^{-1} (bending) related to this bond. After the heat treatment the Si-O peak is shifted to 1025cm^{-1}, while at 790cm^{-1} it is visible the Si-C bond of the Si-O-C ladder. [40]

The relevant peaks of Si-O-Si and Si-C_6H_5 respectively at 1020cm^{-1} and 1250cm^{-1} could cover a peak at 1120cm^{-1} related to the methyl group (Si-CH_3).[42]

The intensity of the peaks is not related to quantitative considerations, because the three analysis are conduced using different amount of active material. For this reason, the FTIR gives qualitative results, which are interesting for this study.

Moreover, it is possible to observe that the rule of the catalyst is exclusively to bind the molecule structures without acting as vulcanizer, disappearing from the material after the heat treatment, avoiding the presence of the aminic bonds (C-N, that would be positioned at 1290cm^{-1}, or Si-N).

Here is the FTIR plot of the material, before and after pyrolysis, with two different amounts of graphite:

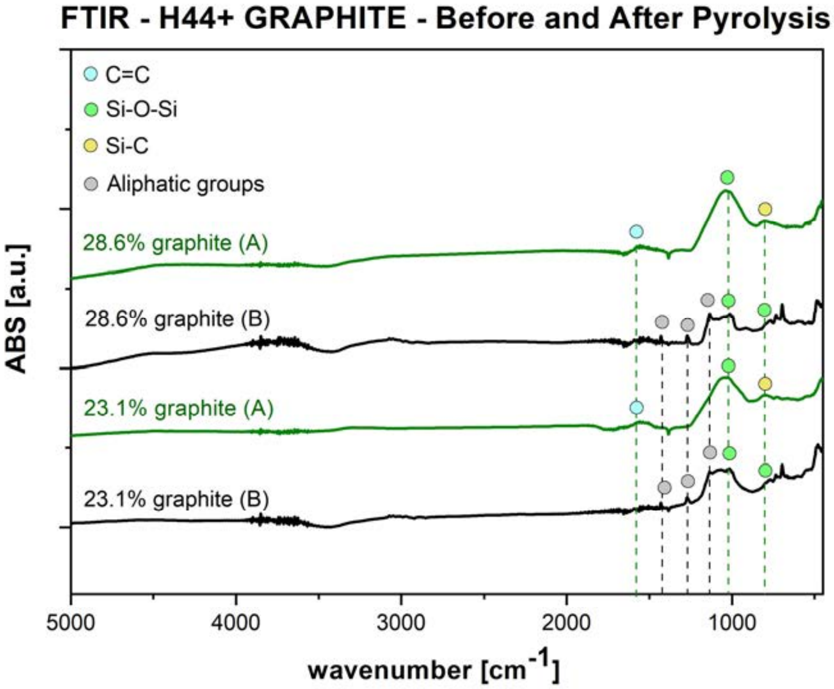

Figure 2.31 *FTIR results for H44+ graphite before and after pyrolysis, different amount of filler*

The main differences found in the H44 development are here confirmed and in particular the aliphatic groups (CH_3 and C_6H_5) are dissolved after the pyrolysis treatment, while the Si-O-Si bond, which has two peaks before the heat treatment, is then shift all in one peak at 1025cm^{-1}, allowing the Si-C peak to form at 800cm^{-1}. In this plot it is also possible to see a minor peak, covered by the moisture absorption noise, due to the use of a KBr disk, at 1580cm^{-1} which is related to the double bond C=C generated in the carbon phase, as reported in the following picture.[28]

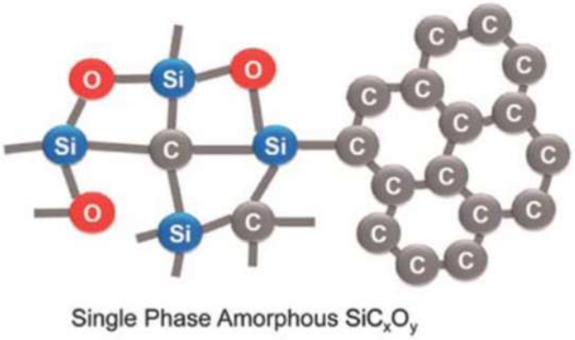

Figure 2.32 *Microstructure of the derived ceramic after the pyrolysis treatment at 1100°C in inert atmosphere*[28]

The same trend is verified in the following plot, where a FTIR of the pyrolyzed material with different amount of graphite is reported:

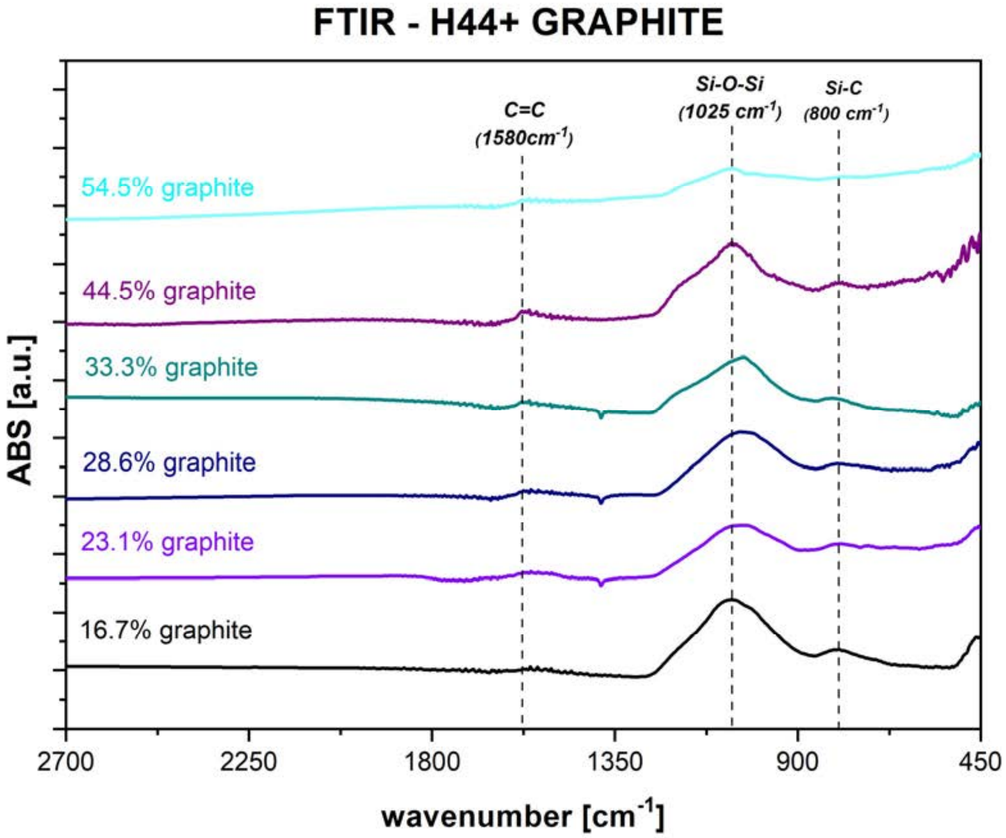

Figure 2.33 *FTIR results of H44 + graphite, different amount of filler*

As expected, in any case there is a high peak related to the Si-O-Si bond at 1025cm^{-1}, besides a shorter peak for Si-C at 800cm^{-1} due to the amorphous structure.

Again, at 1580cm^{-1} it is possible to notice the formation of a little peak related to the double bond C=C related to the graphite powder added.[43] This is in particular evident at higher amount of filler.

The same results are verified also for the materials produced blending the preceramic polymer with carbon fibers and with carbon nanoplatelets as reported in the following two plots.

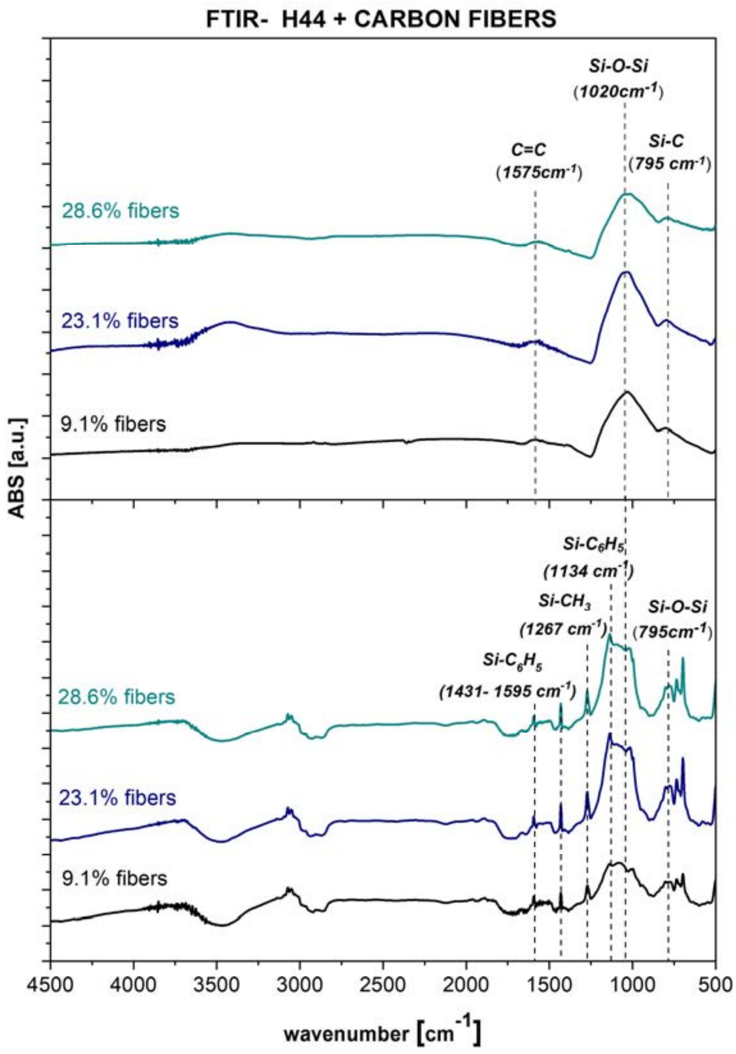

Figure 2.34 *FTIR of H44+carbon fibers before (below) and after (top) the pyrolysis*

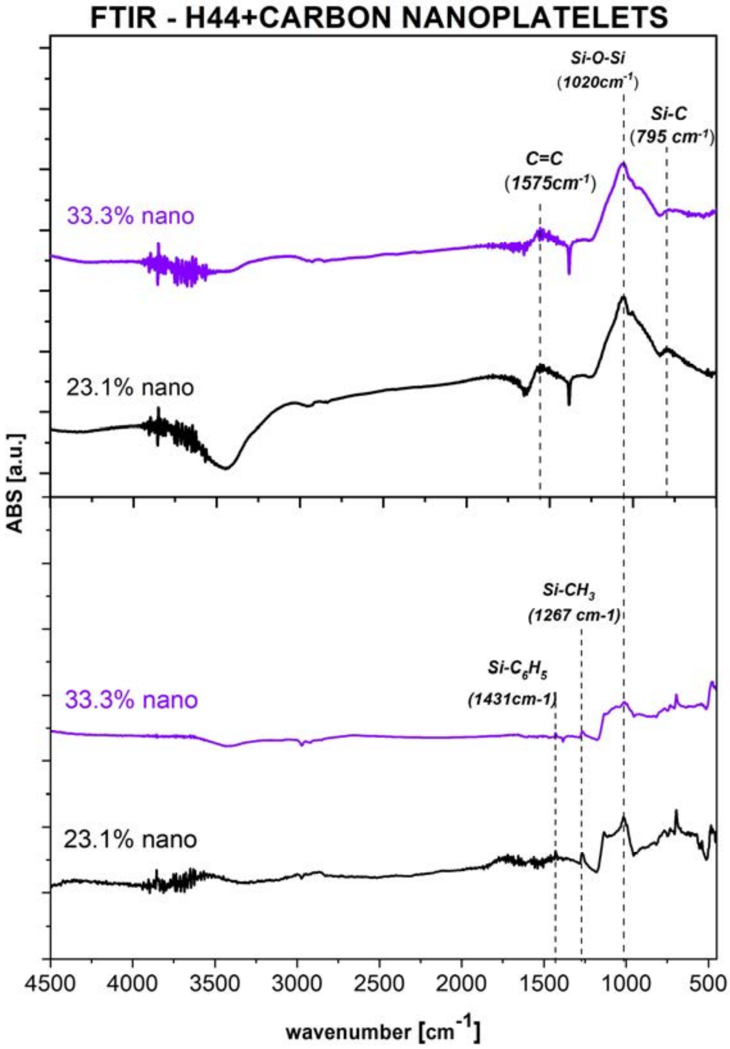

Figure 2.35 *FTIR of H44+carbon nanoplatelets before (below) and after (top) the pyrolysis*

The unvaried attitude of the materials with the three filler is suggesting that the final chemical bonds of the microstructure are the same. No aliphatic groups remain proving the complete transformation of the polymer into an inorganic glass.

The phases present are mainly two as expected: SiOC amorphous phase (separated in SiO_2 and SiOC in base of the quantity of carbon) in which is dispersed the carbon filler and the graphitic carbon (sp_2), gained from the pyrolysis of the preceramic polymer, of varying degree of order, as shown in the following figure. For a high amount of carbon, as in this case, it is possible to form a continuous phase of the C-rich SiOC which is disposed over the carbon graphite clusters.[28]

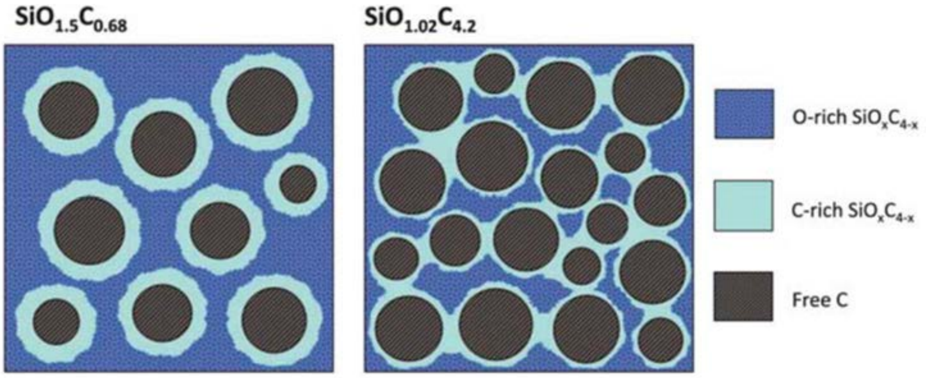

Figure 2.36 *2D structure model of low (left) and high (right) carbon containing SiOC, pyrolyzed at 1100°C in inert atmosphere*

2.3.4 Raman Spectroscopy (RMN)

As reported above, Raman Spectroscopy is in general more addicted for studying inorganic materials. This test is generally faster than FTIR because no sample preparation is needed and there are no limitations regard the thickness, dilution and present of moisture, which are producing the signal saturation in FTIR.

Moreover, because of the high sensitivity of the Raman Spectroscopy to the homo-nuclear molecular bond, such as C=C and C-C, which are polarized during the vibration caused by the laser excitation, is here reported an analysis on the three final materials pyrolyzed, in order to analyse the degree of ordering of the carbon phase.

Raman Analysis is conduced using a LabRAM ARAMIS – Horiba Jobin Yvon spectrometer, equipped with a Helium Neon Laser, with a wavelength λ= 633nm, using a 10x optic and a red filter to reduce the intensity of the signal.

The samples used are in powder for all the SiOC + filler, while the pure SiOC is tested from the 3D-printed sample directly.

The specimens are simply attached to a sample holder and no other preparations are needed.

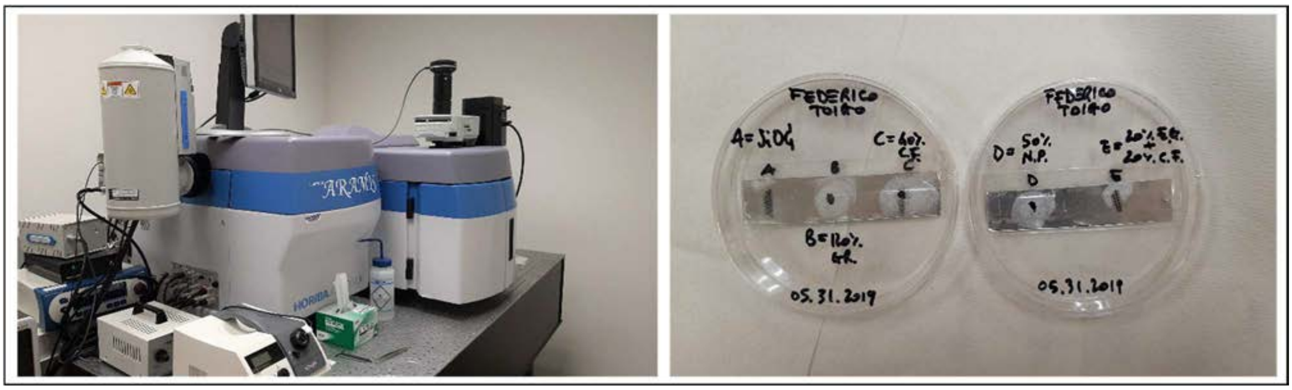

Figure 2.37 *LabRAM ARAMIS – Horiba Jobin Yvon RMN spectrometer (left); samples analysed (right)*

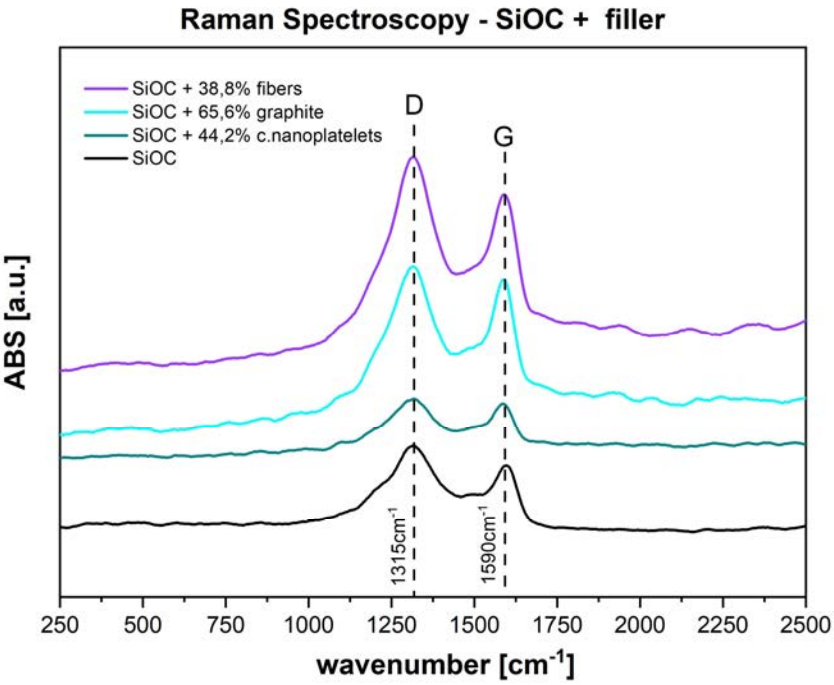

Figure 2.38 *RMN results for SiOC pure and SiOC+ carbon fillers*

The materials are compared to each other with the basic material of SiOC produced starting from H44, at the same conditions.

Both the curves show strong D and G peak, which are related to the Stokes and Anti-Stokes scattering: the D band is generated to the disorder induced by the vibration of the six-fold aromatic ring, while the G band is generated by the plane bond stretching of the sp_2 hybridized carbon atoms.[44]

In base of the intensity, the position and the width it is possible to understand the structural organization of the carbon sources.

In this case, for the pure SiOC, the intensity of the D band is higher than the G band due to the high disorder of the carbon source, facilitated by an amorphous microstructure.[44] This situation could be overturned if the heat treatment is conduced at higher temperatures (≈2000°C), as shown in previous works.[28] The SiOC trend is followed by the SiOC + carbon fibers and SiOC + graphite filler, but a little exception is ascribable to the material with nanoplatelets, which show similar intensities of the two bend, probably because of the filler, which supports a more organized structure of the carbon in the microstructure, due to the size of the particles and the low amount of carbon planes.

The intensity of the two bands increase proportionally with the amount of filler, but it has to be considered also that narrow peaks would be related to the nanocrystalline size of the carbon generated.[44]

The D band for pure graphite should be positioned at a wavenumber of 1350cm^{-1}, while the G band at 1580cm^{-1}, while in this case they are all shifted at 1315cm^{-1} and 1590cm^{-1} respectively:
the shift of the G band is attesting the presence of nanocrystalline graphite.

The chemical microstructure is studied in-depth with the analysis just reported.
It is now investigated the structural morphology of the samples realized with the three different fillers.

2.4 Scanning Electron Microscopy - SEM

In order to have a good image from the study of the sample topography with a scanning electron microscope (SEM), the samples need to have two main prerequisites:

- Electrically conductive: allowing the electrons of the irradiating beam flowing on the surface of the sample and discharging on the base, avoiding any trap of the electron which would decrease the quality of the image;
- Not sensitive to the beam: the high energy of the electron beam could deteriorate the material because of the localized heat generated, damaging the morphology of the sample.

In these cases, the specimens need to be coated with a metallic material (generally gold, silver, platinum, chrome, etc.) which allows the electrons to flow and discharge, avoiding any localized charging and heating of the sample.
In this research the coating of the SiOC is not needed, because its electrical conductivity, due to the presence of the free carbon formed during the pyrolysis process, even though it is limited, allows to reach good images without damaging the samples.

The analysis is conduced with an ESEM, Quanta 200 (FEIItalia SRL, Milano, Italy) and a Carl Zeiss EVO 10 scanning electron microscope, working in high vacuum (10^{-2}, 10^{-3} Pa), allowing to gain high magnifications of 1600x, with a high resolution, till 5µm. This experiment does not allow to study the dispersion of the nanoplatelets because of their tiny dimension, detectable with a transmission electron microscope (TEM), but this is beyond the purpose of this research. For the other two fillers, graphite and carbon fibers, the investigation is led not only with the secondary electrons (which give the image of the surface, gaining a 3-dimensional shape of the sample), but also in backscattering (BSD) in order to analyse the uniformity of the filler, more visible in the inner part of the material.
The samples are analysed both in plane and in section and the electrodes are disposed in a sample

holder, attached to a carbon conductive tape, which encourage the electron conductivity on the sample, for the reasons previously mentioned.

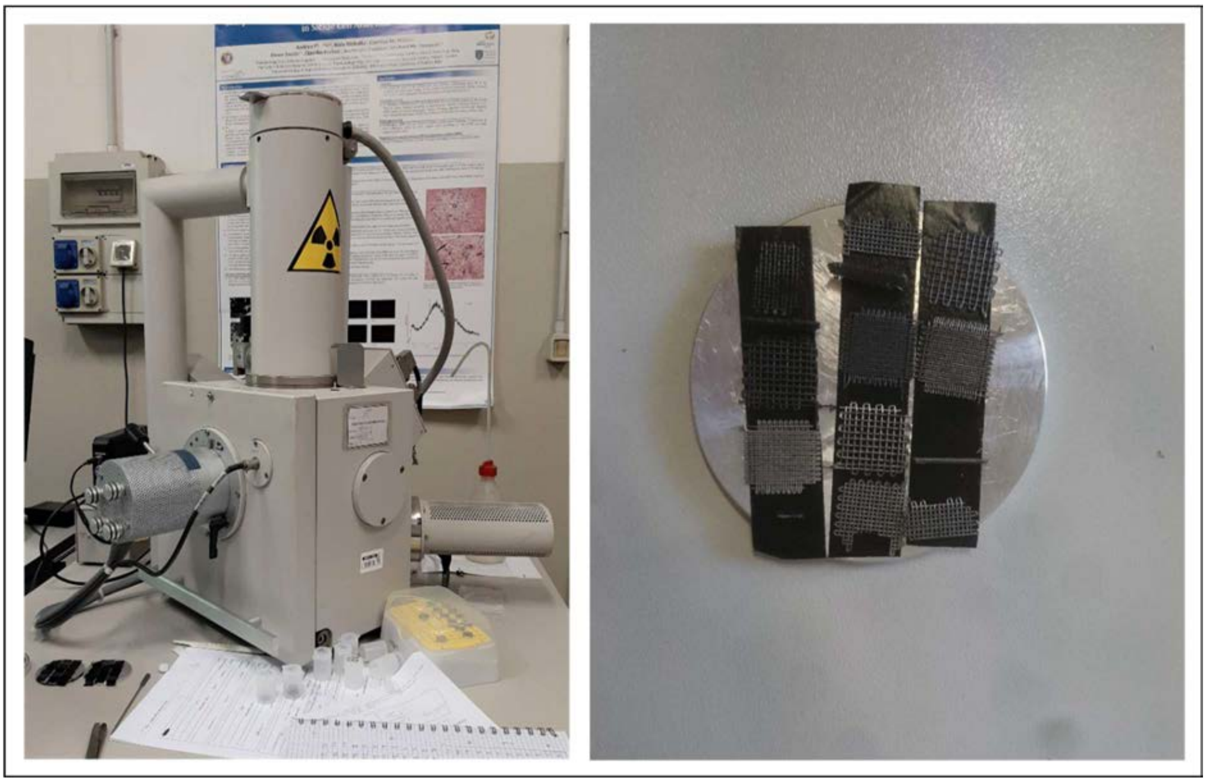

Figure 2.39 *ESEM, Quanta 200 (left); samples attached to the carbon conductive tape (right)*

2.4.1 SiOC sample

The first analysis is conduced with the pure SiOC electrode, which makes up a great basis of comparison for the filled samples.
The sample analysed is a 70% structural shape of pure SiOC.

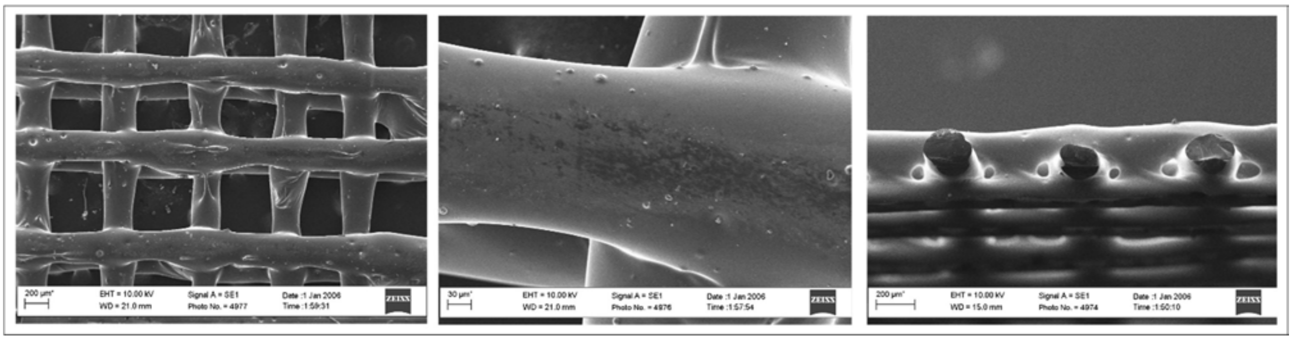

Figure 2.40 SEM of pure SiOC sample

As it is possible to see from the pictures, the material without any filler owns filaments with an inconstant diameter, which is testify by the difficult shape retention after the extruding process from the nozzle. This uneven behaviour is also proved by the non-circular shape of the filament in the picture of the section too and also because of the connections between the first and the third layers, in the interspace among the filaments of the second layer.

Moreover, on the surface it is possible to see the presence of folds, due to the stretching-out caused by the movement of the mechanical harm during printing.

All this “defects” can be avoided by using a filler, which increases the shape retention, obtaining more uniformity of the filaments, as shown further on.

The interspace between the filaments is however not respected, as designed, because of the low precision of the printing process.

The material appears very dense, which is typical of a glass structure, and no voids are present in the structure. The surface is particularly smooth and the high surface area, which is the main parameter to pursue in order to have high ion capacity in the final application, is guaranteed only by the structural shape and not related to the roughness or porosity of the sample.

2.4.2 SiOC + GRAPHITE samples

The investigation is now focused on the samples made of SiOC + Graphite filler with different amount of powder graphite and different structural shapes. In particular the experiment has been performed on two samples with the same amount of filler (16.7%) and different structural shape (80-70%), in order to achieve general conclusions in base of different quantities and structural porosities.

1) *16.7% Graphite – 80% Structural Porosity*

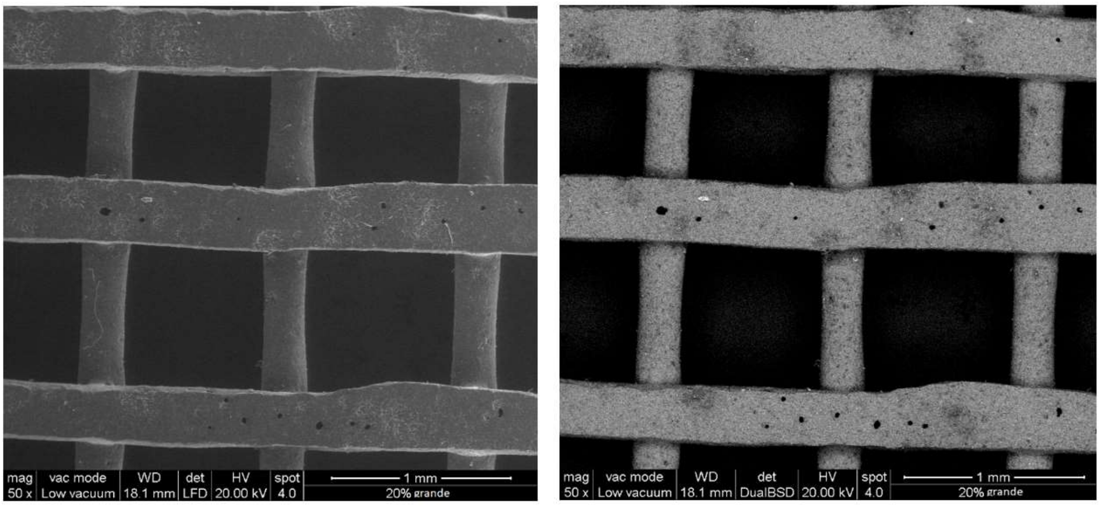

Figure 2.41 *SEM analysis on H44+graphite 16.7% sample - structural porosity 80% (50X magnification)*

These pictures are taken with a magnification of 50x and are related to the samples with 16.7% of filler (considering the total amount of elements in the ink).

As shown, even by adding a little amount of filler, the structure gains a uniform pattern: the filaments have still some diameter variations, in fact they register dimensions between 217µm and 377µm (the nozzle used has an inner diameter of 250µm). The higher dimension of the filament diameter, compared to the expected length, is due to the low viscosity of the material (look at the isopropanol added for this ink that is higher than the amount performed in the interpolation) which does not allow the perfect retention of the material, but it lets it lay down on the holder.

In the picture there are also visible some voids (black spots) because the picture is taken on the surface, which is in contact to the substrate during the 3D printing: some isopropanol could be trapped and the consequence is that it releases these voids on the surface.

The SEM analysis gives the pictures due to the interaction between the incident electrons of the beam and atoms on the surface of the material. There are two types of electrons dedicated to the interactions: the secondary electrons, which gives the surface information due to the inelastic interaction, and the backscattered electrons, which achieve the inner portion of the material, by giving more details on the structure of the material, especially if there are fillers, as in this case.

The backscattering acquisition is indeed more sensitive to the atomic number (Z) of the atoms, and in particular higher is Z and brighter is the image: for this reason the graphite, made of carbon, which has an atomic number of 6 is darker than the Si-C-O matrix, in which the silicon has Z=14 and the oxygen Z=8 (higher respect the carbon). Even though, the variation of the atomic number is not so marked and the similar colour of the phases does not allow to determine the areal fraction of the graphite phase compared to the amorphous SiOC matrix with an image analyser software.

In the BSD picture above it is also possible to notice how the filler is disposed on the microstructure: there are portions in which the powder is more condensed and these are identified by the darker areas.

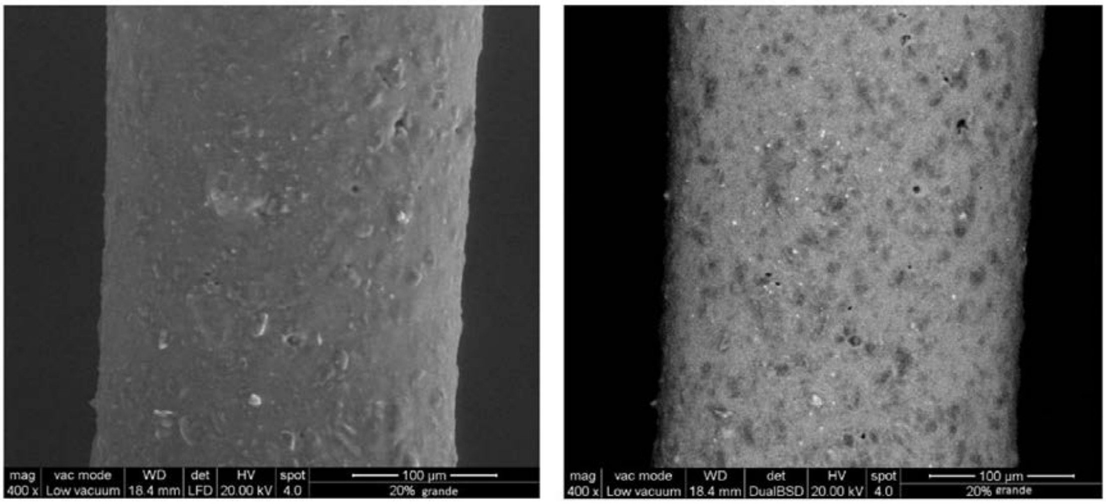

Figure 2.42 *SEM analysis on H44+graphite 16.7% sample - structural porosity 80% (400X magnification)*

With a higher magnification (400x) it is possible to see how the particles enhance the roughness of the surface, because of their disposition on the material, even if this is more evident with higher amount of filler as is shown further on.

The white spots on the surface are analysed with an Energy Dispersive X-ray Spectrometer (EDS), in which they result as Iron (Fe), probably deposited on the surface of the specimens during the heat treatment process due to impurities attached to the surface of the tube.

The black spots in the BSD are the graphite powders submerged on the SiOC matrix (light grey): their shape is not circular and moreover irregular.

2) *16.7% Graphite – 70% structural porosity*

Another analysis is conduced for the same material, but with a different structural porosity (70% instead of 80%).

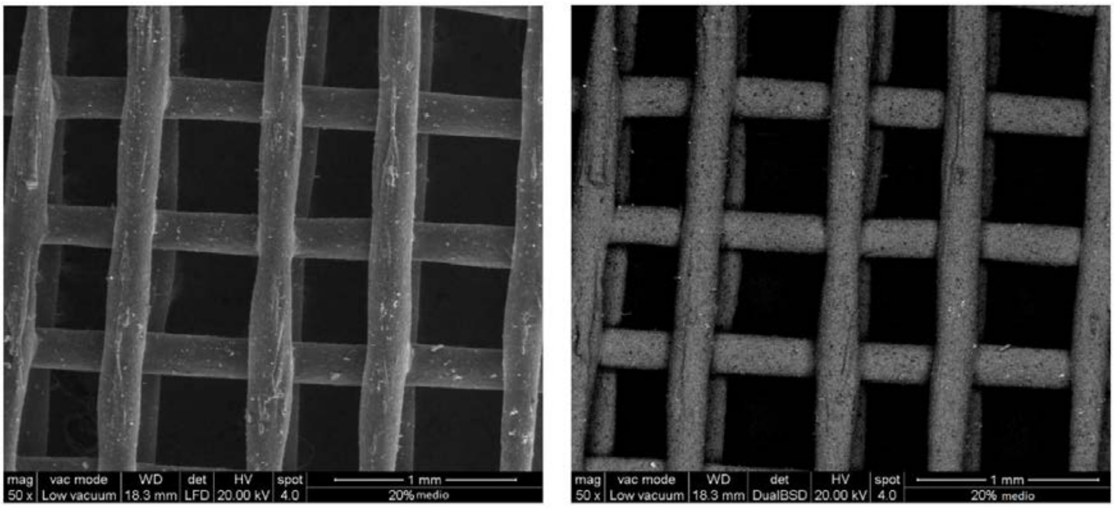

Figure 2.43 *SEM analysis on H44+graphite 16.7% sample - structural porosity 70% (50X magnification)*

In this case the filament diameter dimension varies between 230 and 190µm, so below the standard 250µm of the nozzle: in this case the amount of isopropanol is lower than the amount performed in the interpolation, resulting more viscous than the ink previously studied with the 80% structural porosity, avoiding the filament laying down on the substrate.
This phenomenon is also testified by the presence of the folds, disposed in the direction of the flow, which suggest a stretching of the material during the printing due to the high viscosity (low amount of solvent).

Also, the roughness, seen in the 400x magnification picture, is apparently increased because of the decrease of the filament dimension with higher probability of the powder to be disposed on the surface.

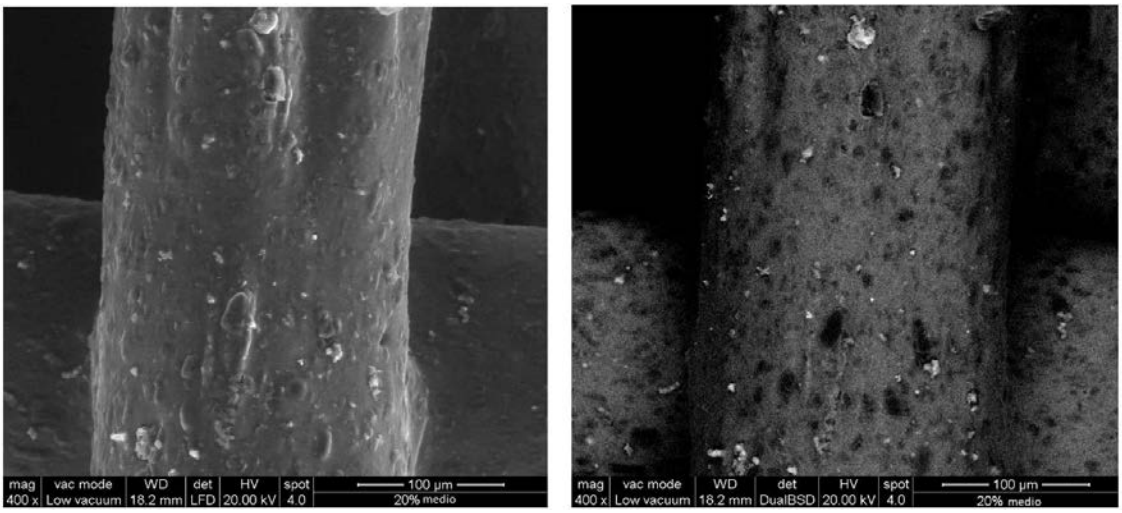

Figure 2.44 *SEM analysis on H44+graphite 16.7% sample - structural porosity 70% (400X magnification)*

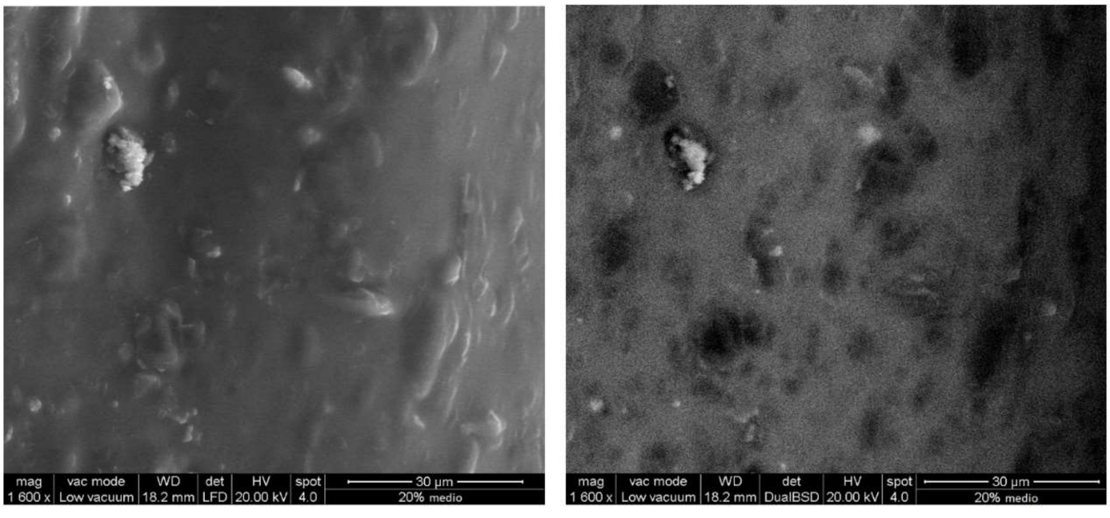

Figure 2.45 *SEM analysis on H44+graphite 16.7% sample - structural porosity 70% (1600X magnification)*

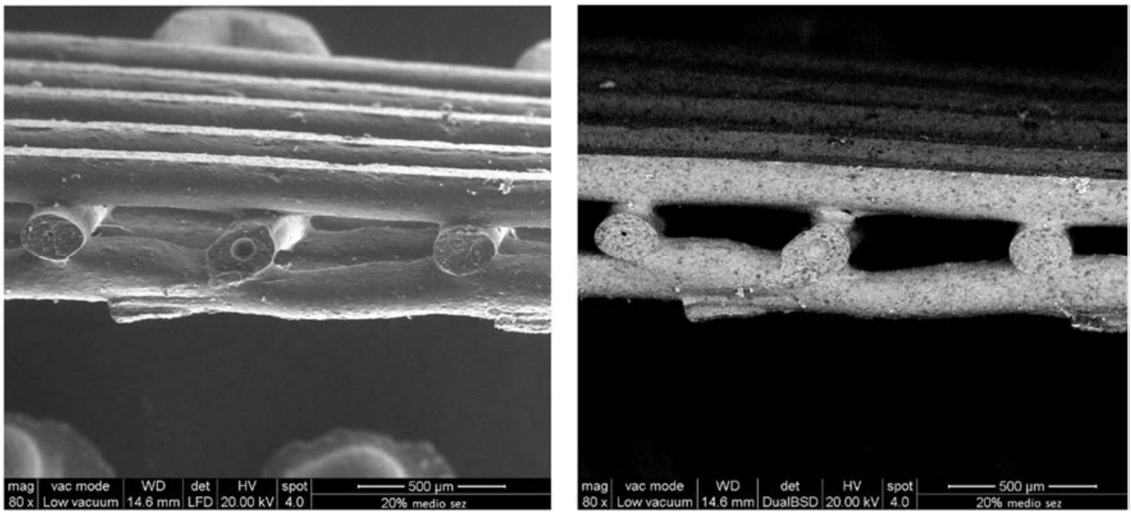

Figure 2.46 *SEM analysis on H44+graphite 16.7% sample - structural porosity 70% (section-80X magnification)*

From the section picture it is also possible to see how the filaments preserve more or less their shape and the section of the filaments are still circular. This behaviour is caused by the increasing amount of filler. The filaments are also well attached layer-by-layer, generating welding with low curvature, decreasing the possibility of forming cracks between layers.

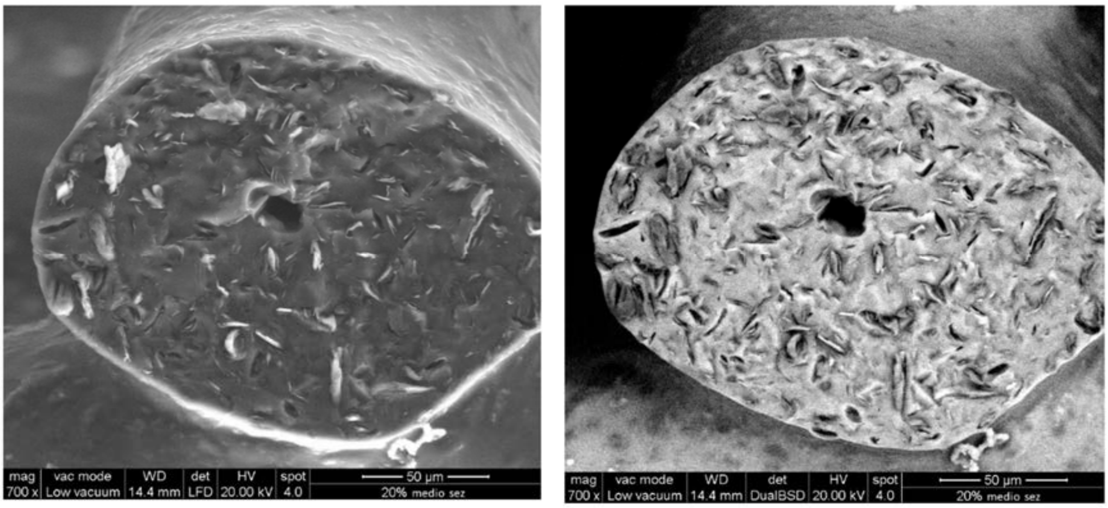

Figure 2.47 *SEM analysis on H44+graphite 16.7% sample - structural porosity 70% (section-700X magnification)*

From the pictures of the section at a magnification of 700x it is possible to see the disposition of the graphite particles, which appear like filaments because of the orientation generated by the shear stress applied during the extrusion.

It also seems that the graphite does not attach perfectly to the matrix because some black portions are visible near the surface of the particles, suggesting the break of the interfaces because of the different thermal expansion between the SiOC and the graphite, in particular achieving high temperatures as in the pyrolysis process.[45,46] In the parallel plane this detachment is not seen probably because of the different thermal expansion between the different side of the hexagonal cell, characteristic of the graphitic carbon.

Below there are illustrated the BSD results obtained for different amounts of graphite respectively of 16.7%, 33.3% and 50% (compared to the total amount of the ink prepared):

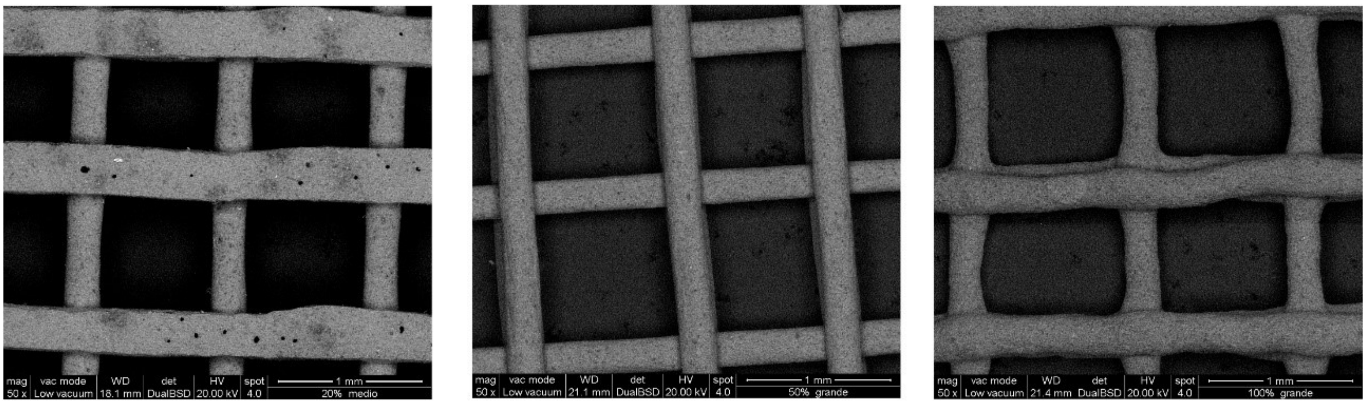

Figure 2.48 *SEM analysis on H44+graphite different amount of filler: 16.7%, 33.3% and 50%*

From these pictures it is possible to notice how the increase of darkness is proportional to the amount of filler introduced.

Moreover, it can be noticed that by increasing the amount of filler beyond 44.5%, the net-shape of the electrode is distorted by the high quantity of powder which produces accidental movements of the filament when extruded, due to the low amount of polymer compared to the solid material.

The increasing addition of graphite in the material also increases the roughness of the material, slightly increasing the surface area of the sample. The SiOC percentage decreases inversely proportional, allowing the filler powder to occupy higher volumes and increasing the probability of disposition on the surface.

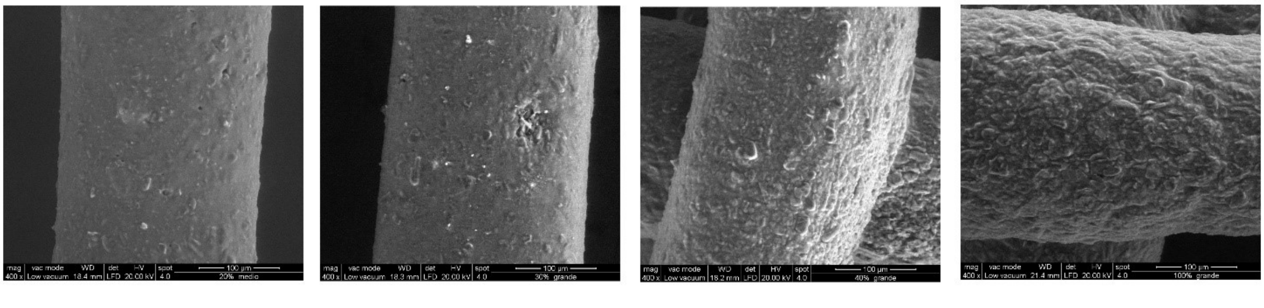

Figure 2.49 *SEM analysis: increasing of roughness increasing the content of graphite as filler (from left to right)*

In order to achieve both high electrical conductivity and ion capacity for the application of this material, such as electrodes, it is important to balance the quantity of filler because on one hand the carbons enhance the electrical conductivity, but on the other hand the SiOC matrix increases the ion capacity.

In the 50% structural porosity it is more evident the different length of the distance between the filaments due to the imprecise movement of printing. Even though the average distance (mediated between the wider and the shorter) is similar to the length designed. This observation is important for subsequent considerations.

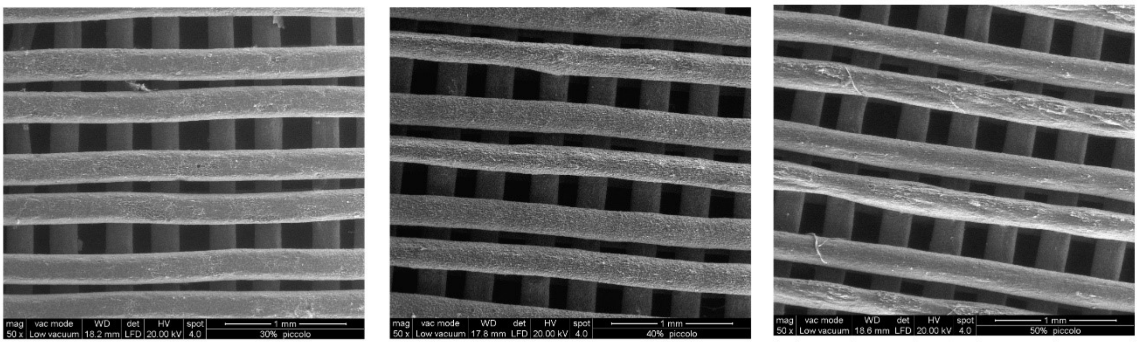

Figure 2.50 SEM analysis: different lengths of the interspaces

In the following pictures, the increase of filler in the material unquestionably testifies the high shape retention, which allows to gain a perfect rectilinear shape (till 44.5% of filler) with a good mechanical support generated by the filler loaded in the ink.

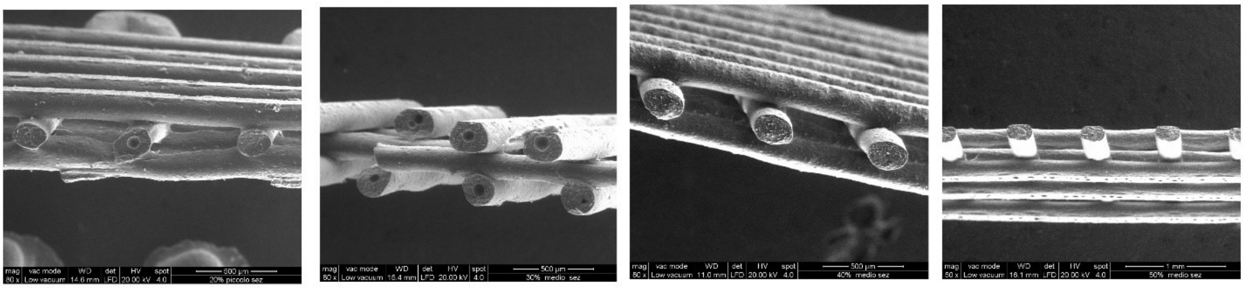

Figure 2.51 *SEM analysis: section of the sample increasing the amount of graphite filler (from left to right)*

2.4.3 Analysis of structural Porosity – Graphite

From the pictures obtained by using the SEM, an analysis on the structural dimensions is taken in order to understand the variations of the structural porosity before and after the heat treatment.

The length of the initial sample is considered equal to the dimensions designed for the G-Code set on the printing machine (50-70-80% structural shape); the porosity of the final samples is in this way calculated, taking the length measurements from the SEM pictures:

$$P\% = \frac{d}{d+i} \tag{2.6}$$

Where d is the dimension of the filament and i is the dimension of the interspace between the filaments, as reported in the following picture.

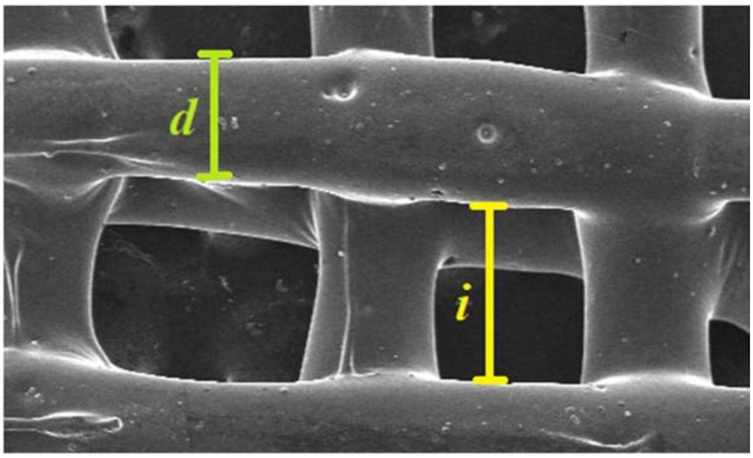

Figure 2.52 *SEM analysis in which are indicated the dimension of the filament (d) and the interspace distance (i)*

The measurements are taken with ImageJ software (Image Processing and Analysis in Java) and the dimension of the filaments and interspace are averaged with a set of 30 length, taken in different parts of the images, due to the possible change of diameters of the filaments and the variation of the interspaces due to the imprecise net-shape pattern printed.

The measurements are compared between different type of porosity and different type of filler amounts.

For the graphite are analysed the 23.1%, 28.6%, 33.3% and 44.5% of filler in the three different structural porosities (50-70-80%).

1) *23.1% Graphite*

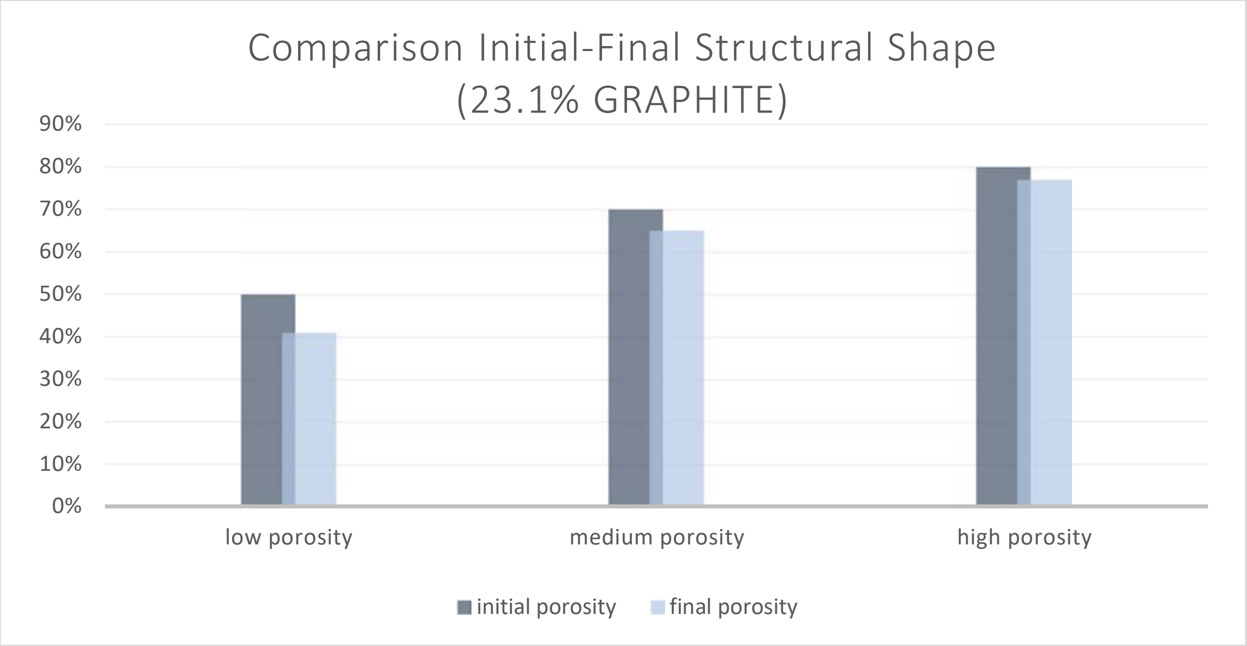

Figure 2.53 *schematic variation of porosity before and after the treatment for the three different structural shapes designed - 23.1% graphite filler*

For the samples containing 23.1% of graphite filler it is possible to note that after the heat treatment the porosity is reduced compared to the initial one, as expected.

This is due to the thermal shrinkage which happens during the pyrolysis process, especially between 400-800°C. [47]

Moreover, the variation is inversely proportional with the amount of filler:

in the low porosity sample the porosity is reduced of 9% (41% final measurement), in the medium porosity sample, it is decreased of 5% (65% final) and in the high porosity sample it is decreased of 3% (77%).

This proves that, with high porosity, the final dimensions of the samples are not deviating so much from the initial ones.

2) 28.6% and 33.3% Graphite

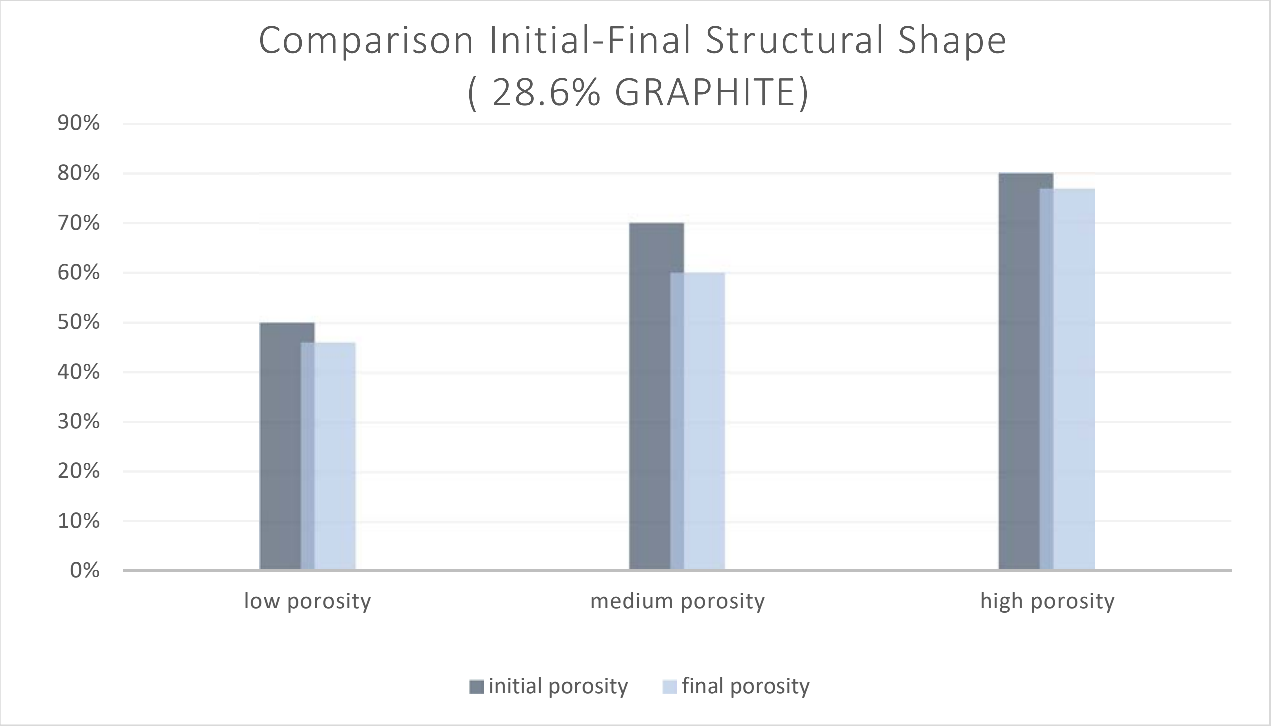

Figure 2.54 *schematic variation of porosity before and after the treatment for the three different structural shapes designed - 28.6% graphite filler*

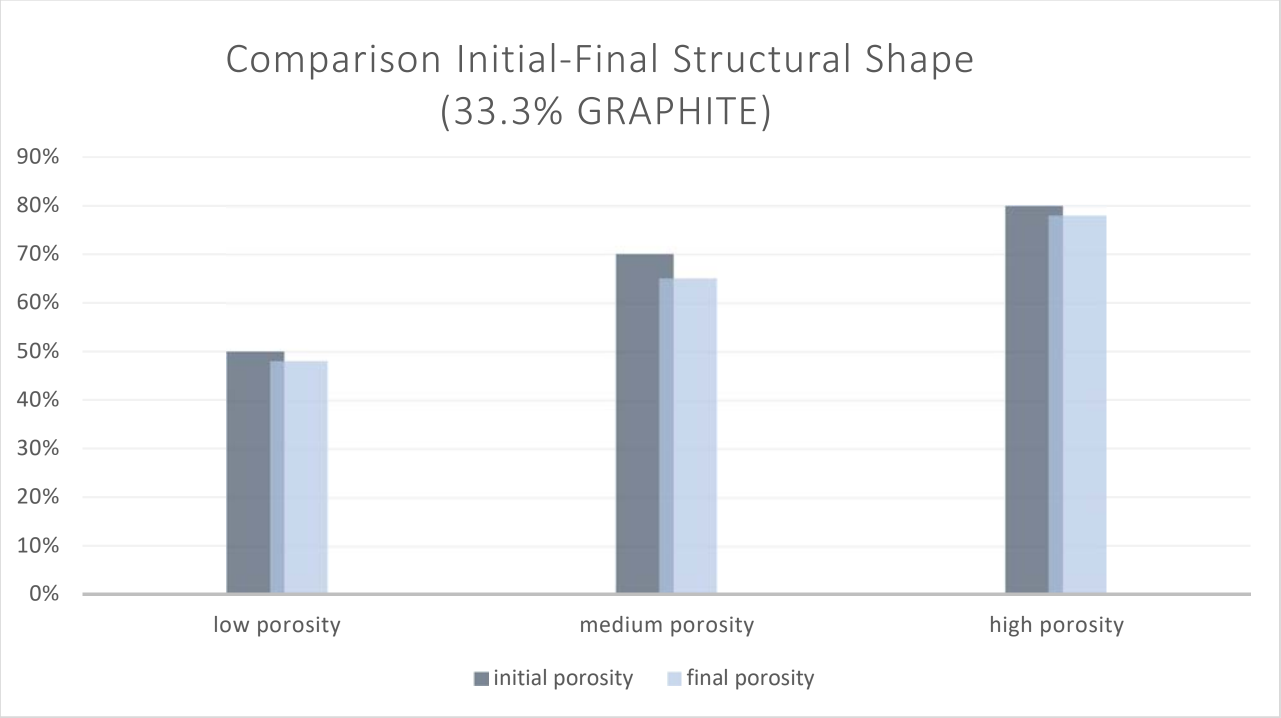

Figure 2.55 *schematic variation of porosity before and after the treatment for the three different structural shapes designed -33.3% graphite filler*

The samples including an amount of filler of 28.6% and 33.3% show a slightly different trend than the previous ones. In any case the final porosity decreases with respect to the initial one, but the variation is not proportional to the amount of filler: the higher variation is in both cases (28.6-33.3%) identified at a medium porosity (decreased respectively of 10% and 5%), while the decrease in the low and high structural porosity is mild.

3) *44.5% Graphite*

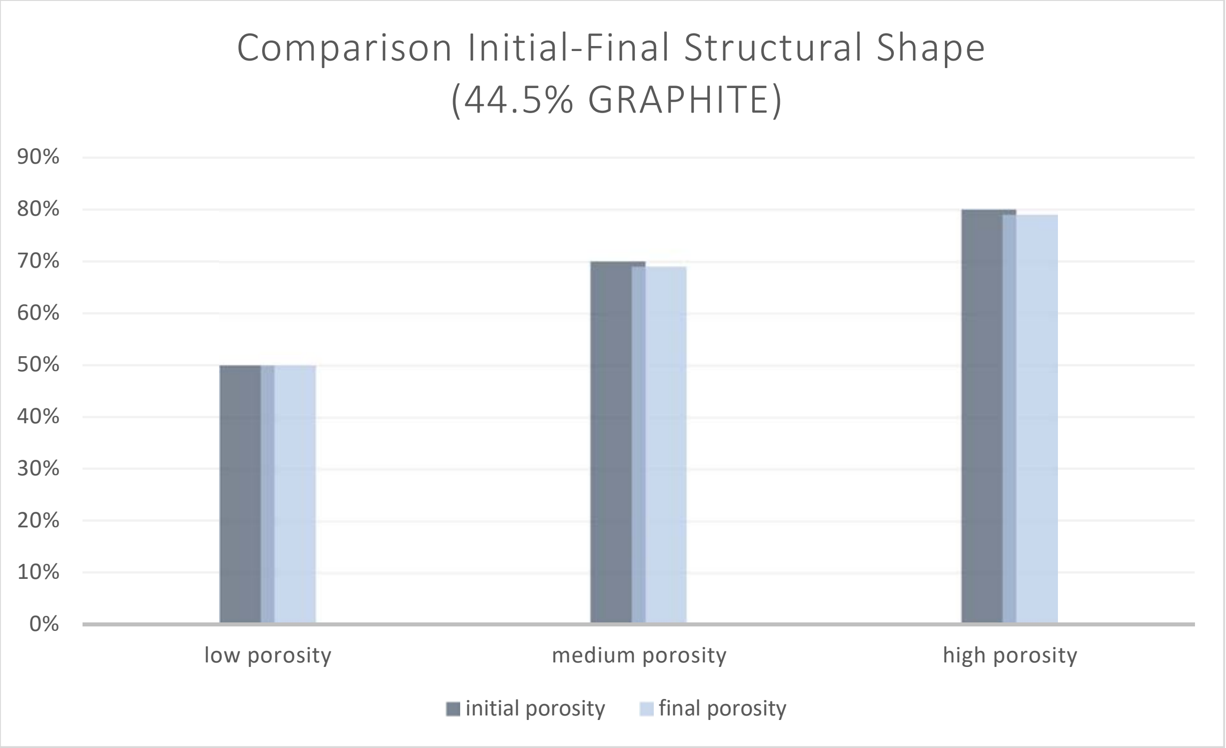

Figure 2.55 *schematic variation of porosity before and after the treatment for the three different structural shapes designed - 44.5% graphite filler*

The 44.5% graphite sample shows a negligible variation of the structural porosity, after the pyrolysis (<1%), demonstrating a higher shape retention for the materials containing an increasing amount of filler, as previously mentioned.

Indeed, the increasing amount of filler does not only allow to have a great conservation of the geometrical shape during printing, but it also preserve the initial shape after the heat treatment, inhibiting the shrinkage expected.

These considerations are summarized in the following plot, where the real porosity is converging to the theoretical one, increasing the amount of filler used.

For the medium structural porosity, an anomaly can be observed with a low amount of filler, where the porosity momentarily decreases, and then increases, as expected.

The high structural porosity samples show the most stable geometry and for this reason they have to be chosen in applications in which dimensional variations are not acceptable.

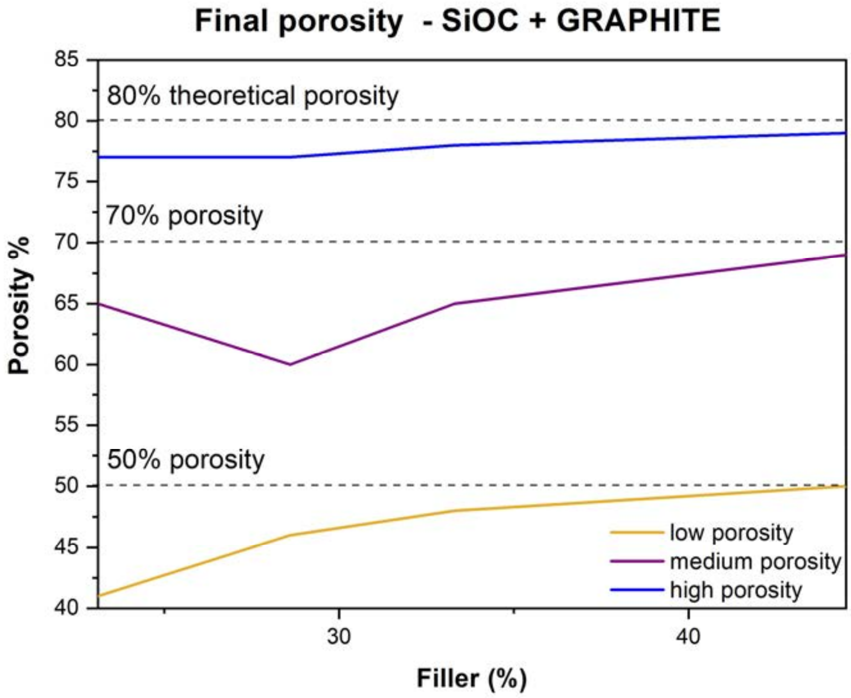

Figure 2.56 *variation of porosity compared to the theoretical values (dotted) for the three different structural shapes designed, considering different amount of graphite filler*

2.4.4 SiOC + CARBON FIBERS samples

The SEM experiment enables to analyse the morphology of the SiOC + Carbon Fibers samples, such as the samples loaded with graphite previously analysed.

Here are reported the backscattered images of 4 samples with the same structural porosity, but an increasing amount of filler.

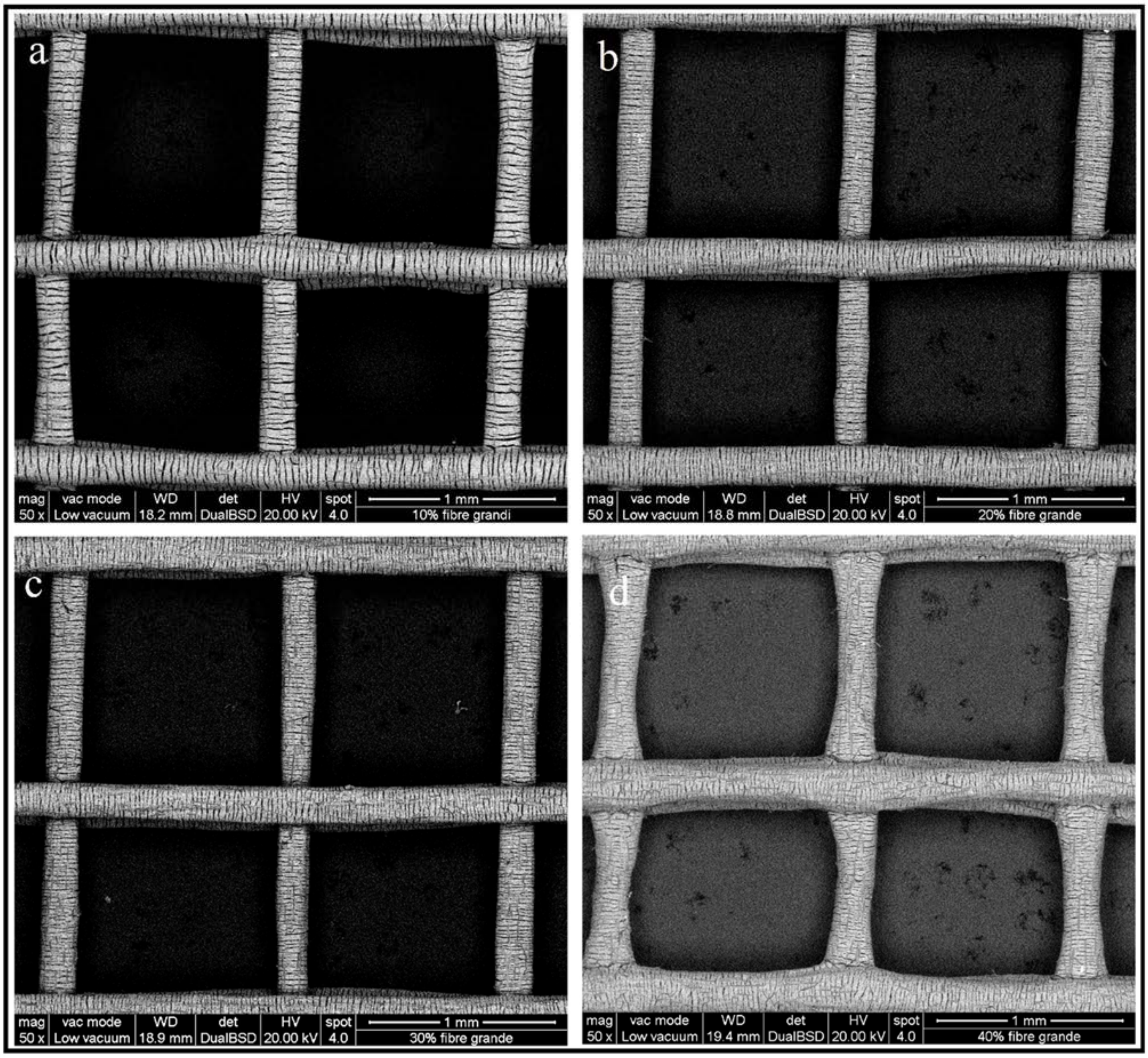

Figure 2.57 *SEM analysis: increasing of cracks proportional to the amount of carbon fibers used as filler (from a to d): a) 9.1% carbon fibers; b)16.7% carbon fibers; c)28.6% carbon fibers; d) 33.3% carbon fibers.*

As shown in this figure, by adding carbon fibers, due to the anisotropy thermal expansion of this fillers, all the samples show surface cracks, produced during the thermal treatment, which are mainly arranged transversely to the filaments. This characteristic is surely negative, considering the mechanical strength of the material, but on the other hand it is desired to have a high surface area, allowing the lithium ion to penetrate the inner part of the sample, obtaining the SiOC as much as possible. It should also be considered that by increasing the amount of filler the SiOC matrix diminishes, decreasing the ion capacity.

As it is possible to see, the increasing amount of filler apparently increases the quantity of cracks produced. The geometry of the sample, in addition to a possible increase in length due to the expansive cracks, has maintained the proper shape compared to the only SiOC samples. Only with the highest amount of filler (d), the sample shows a slight deformation of the shape of the net, as shown by the graphite with the highest amounts due to the much quantity of filler, which distorts the filament deposition during printing. Furthermore, the cracks are also arranged longitudinally to the filaments, mainly affecting the mechanical properties.

For this sample it should be better to consider a good compromise between SiOC/Carbon Fiber amount and mechanical properties in order to have functional electrodes, not only as batteries elements but also as structural parts.

By increasing the magnification, it is also possible to see how the fibers are arranged longitudinally to the flow of printing (left figure), as expected and demonstrated in previous works, due to the shear stress acting in the material. [48,9] Moreover, the fibers in the interior part of the material keep the matrix portions joined, acting as a true mechanical reinforcement, also thanks to the good interface between fibers and SiOC.

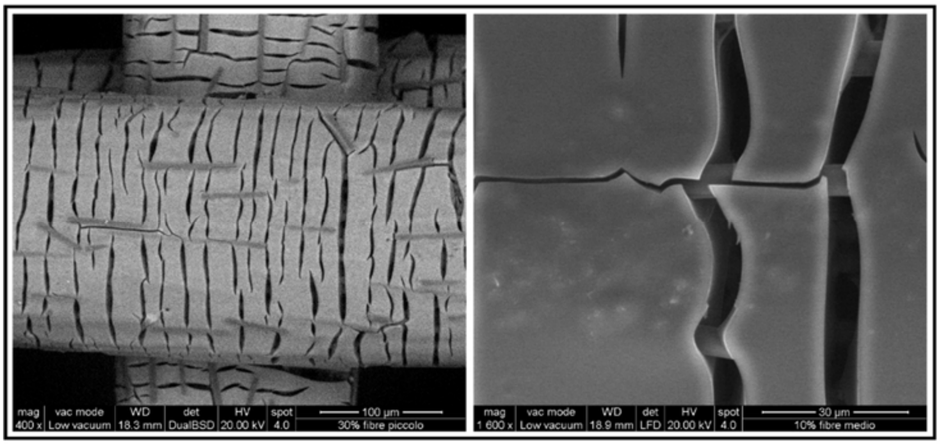

Figure 2.58 *SEM analysis: alignment of the fibers (left); fibers inside the material connecting the bulk SiOC matrix parts.*

The section of the filament, obtained by breaking the sample in flection, well demonstrates the effectiveness of the interface between the fibers and the matrix, in fact the fibers pulled out of the structure are much more compared to the fibers broken by fragile fracture (which are related in the Debounding work, smaller than the other about 1/10-1/100).

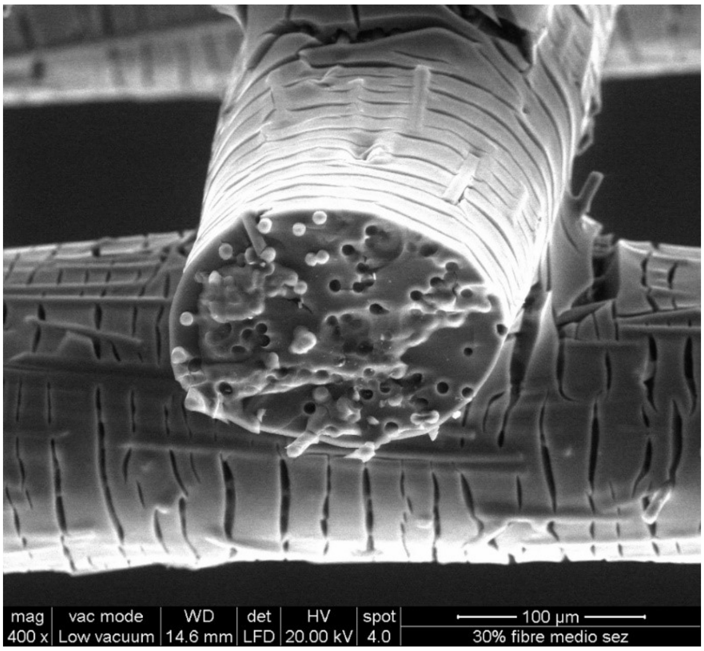

Figure 2.59 *SEM analysis: section of the SiOC+ carbon fibers with presence of broken fibers and voids.*

The pictures above show that the cracks produced are mainly superficial and they do not affect the middle of the filament, guaranteeing a better condition of mechanical resistance.

2.4.5 Analysis of structural Porosity – Carbon fibers

The dimensional analysis is also carried out for the SiOC + Carbon Fibers filler, in the same way as the previous study for graphite filler.

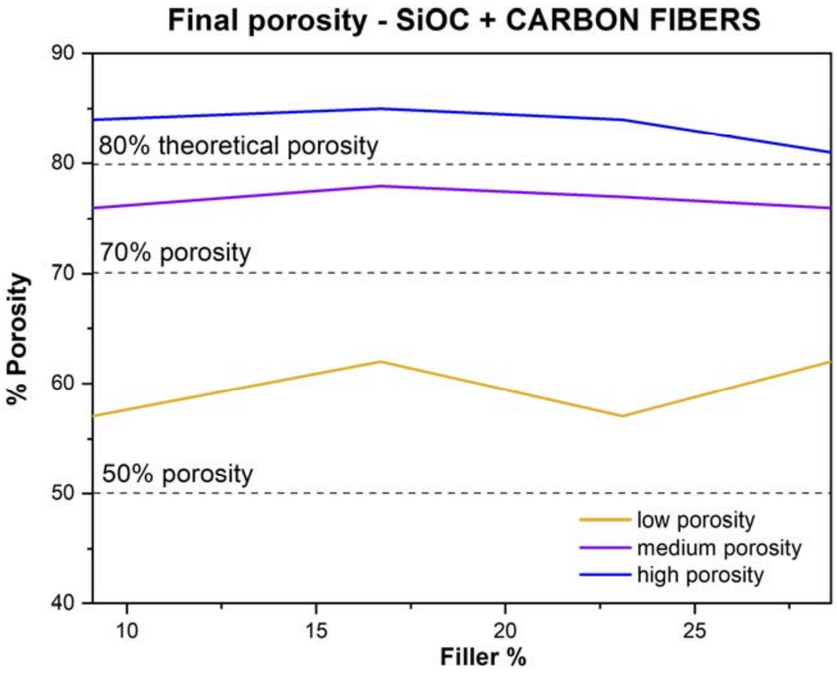

Figure 2.60 *variation of porosity compared to the theoretical values (dotted) for the three different structural shapes designed, considering different amount of carbon fiber filler*

The structural porosity achieved for the material is higher than the designed theoretical one because of the expansion cracks created during the heat treatment; in particular a highest variation is noticed for the lowest porosity (12% more than the theoretical value); this deviation decreases with higher structural porosity, recording an average variation of 9.5% for low structural porosity, 6.75% for medium structural porosity and 4% for high structural porosity, attesting again the high structural porosity as the most reliable in terms of structural geometry, considering the shape designed.

Also the variation of the porosity deviations, considering the different amounts of fillers, is not predictable with in the lowest porosity design, but it is increasingly more stable at higher structural porosities.

2.4.6 SiOC + NANOPLATELETS samples

Compared to the previous materials loaded with filler, the SiOC + carbon nanoplatelets have a different roughness due to the small size of the nanoplatelets, which affect the surface on the nanoscale scale, not visible with a SEM analysis.

In this case, the increase in the surface area of the sample would be negligible compared to a micrometric roughness showed in the previous samples, even if this parameter should not affect the final results of capacity in the batteries.

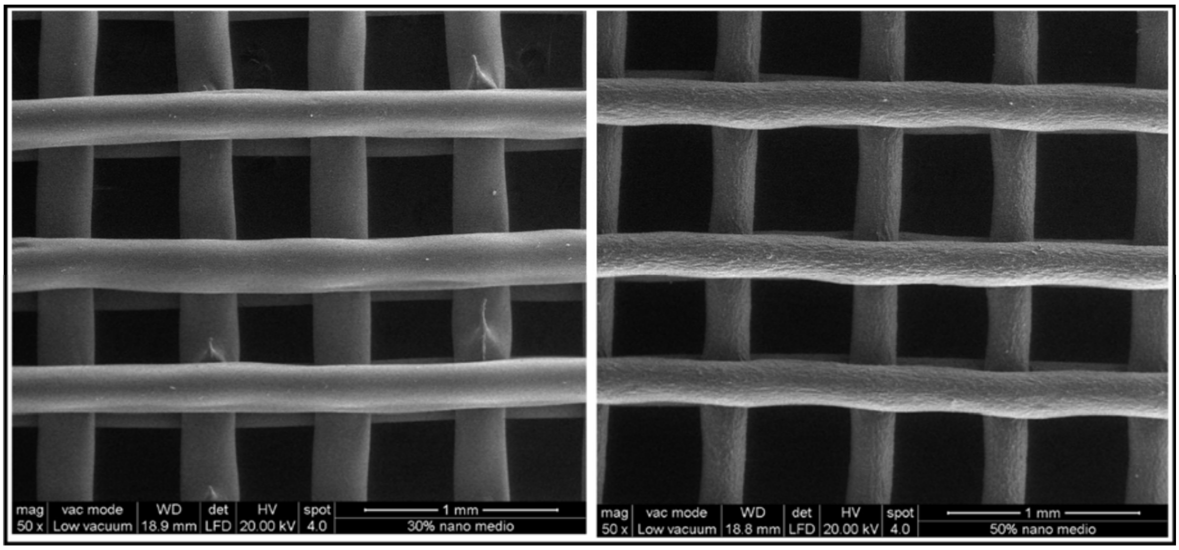

Figure 2.61 *SEM analysis: morphology of the SiOC + 23.1% nanoplatelets (left) and SiOC+ 33.3% nanoplatelets (right)*

Moreover, from the SEM analysis it is not possible to understand the uniformity of the nanoplatelets in the material and the adhesion to the matrix, but from the section of the filament, it seems they have been aggregated because of the micrometric pattern formed.

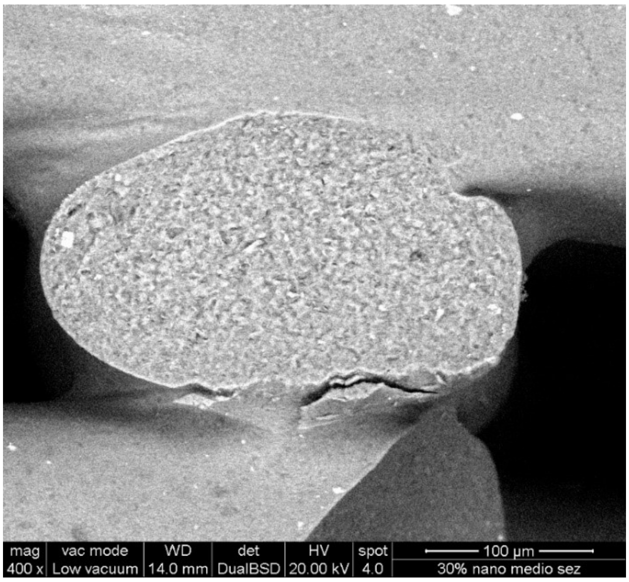

Figure 2.62 *section of the SiOC+ carbon nanoplatelets sample*

Considering the different % of filler analysed in this case, the shrinkage of the material decreases with the increase in the amount of filler and in particular the high porosity is again the best choice for this purpose.

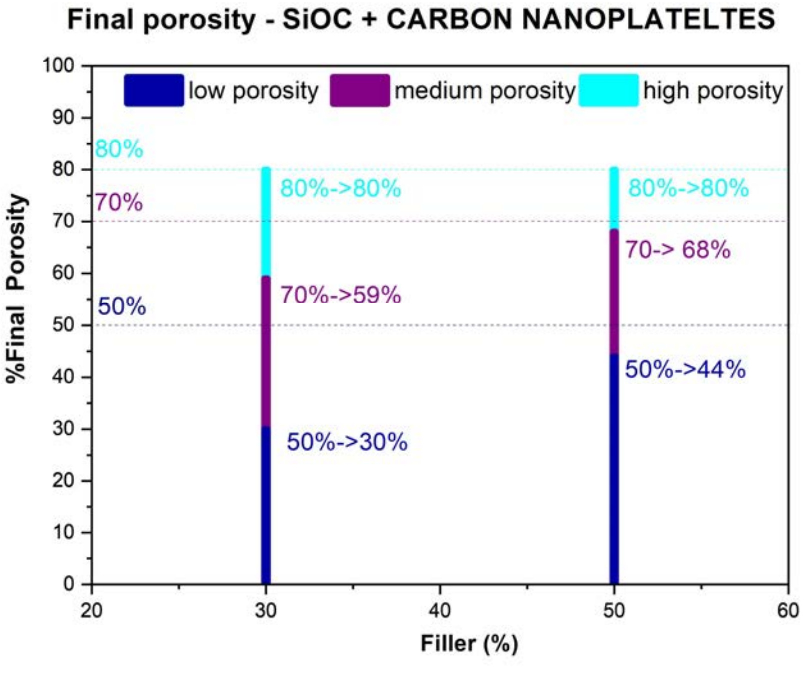

Figure 2.63 *variation of porosity compared to the theoretical values (dotted) for the three different structural shapes designed, considering different amount of carbon nanoplatelet filler*

Moreover, the samples made with carbon nanoplatelets do not show any shrinkage using the high porosity structure, so they could be considered as the best geometrical reliability of all the samples.

Chapter n.3

Half- Cell Assembly
and
Characterization

The electrodes produced and characterized till now, are ready to be assembled in the half-cell and subsequently studied to understand their electrochemical behaviour.

In this chapter it is shown the procedure of preparing lithium-ion half-cells starting from SiOC + graphite in powder (traditional method) and 3D printed (innovative method), with the samples prepared.

Both methods are compared in their practical development and a short financial statement is discussed, where it is possible to understand the main economic advantage by using the innovative process instead of the traditional.

The study is then focused on testing the half-cells prepared in a charge/discharge test in which the samples are tested, in a repeated series of charge and discharge cycles, using constant voltage (CV), in order to determine their capacity, their stability and the efficiency achievable using these advanced electrodes.

The electrodes used are chosen among the wide set of the different materials prepared in order to draw the conclusion based on of the filler used, the amount, comparing the results with the electrodes made with the equivalent material in powder (traditional method).

The goal of this study is to achieve high capacity, as well as guaranteeing high cycle stability, which could be downgraded by the deterioration of the half-cell.

3.1 Electrodes Material

In order to analyze the particular material of the sample prepared, the cell has to be constructed with a reference electrode (RE) coupled with the 3D printed working electrode (WE). In this way the so-called half-cell is prepared, and it is possible to exclusively investigate the contribution of the single electrode (WE) ton the electrochemical properties, disregarding the counter electrode (CE), typical of the two electrodes system of the full cell. Moreover, it is possible to compare the results with the current state of the art present in previous published reports. in which these devices are prepared as described, indeed this approach is very common in research and development.[49] For this reason, in this work half-cells instead of full cell are assembled, with the cathode electrode made of pure lithium, which is considered a reference electrode in the scientific society, considering its potential zero (V=0), even though it has a potential of -3.05V vs. standard hydrogen electrode (SHE). In this way the SiOC based 3D printed electrode works as an anode electrode.

In this research two type of electrodes are prepared with different techniques: the innovative 3D printed electrodes, described so far, and the traditional electrodes, prepared from the same material, but in powder, following an extra process here described.

3.1.1 Traditional method

The traditional electrodes are prepared with the Doctor Blade method (tape casting), which is an outspreading technique that in this case allows to obtain a thin film of active material on a large copper foil.

The electrodes produced with this technique are made with three types of material, adequately selected during the work, in base of the results obtained with the 3D printed electrodes, and in particular:

- Pure SiOC (no filler);
- SiOC + 23.1% Graphite;
- SiOC + 23.1% Carbon Fibers.

These materials are produced in the same conditions of the 3D printed samples, but are grinded in powder.

The process of producing the traditional electrode follows these steps:

- Mix the active material with carbon black (CB, acetylene, 50% compressed,99.9+%, Alfa Aesar, Germany), used as electrically conductive element, and Poly(vinylidene) fluoride (PVDF, %, Sigma-Aldrich, St. Louis, MO, USA), used as binder, each respectively in the following proportion 80:10:10;
- Add N-Methyl Pyrrolidone (NMP, anhydrous, 99.5%, Sigma-Aldrich) as solvent, as much as needed to produce a slurry and mix for 20 minutes until the mixture is completely homogeneous;
- Depose the mixture on a pure copper foil (254µm thickness, Copper foil 99.9%) with a high precision blade having 25.4µm gap;
- Dry the coating at 80°C, at least for 12hours, till the solvent is completely evaporated and then punch the electrode (12mm diameter).

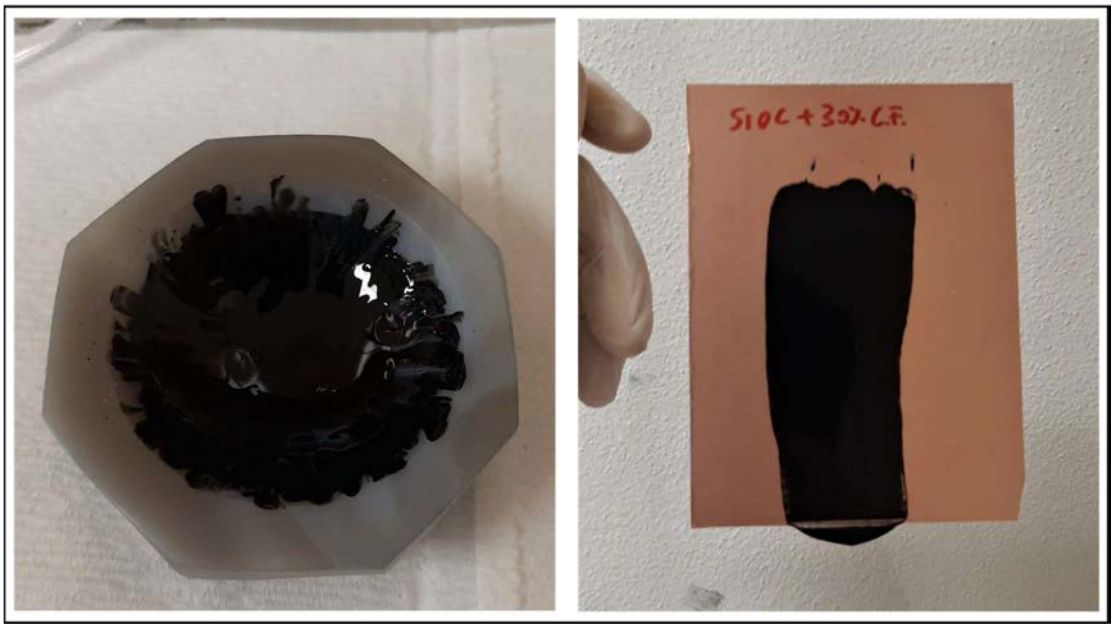

Figure 3.1 *mortar with the slurry prepared (left); tape casting of the slurry in the copper foil (right)*

The amount of CB and PVDF is negligible, compared to the quantity of active material and for this reason they are not considered in the calculation of the specific capacities.

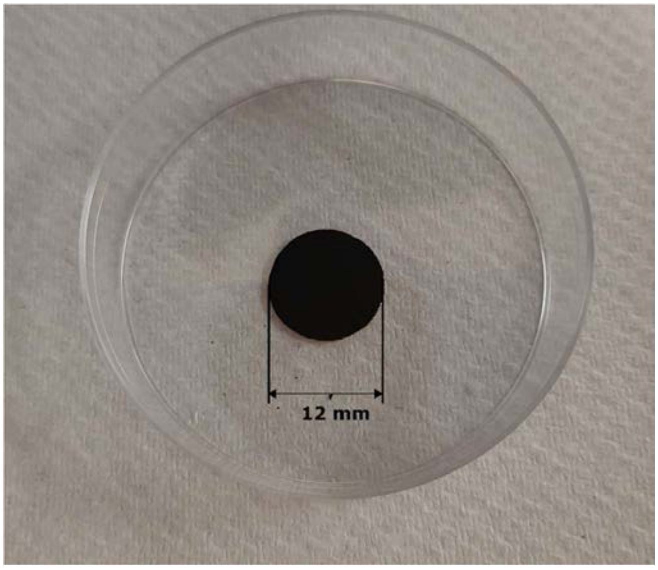

Figure 3.2 *SiOC+ carbon fibers electrode prepared with the traditional method*

3.2 Half-Cell Assembly

Lithium ion half-cells are produced in a glove box (UnilabProSP-MBRAUN) that inhibits the O_2 and H_2O contact with the lithium cathode and electrolyte: as it is known, lithium is highly reactive, having only one electron in its external orbital.

The glove box guarantees values of O_2 and H_2O below 1ppm since it is filled constantly with inert argon gas.

The half-cell is assembled in a two-electrodes coin cell with the active material, as a working electrode, and the lithium electrode (99.9% purity, 0.75mm thickness, Alfa Aesar, Germany), as reference, which is a source of lithium ions during charging and a tank during discharging.[49] The electrolyte used is 1M lithium hexafluorophosfate ($LiPF_6$) in lithium carbonate EC/DMC=50/50 (v/v), (Sigma-Aldrich). A glassy microporous filter is used as separator in order to avoid any contact between the two electrodes that would produce shortcuts.

The coin-cell is assembled by positioning a spring in the bottom chasing, followed by the stainless-steel spacer conveniently sticked to the lithium reference electrode; a few drops (6-7) of the liquid electrolyte are deposited on top and a glass filter is superimposed; other 4 drops of electrolyte are added in order to soak the filter and finally the active material electrode is laid above, followed by the stainless-steel spacer and the top chasing.
The procedure is represented in the following picture:

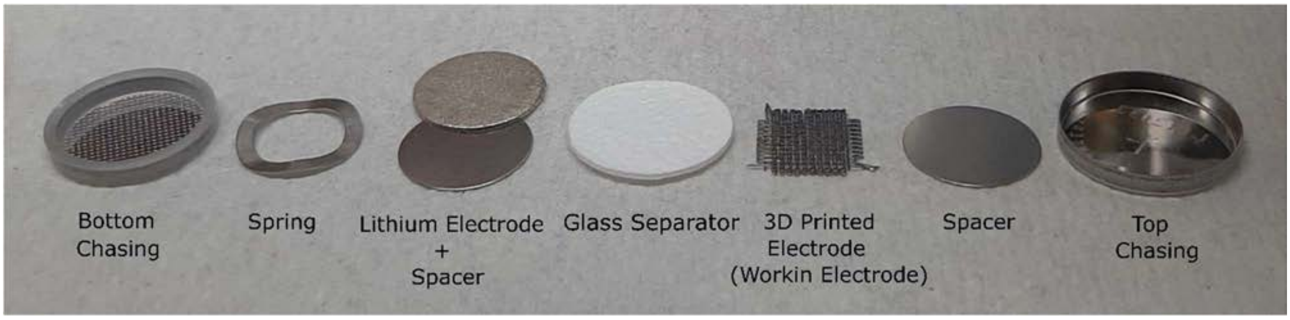

Figure 3.3 *elements of the lithium- ion half-cell assembly*

The assembled coin-cell is then hermetically crimped with a hydraulic compressor which applies a pressure of 0.9torr. The whole manipulation of the objects is carried out with plastic tweezers to avoid any shortcut that could compromise the performance of the system.

The electrodes produced with the traditional method and the 3D printed electrodes are likewise inserted into the cell.
The cell voltage is tested with a multimeter and it is expected to be around 2.5V.
Then it is removed from the glove box and cured for 20-24hours before the test in order to allow the electrodes to be fully embedded in the electrolyte, previously absorbed into the glass filter.

3.3 Galvanostatic Charge Discharge (GCD) Test

In order to determine the most important electrochemical properties of the analyzed materials, a galvanostatic charge discharge test is performed for a selection of samples, suitably chosen from the samples produced, in base of the results obtained during the investigation: this test is a powerful technique to determine the specific charge capacity and the efficiency of the cell.

The system used is an Arbin Instrument BT-2000 battery test device and the potential of the cells is monitored between 0.01V and 2.5V, cut-off voltage window, collecting the potential values with a scan rate of 0.005V, imposing constant current densities every 5 cycles.
The potential window is set to a maximum of 2.5V in order to stay in safe conditions, avoiding any degradation of the electrolyte, gas formation, temperature increases, which could decrease the life of the cell, or even produce explosions.
This technique should not be confused with the other typical analysis called Cyclic Voltammetry (CV) in which the potential is set and the current density is controlled.
The program is set with the following current densities during the charging process:

- 5 cycles at 50mA/g
- 5 cycles at 100mA/g
- 5 cycles at 150mA/g
- 5 cycles at 200mA/g
- 29 cycles at 50mA/g

The discharge process is carried out with a current density of 50mA/g in each cycle, with a reverse polarity with respect to the charge, pursuing an asymmetric charge/discharge program.
It is expected that by increasing the current density the specific charge, the capacity of the cell decreases because the lithium ions available in the electrolyte have no time to intercalate in the active site of the working electrode. Another typical phenomenon of the graphite electrode, with high current rates, is the exfoliation of the material with a consequent degradation. [50] In order to produce batteries with low recharging time, frequently required in the electronical application such as in hybrid or electrical vehicles, the batteries should work at high current rates, lacking of capacity; for this reason the research and development are focusing on the search of new materials capable of working in those condition, achieving high capacity results, in addition to constant efficiencies.

The final cycling of the program is set back to the initial current density (50mA/g) in order to verify the stability and the cyclability of the material after 20 cycles of lithiation and delithiation, which could have degraded the electrode material (especially at high current rates).

Figure 3.4 *Arbin Instrument BT-2000 battery test device*

The plot obtained from this analysis is a voltage against time, in fact the instrument constantly monitors the potential of the examined material compared to the reference electrode (lithium electrode) over time. This parameter depends on the internal resistance of the cell, as in a RC system with a current generator, and in particular:

$$V(t) = iR + tC \cdot i(V) \tag{3.1}$$

Where i is the current, R is the resistance, t is the time and C is the capacity.

In this research, the 3D printed electrodes have previously been tested with the program just mentioned, but the cyclability show is so fast that the experiment needs to be stopped from the beginning.

This is reasonable because, for this type of 3D-shaped electrodes, the solid electrolyte interface (SEI), which is created by the decomposition of organic and inorganic compounds during the firsts cycle, [51] needs more time to be formed: this is indeed fundamental in silicon electrodes because it regulates the lithium ion kinetic in the silicon, in addition to monitoring the electrons, transferred from the reference electrode, to be placed on the surface of the 3D sample.[52] The SEI, on the other hand increases the internal resistivity, being the major contribution to the irreversible charge in the first cycle, but it is also important, not only for the charging process, but also for the safety of the cell and for the cyclability degradation.[53]

In order to allow the SEI formation, the first discharging process is set to a current density of 3mA/g: the process is so low that it needs to be stopped after at least 1 day, going back to 50mA/g where the cell starts cycling properly. During the following discussion it is shown how the time of pre-set affects the final capacity results.

On the other hand, the traditional electrodes do not need any pre-set condition and they are performed starting directly from a current density of 50mA/g, due to their active thin layer, totally open to host lithium ion, producing directly the SEI.

The results of the GCD are discussed below, considering the charge capacity for each cycle and the respective efficiency. The cells compared have electrodes properly selected and the following section are divided as follow:

1. Different types of fillers in 3D printed electrodes: §3.3.1
   3D printed SiOC vs 3D printed SiOC + 23.1% Graphite/ 23.1%C.F./ 23.1%N.P., 70%p.;

2. Influence of the structural shape and of the pre-set conditions: §3.3.2
   3D printed SiOC + 23.1%, 50%p. vs 70%p vs 80%p.

3. Influence of the amount of filler in the 3D printed samples: §3.3.3
   3D printed SiOC + C.F. 23.1% 70%p. vs 3D printed SiOC + C.F. 28.6%, 80%p.;

4. Comparison of the innovative 3D printed electrodes with traditional electrodes: §3.3.4
   SiOC + 23.1% Graphite (3D vs traditional) and SiOC + 23.1%C.F. (3D vs traditional);

5. Etching with Ozone Procleaner and with Hydrofluoric Acid (HF): §3.3.5
   SiOC + 23.1% C.F.

3.3.1 Different types of fillers in 3D printed electrodes

First of all, it is interesting to investigate the different behavior of the materials produced in base of their filler used. For this reason, here are compared three different types of 3D printed electrodes with the same structural porosity, but with the three different types of filler added, even if with the same quantity (23.1%).

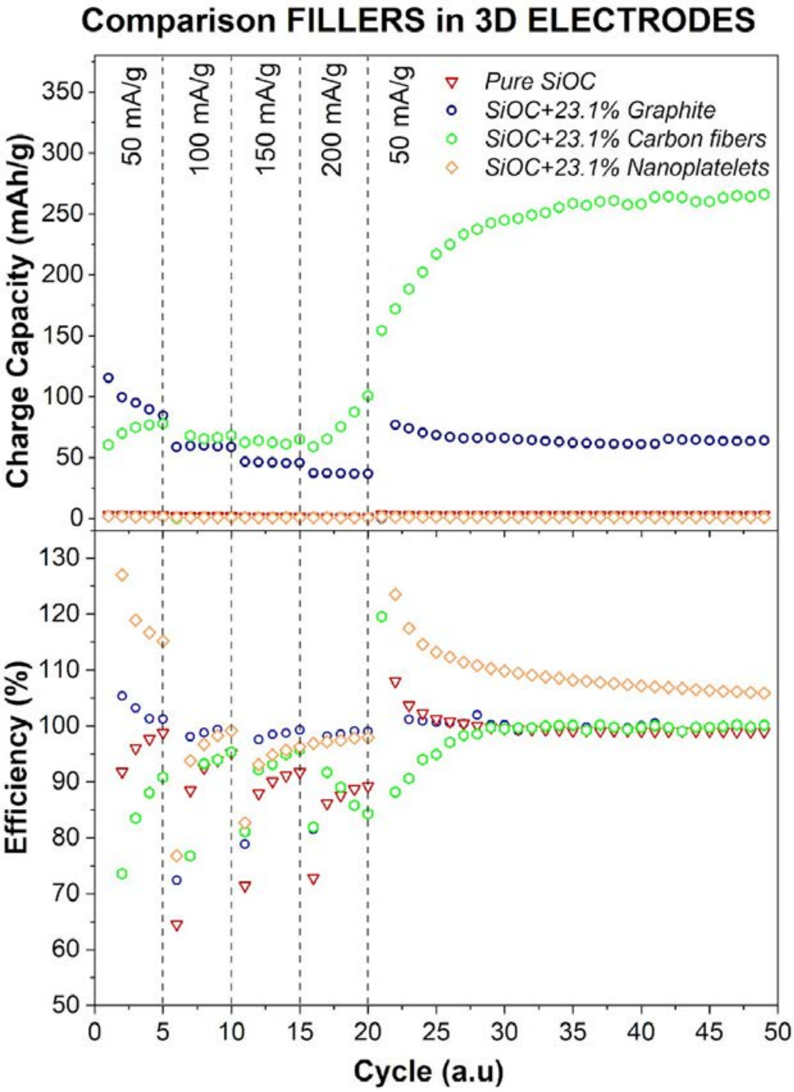

Figure 3.5 *GCD analysis: capacity and efficiency comparison between three electrodes made of SiOC + different fillers*

The 3D printed electrodes prepared with carbon fibers and graphite show the highest specific capacity results with a maximum charge capacity of 99.7mAh/g for the SiOC + 23.1%graphite and 266mAh/g for the SiOC + 23.1%carbon fibers.

The better results obtained with these two fillers are certainly due to the higher electrical conductivity enhanced by introducing the carbon sources in the material, which allow the electrons to place themselves on a higher surface of the specimens, attracting more lithium ions to the surface.

Table 3.1 *Values of specific capacity (max and mean), mean efficiency and max volume capacity for different SiOC+filler electrodes*

ELECTRODE MATERIAL	*MAX SPECIFIC CHARGE CAPACITY (mAh/g)*	*MEAN CHARGE CAPACITY (mAh/g)*	*MEAN EFFICIENCY (%)*	*MAX VOLUME CAPACITY (mAh/cm^3)*
SiOC	3.24	2.26	99.69	0.46
SiOC+23.1%Gr.	119.6	61.59	98.45	35.27
SiOC+23.1%C.F.	265.97	170.9	93.5	50.7
SiOC+23.1%N.P.	1.91	0.93	124.6	1.45

Moreover, the highest values obtained with the carbon fibers are expected (from the SEM analysis) and can be traced back to the cracks present in the surface, which have enormously increased the surface area achievable by the lithium ions, which are intercalated in the electrode material, even if the mechanical properties of the sample are surely decreased. However, this material does not exhibit a stable behavior, indeed the specific capacity slightly decreases with higher current densities, but at 200mA/g it suddenly increases achieving the best results in the last 29 cycles, when the current density returns to 50mA/g. This can be explained by an expansion of the material due to the ion absorption, which allows to further increase the surface area, gaining higher values. The efficiency of this sample also fluctuates very easily in the first 20 cycles, suggesting unstable conditions during the cycling process, resulting in less fading.

On the other hand, the stability of the cycles for the graphite electrodes is better, showing high efficiencies (mean of 98.45%): its trend is more predictable, in fact the specific charge capacity decreases with the increase in the density of the current imposed, as expected, because of the shorter time permitted to the lithium ions to intercalate. Furthermore, it is possible to see how the cell reduces its charging capacity going back to 50mA/g in the last 29 cycles, with results similar to the 5 cycles previously performed at 100mA/g: this behavior is due to an electrode degradation.

The nanoplatelets are the only filler which does nor cycle at all and this is identified both for the negligible specific capacity and for the poor efficiency achieved. This is possibly due to the ineffective ability of the electrolyte to produce the SEI on the surface and, as it's possible to understand later in the discussion of other samples, it has been demonstrated that the time of pre-set at low current density affects the results. Based on this, the nanoplatelets samples, which were tested with the two different amounts of 23.1% and 33.3%, are here pre-set for a time of 24hours, probably not enough for the material at hand.

The loss of capacity of the first cycle, correlated with a loss of efficiency, which would be significant to understand the SEI formation, is not here discussed for the graphite and nanoplatelets fillers, because all the half-cells are tested after a pre-set at lower current density. For this reason, here the differential capacity plot not reported, in which it should be possible to identify, in the first cycle, the SiOC lithiation, the Li_xSiOC formation, and the SEI formation corresponding the reduction peaks in the lithiation process, and an oxidation during delithiation.[54]
It is remembered that the delithiation occurs during charging, while the lithiation occurs during discharging, just because a half-cell is treated in this study.

On the other hand, here is reported the differentiated analysis, which is extrapolated from a manipulation of the data obtained with the GCD, of one of the SiOC+carbon fiber samples and in particular of the best sample analysed: SiOC+ 23.1% C.F: this half-cell, in fact, shows a reduction in efficiency in the first cycles, due to the SEI formation.
Only the 1st , 2nd and 49th cycles are studied.

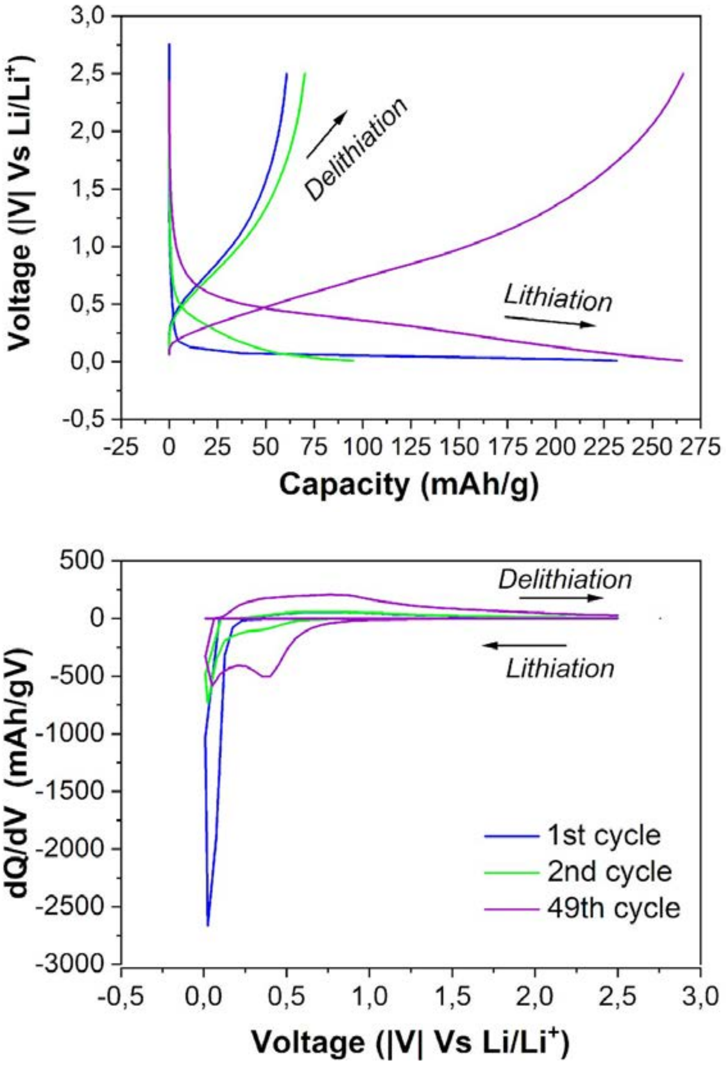

Figure 3.6 *Differential capacity analysis for the first, second and last cycle of SiOC+28.6% carbon fibers*

As shown in the analysis, the peak present in the 49th cycle at 365mV is related to the LixSiOC lithiation, while the broad peak at 500mV is related to its delithiation. In the 1st and 2nd cycle there is a single peak at 27mV which is due to the carbon lithiation. The SEI formation happens in the second cycle with a peak at 520mV during lithiation. The other peaks present are in accordance with the literature.[25]

The other graphs of differentiated capacity, for the materials produced with this filler, are similar to this just analyzed, as expected.

The specific capacity results obtained should be compared with the commercial graphite electrodes produced with the traditional method which provide specific capacities of 372mAh/g.[20] The results obtained with the 3D printed electrodes are surely minor than the traditional values, but if is considered the total capacity achievable with these samples, the circumstances are reversed, even if the total weight of the electrode would affect the final weight of the batteries.

On the other hand, the low specific capacity of the 3D printed electrodes is surely caused by the low surface area of the material; the electrical conductivity of the active material is measured in the three samples, demonstrating the active role of this element in the electrodes, which promotes the electrons to achieve the active material, increasing the intercalation of the ions. The resistivity of the materials produced is here reported:

Table 3.2 *Values of electrical resistance for the three electrodes produced with the same amount but different type of filler*

SiOC+Graphite 23.1%	SiOC+Carbon Fibers 23.1%	SiOC+Carbon N.P. 23.1%
0.132 kΩ	28.1 kΩ	1.117 kΩ

As it is possible to see from the table, the graphite seems to be the most conductive element but, on the other hand, the carbon fiber samples have a higher surface area, achieving better results even if it is the most resistive. The material with carbon nanoplatelets seems promising because it has the proper conductivity, but it must be performed in different conditions.

The obtained volume capacity is calculated considering the electrodes as bulk samples with a thickness of 0.075cm and a square area respectively of 1.4x1.4cm^2 for the carbon fiber samples and 1.2x1.2cm^2 for the graphite specimens. In reality the volume should be a little lower than the one considered, increasing even more the volume capacity calculated. The values are not comparable with the traditional silicon electrodes which show values over 393mAh/cm^3 [54], but are promising compared with the values obtained for 3D printed electrodes published recently, which show an anode achieving specific capacity around 7mAh/cm^3 at a current density of 20mA/g,[55] compared to the maximum values achieved in this research of 50.7mAh/cm^3 at a current rate of 50mA/g for SiOC+23.1%C.F..

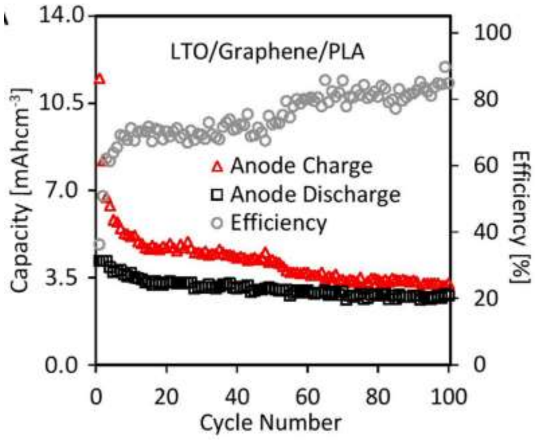

Figure 3.7 *Specific capacity for 3D printed anodes reported in literature*[55]

3.3.2 Influence of the structural shape and of the pre-set conditions

This section shows the results of the three different types of structural shapes (50-70-80% porosity) using the same material: SiOC+23.1%Graphite.

The behavior of this sample has already been studied in the previous section §3.3.1 but here is shown the result for another half-cell prepared with the same material and shape (70%), using a different time of the pre-set process, demonstrating how this affects the final results related to the specific capacity.

The three electrodes analysed are:

- SiOC+23.1% Graphite 50%structural porosity;
- SiOC+23.1% Graphite 70%structural porosity;
- SiOC+23.1% Graphite 80%structural porosity.

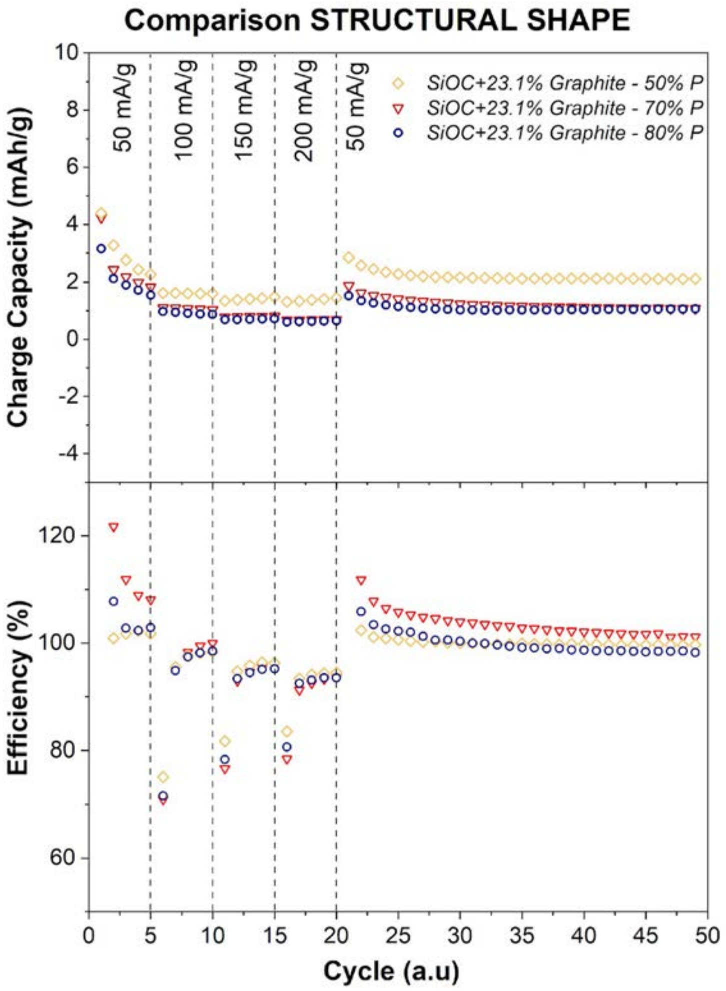

Figure 3.5 *GCD analysis: capacity and efficiency comparison between three electrodes made of SiOC+ graphite (same amount) with different structural porosities*

The specific capacities obtained are very small, compared to the values obtained with the previous sample in §3.3.1 and this is attributable to the shorter pre-set time, opportunely set to study the influence of this process on the final results.

In particular the sample analyzed is discharged (lithiated) at 3mA/g for 81.5hours, allowing more time to stabilize the conditions of working, forming the SEI on the surface of the working electrode, while the second electrode, here evaluated, is pre-set for one night (12hours), achieving a much smaller specific capacity from the first cycles (2.43mAh/g of the second cycle instead of 119.6mAh/g, approximately 2% of the first result).

The same pre-set time of the last sample is also used for the electrodes composed of carbon fibers, but in this case the values obtained are remarkably better, compared to the graphite filler, as shown in the previous section §3.3.1, demonstrating that the time of pre-set does not only influence the result, but it also depends on the type of filler used in the material.

This also explains the behavior of the carbon nanoplatelets filler, which shows low capacities with a one night pre-set, as used for the carbon fibers samples.

Table 3.3 *Values of specific capacity (max and mean), mean efficiency and max volume capacity for SiOC+ graphite electrodes with different structural porosity*

ELECTRODE	*MAX SPECIFIC CHARGE CAPACITY (mAh/g)*	*MEAN CHARGE CAPACITY (mAh/g)*	*MEAN EFFICIENCY (%)*	*MAX VOLUME CAPACITY (mAh/cm^3)*
50% Structural Porosity	3.26	2.02	99.58	14.95
70% Structural Porosity	2.43	1.19	103.56	8.31
80% Structural Porosity	2.13	1.04	100	5.61

This table does not show the values for the first cycle (which are the maximum) because those results are invalidated by the previous pre-set program, showing a higher charging capacity than the discharge capacity. This happens because the lithium ions are already intercalated in the active material and for this reason they need to be discarded.

The results seem somehow correlated to the shape of the sample, even if the values are not so different from each other. If the structure has more porosity in the same space, it means that the material used is less compared to the others, moreover the surface area of those samples should decrease proportionally with the increase of the porosity. This seems to be verified by the results, indeed the 50% porosity has higher specific capacity compared to the other structures. Nevertheless, the difference of the surface area between the three structures is not so emphasized and the results of the following half-cells investigated could be compared with each other, even if with different structural porosity (especially if compared between 70 and 80% where the difference is moderate, as seen in the Charge/Cycle scattered plot).

By the way, the three samples follow the cyclability expected, diminishing the specific capacity with an increase in current density, with a large recovery of charge going back to 50mA/g, attesting the low degradation of the material during the cycling process.

The very high efficiency is always guaranteed, even if there are fluctuating values especially changing the current density, ascribable to instrumental errors.

Furthermore, the specific volume capacities are still reasonable results compared to the current 3D printed samples studied in the scientific community, in particular for a structural porosity of 50% and 70%.

3.3.3 Influence of the amount of filler in the 3D printed samples

The amount of filler is surely decisive in the results of the final capacity of the half-cell and, in order to investigate this behavior, two samples with a different amount of filler are here investigated, in particular choosing the best sample performed till now:

- 3D printed SiOC + C.F. 23.1% 70%p.
- 3D printed SiOC + C.F. 28.6%, 80%p.

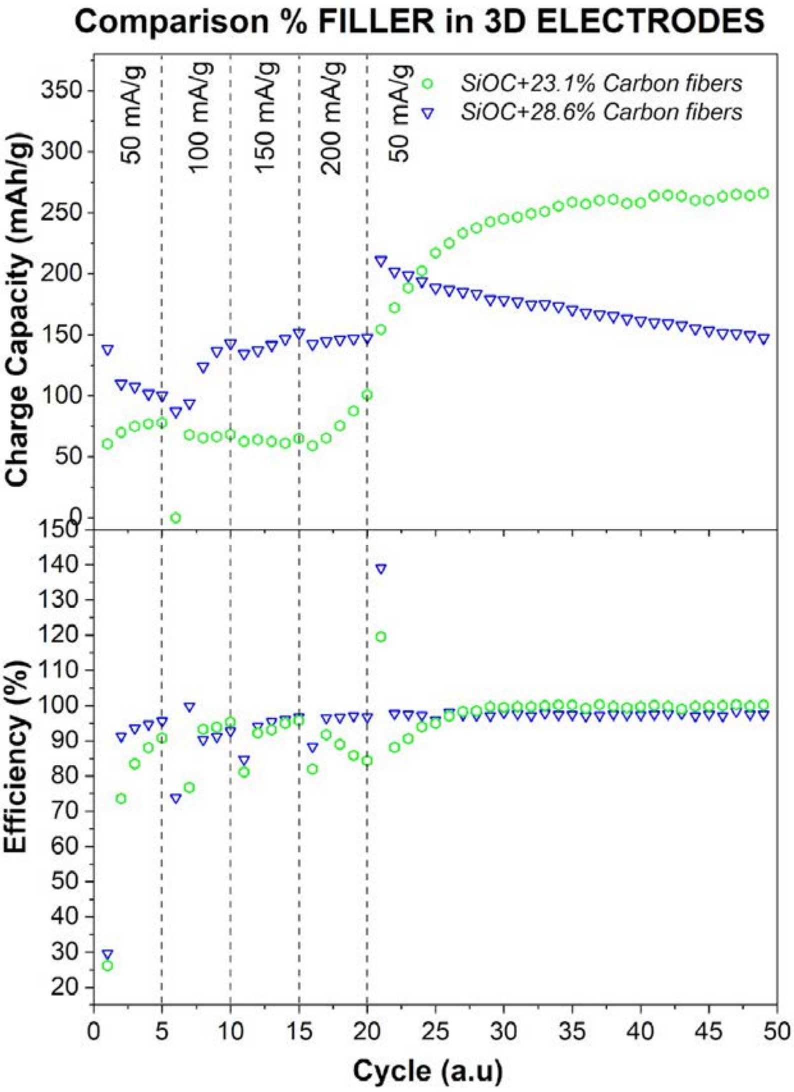

Figure 3.6 *GCD analysis: capacity and efficiency comparison between two electrodes made of SiOC+ carbon fibers with different amount of filler*

In this way it is possible to see that the results of the charge capacity achieved with a higher amount (28.6%) of filler, are slightly higher compared to the results obtained with 23.1%,up to high current densities (200mA/g) but, going back to 50mA/g, the situation is overturned and the material with less filler is showing higher results because of its less degradation.

Moreover, the material with an amount of 23.1% increases its specific capacity over cycles due to the achievement of stabilizing electrochemical conditions, demonstrated by the inconstant efficiency before 25 cycles (mean 84.8%), while the material with higher amount of filler seems more stable up to the beginning (mean 89.7%). Furthermore, the higher values reached with a low quantity of carbon fibers, going back to the starting current density condition, could be caused by higher expansion of the material.

These concepts prove that the influence of the amount of carbon fibers surely depends on the electrical conductivity of the material (proportional to the carbon amount), but at the same time the material seems to degrade more easily with higher amount of filler, achieving higher fading over 20 cycles. In this way, a good compromise between high conductivity and stable cyclability should be found.

Table 3.4 *Values of specific capacity (max and mean), mean efficiency for SiOC+ carbon fibers electrodes with different amount of filler*

ELECTRODE MATERIAL	***MAX SPECIFIC CHARGE CAPACITY First 20 cycles (mAh/g)***	***MEAN SPECIFIC CHARGE CAPACITY After 20 cycles (mAh/g)***	***MEAN EFFICIENCY First 20 Cycles (%)***
SiOC+23.1%C.F.	101	242.8	84.8
SiOC+28.6%C.F.	151.5	171.9	89.7

The more stable condition of the 23.1%C.F, going back to 50mA/g, could be attributable to the higher amount of SiOC in the material, which encourages the ion conductivity, as already mentioned in section §2.4.2.

3.3.4 Comparison of the innovative 3D printed electrodes with traditional electrodes

In order to verify if the material is competitive with the actual electrodes industrially used, the traditional electrodes are manufactured as described in §3.1.1 for two different materials:

- SiOC + C.F. 23.1%;
- SiOC + Graphite 23.1%.

Both materials are also compared with the equivalent 3D printed electrodes, previously studied.

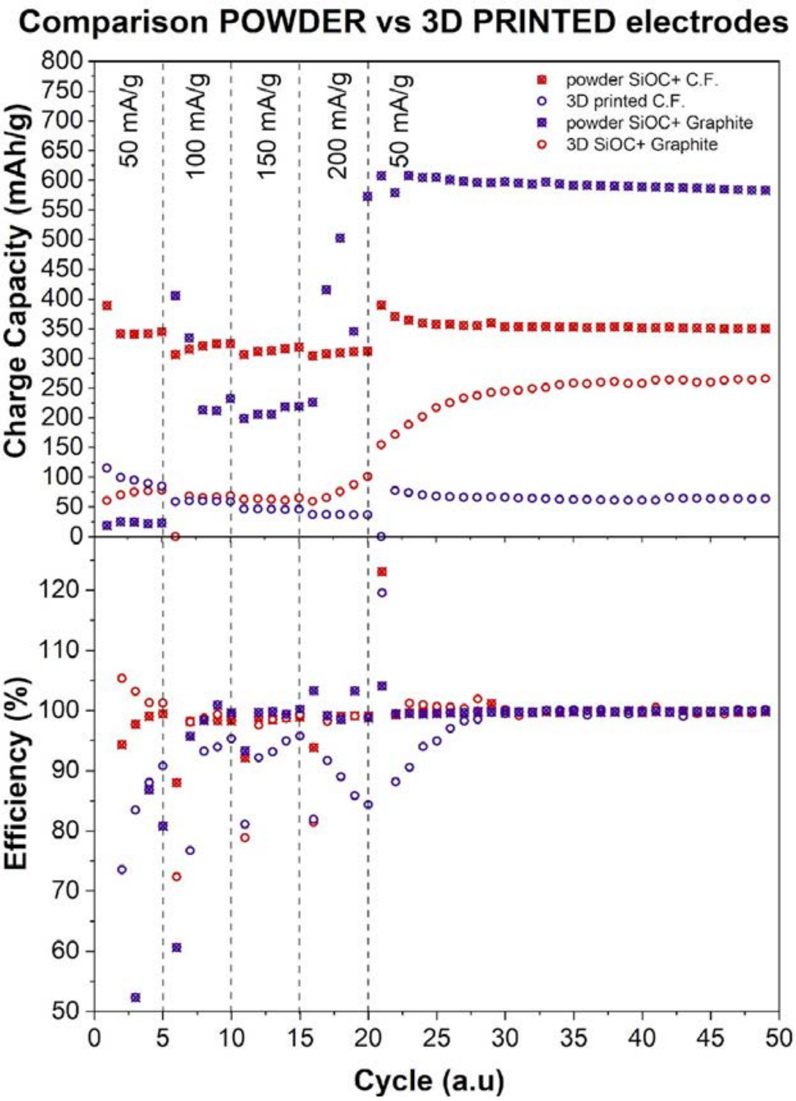

Figure 3.7 *GCD analysis: capacity and efficiency comparison between 3D printed and traditional electrodes*

As it is illustrated from these results, the two traditional electrodes show specific respectable values of capacity compared to the graphitic electrodes produced nowadays (372mAh/g), as it is demonstrated with silicon electrodes in several works previously published.[54,56 , 57]

Table 3.5 *Values of specific capacity (max and mean), mean efficiency for 3D printed and traditional SiOC+ graphite/carbon fibers electrodes*

ELECTRODE MATERIAL	*MAX SPECIFIC CHARGE CAPACITY (mAh/g)*	*MEAN CHARGE CAPACITY (mAh/g)*	*MEAN EFFICIENCY (%)*
Powder-SiOC+Graphite	607.63	444.96	94.54
3D-printed-SiOC+Graphite	119.6	61.59	98.45
Powder-SiOC+C.F.	389.97	342.33	98.18
Powder-SiOC+C.F.	265.97	170.9	93.5

The 3D printed SiOC+Carbon Fibers sample produced has values not very different from the equivalent powder sample, compared to the 3DvsPowder of the SiOC+Graphite.
This well demonstrates that the material with the carbon fibers could at most gain values around 390mAh/g, similar to the graphite electrodes used nowadays, because the cracks produced increase the surface area, enhancing the specific capacity values; on the other hand, the graphite 3D-sample, not only has low values compared to equivalent SiOC+Carbon Fiber sample, but it is much more lower than the equivalent powder sample.
For this reason the SiOC+Graphite material is a more promising material, but its 3D shape does not perform the best solution to exploit its potential, while the material with carbon fibers, even if it is less encouraging than the other, its 3D shape gains converging values to the equivalent powder, and even more than the 3D SiOC + graphite.

Moreover, the carbon fibers sample shows a more stable cyclability compared to the graphite powder sample, but also compared to the 3D carbon fibers sample; the 3D graphite sample is more stable compared to its equivalent powder sample and to the 3D carbon fiber sample.

The graphite sample, in order to achieve the best result, should be pre-set for a longer time, as demonstrated in §3.3.2 and the surface area should be increased.
Nevertheless, in the following section the 3D SiOC + Carbon Fibers sample is etched in order to create much more open pores on the structure, further improving its surface area and achieving results much more similar to the equivalent powder sample.

3.3.5 Etching with Ozone Procleaner and with Hydrofluoric Acid (HF)

As the first option for the treatment of the samples, an UV/ozone Procleaner system (BioForce Nanosciences, USA), is used in order to oxidize the surface, creating more superficial roughness, avoiding any destructive method that could further damage the electrodes shape, which is already brittle.

Figure 3.8 *BioForce Nanosciences UV/ozone procleaner*

The following samples are treated for 3hours and the weight is measured before and after the etching treatment, without observing any difference (<0.3mg):

- 3D SiOC + 28.6% C.F._80P
- 3D SiOC + 33.3% N.P._80P

The N.P. sample is treated only to analyze the surface before and after the treatment, because it has the smoothest surface compared to the other samples and the roughness could be more visible with an optical microscope. The sample is then not analyzed because of the low capacity results obtained before; indeed, this sample needs more study to be performed properly.

The microscope analysis does not show any superficial difference before and after the treatment, as shown in the following pictures.

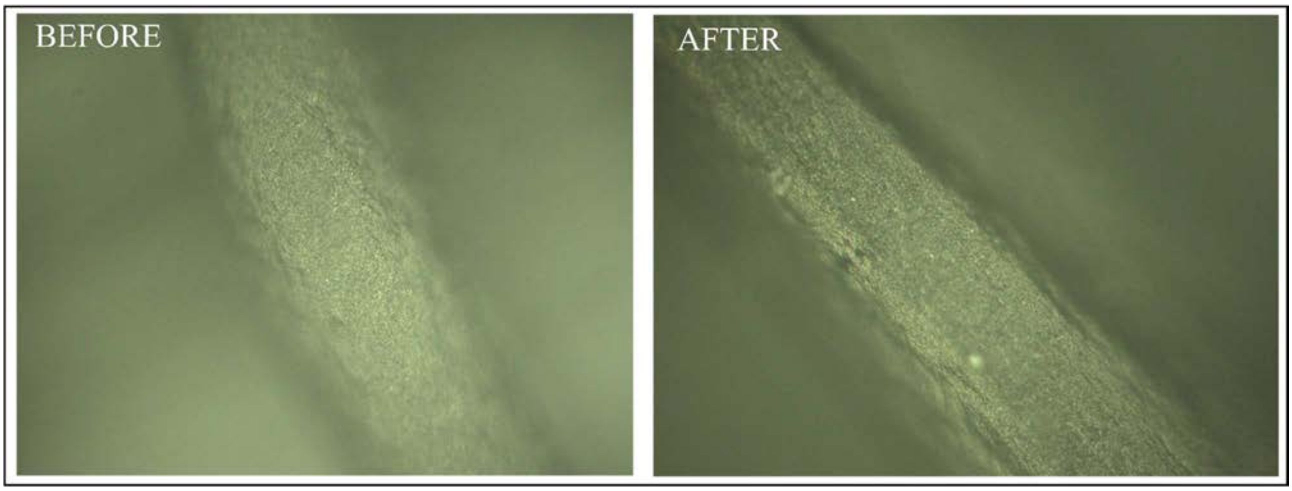

Figure 3.9 *Microscope analysis: filament morphology compared before and after the UV/ozone attack*

The procleaner system is generally used to remove the impurities from the surface of the material due to the UV light in two specific wavelengths, 185cm^{-1} and 284cm^{-1}, generated by a mercury lamp that allows to reduce the molecules on the surface. Atmospheric oxygen (O_2) is decomposed into atomic oxygen (O), by an irradiation of 185cm^{-1}, which combines with the oxygen molecules (O_2) creating ozone O_3; this reacts with the fragments of the waste organic contaminants that split them.

The 284cm^{-1} wavelength, at the same time, decomposes the ozone producing oxygen atoms and atmospheric oxygen: the atomic oxygen (O) is particularly reactive and it oxidizes the fragments of the inorganic materials generating volatilized compounds.

During this process it is assumed that also part of the Si-O bonds, with an energy of 453kJ/mol, and the Si-C, with an energy of 360kJ/mol, would be removed by the energy produced by the 185cm^{-1} UV irradiation which has 647kJ/mol of energy, producing superficial roughness. (values of the bonds energy reached from “Chemistry 5th Edition” by Steven S.Zumdahl and Susan A.Zumdahl)

This method is generally used to clean and sterilize the contaminated surfaces, or at least oxidizing the surface in order to guarantee the proper external layer for the following treatment such as coatings and thin film depositions.

It is also used to produce activating surfaces due to the etching on polymer materials, besides curing due to the UV action.

Two lithium batteries with the same material (40%C.F. 80%P) are here compared: one treated on the uv/ozone procleaner and the other one as a virgin material. They are performed with the same program, set for the previous batteries, but for a maximum of 35 cycles.

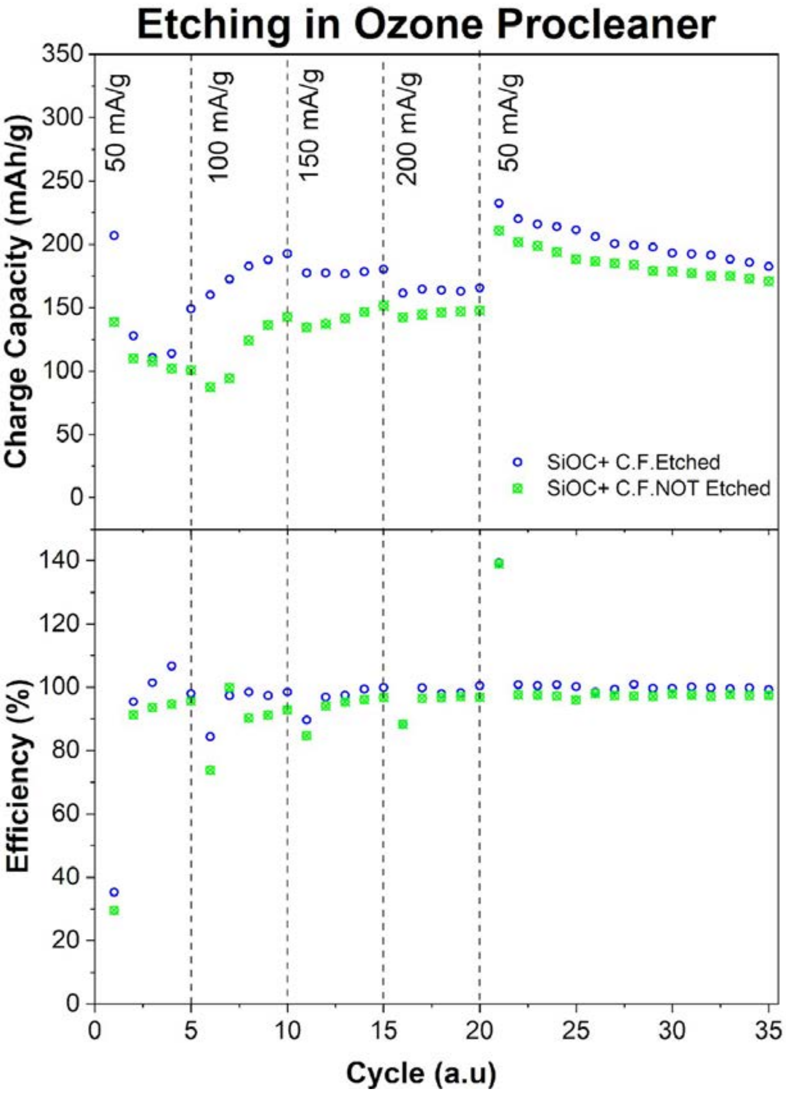

Figure 3.10 *GCD analysis: capacity and efficiency comparison between SiOC+CF samples etched and not etched with UV/ozone attack*

The etching in the ozone procleaner increases the material capacity a little, but it is still similar, especially when the half-cell gains stable condition after 20 cycles.

These results are hardly ascribable to the increase of the nanosized roughness, due to the treatment, because the surface area increases insignificantly.

For best results, the etching with hydrofluoric acid is considered the best option to attack the SiOC matrix, creating a higher porosity in the structure of the material: several studies have shown that by creating micropores (<2nm), higher than the dimension of the ions, the capacitance of the Electrical Double Layer Supercapacitors (EDLS) increases,[29] and the same is expected in the cells. The mesoporous, on the other hand, also contributes to higher values to the enhanced kinetic properties, achieving higher lithium-ion conductivity.
The porosity is achieved by the attack of the hydrofluoric acid, which removes only the silica (SiO_2) present in the microstructure, leaving behind a C-based porous structure.

The treatment used is an etching in 20% aqueous HF solution for 6 hours, after the pyrolysis treatment, with subsequent dry process at 80°C. [58]
The specimen treated is:

- 3D SiOC + 26.1%C.F._70P.

The electrode is analyzed in the same condition as the virgin samples, previously investigated in §3.3.1.

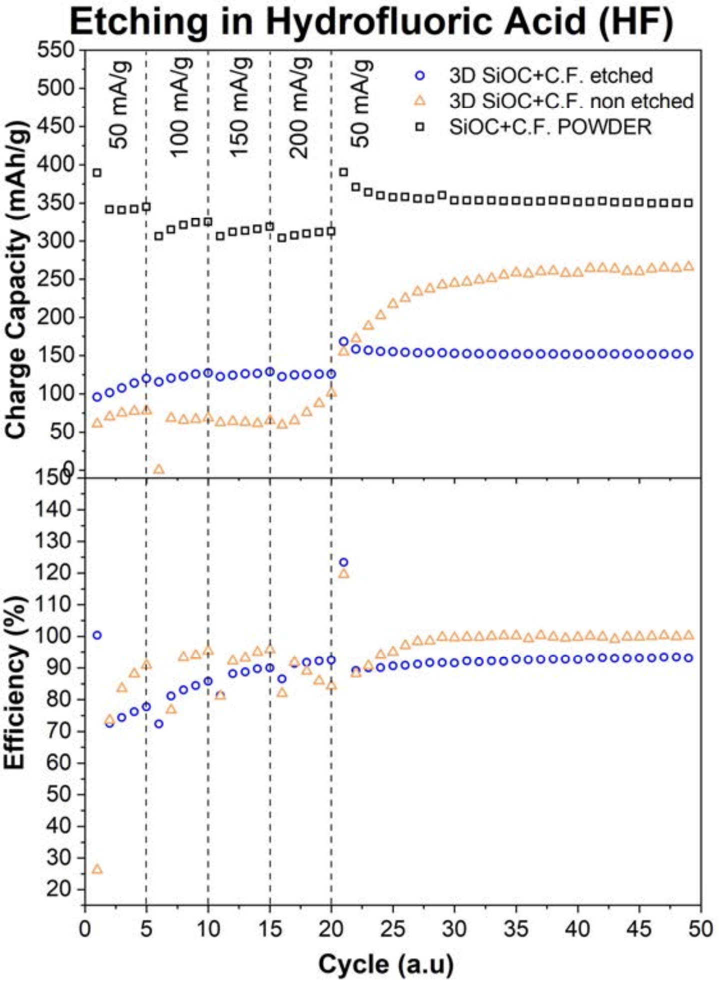

Figure 3.11 *GCD analysis: capacity and efficiency comparison between SiOC+CF samples etched and not etched with HF attack, and SiOC+C.F. traditional electrode*

The etched sample performs slightly better results in the first 20 cycles, achieving also high current density (200mA/g), but going back to 50mA/g the virgin electrode still shows better results.

The unmarkable variation on the specific capacity, as hoped, is possibly due to the poor efficiency of the prepared HF attack, because of the high chemical resistivity of the SiOC matrix, in addition to the non-existence of SiO_2 nanodomains due to the heat treatment of pyrolysis at 1000°C. [7]

3.4 Financial statement

The traditional process needs more steps to produce the electrode, compared to the 3D printed method, wasting more time and materials, which are related with economic loss.
Here is a financial statement which considers only the extra materials used, excluding the wasted time and the dryer consumption, with the following consideration:

- calculation of the saving of material per electrode;

- energy saving for each 3D-printed cell, considering the higher energy achieved for both the electrodes (multiplying the capacity for the potential) differentiating and multiplying for the electricity cost (0.000012USD/kWh);

- calculation of the saving cost of the material for producing 1kWh, considering the total amount of cells needed for producing 1kWh and multiplying the difference for the material saving of each 3D-printed cell.

The report is conduced considering the two best materials in terms of charge capacity:

- 3D printed SiOC + 23.1% Graphite vs Traditional SiOC + 23.1% Graphite;
- 3D printed SiOC + 23.1% Carbon Fibers vs Traditional SiOC + 23.1% Carbon Fibers.

Table 3.6 *Cost saving for cell considering only the material cost*

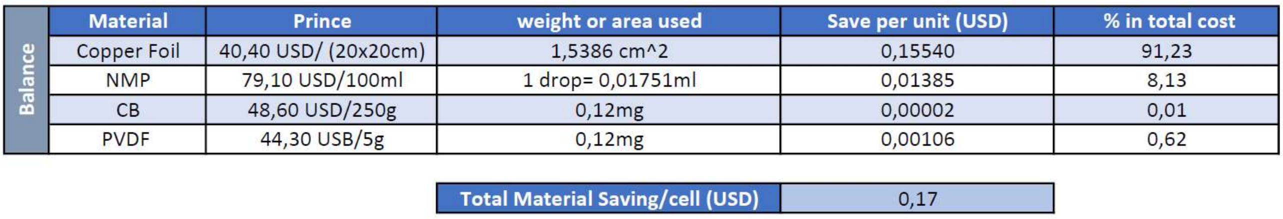

	Material	Prince	weight or area used	Save per unit (USD)	% in total cost
Balance	Copper Foil	40,40 USD/ (20x20cm)	1,5386 cm^2	0,15540	91,23
	NMP	79,10 USD/100ml	1 drop= 0,01751ml	0,01385	8,13
	CB	48,60 USD/250g	0,12mg	0,00002	0,01
	PVDF	44,30 USB/5g	0,12mg	0,00106	0,62

Total Material Saving/cell (USD)	0,17

As reported in the table, regardless of considering the type of electrode, the total material saving for cell is about 17centUSD, which is surely a high cost considering an industrial production. Moreover, two electrodes are provided in a cell, so the cost is at least doubled.

3.4.1 SiOC + 23.1% Graphite electrode

Considering in particular the SiOC + 23.1% Graphite electrode, the electricity cost saving and the cost saving of the material/kWh are calculated as reported in the following table:

Table 3.7 *Electricity cost saving per cell and material cost saving/kWh considering SiOC+ graphite electrode*

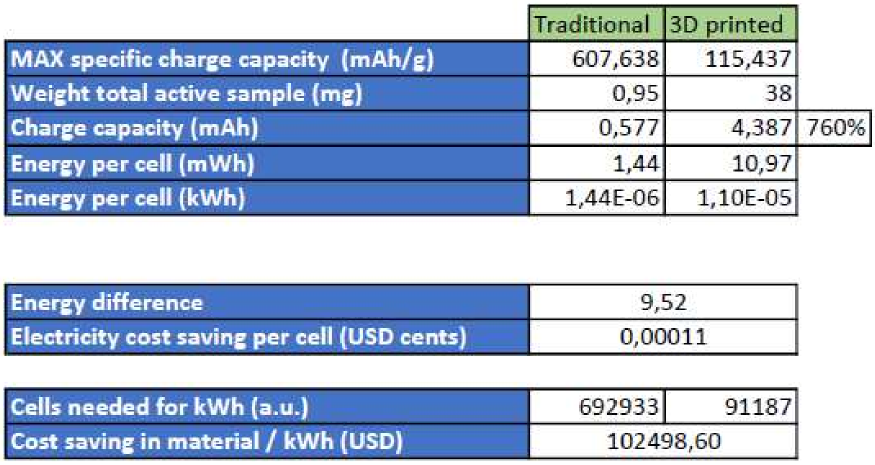

	Traditional	3D printed	
MAX specific charge capacity (mAh/g)	607,638	115,437	
Weight total active sample (mg)	0,95	38	
Charge capacity (mAh)	0,577	4,387	760%
Energy per cell (mWh)	1,44	10,97	
Energy per cell (kWh)	1,44E-06	1,10E-05	

Energy difference	9,52
Electricity cost saving per cell (USD cents)	0,00011

Cells needed for kWh (a.u.)	692933	91187
Cost saving in material / kWh (USD)	102498,60	

Even if the specific charge capacity of the 3D printed electrode is less than the traditional one, the total charge capacity is abundantly higher (760% more capacitive).

For this reason one 3D printed cell is able to produce a total energy of one order greater than a traditional electrode ($\approx 10^{-5}$ kWh instead of $\approx 10^{-6}$ kWh); the electricity cost earned in producing a 3D-printed cell is about (0.00011centUSD).

Considering the number of cells needed to produce 1kWh, the saving on material cost is calculated by giving 102,498.60USD.

3.4.2 SiOC + 23.1% Carbon Fibers electrode

Using a carbon fiber electrode with 23.1% of filler the saving costs are as follow:

Table 3.8 *Electricity cost saving per cell and material cost saving/kWh considering SiOC+ carbon fibers electrode*

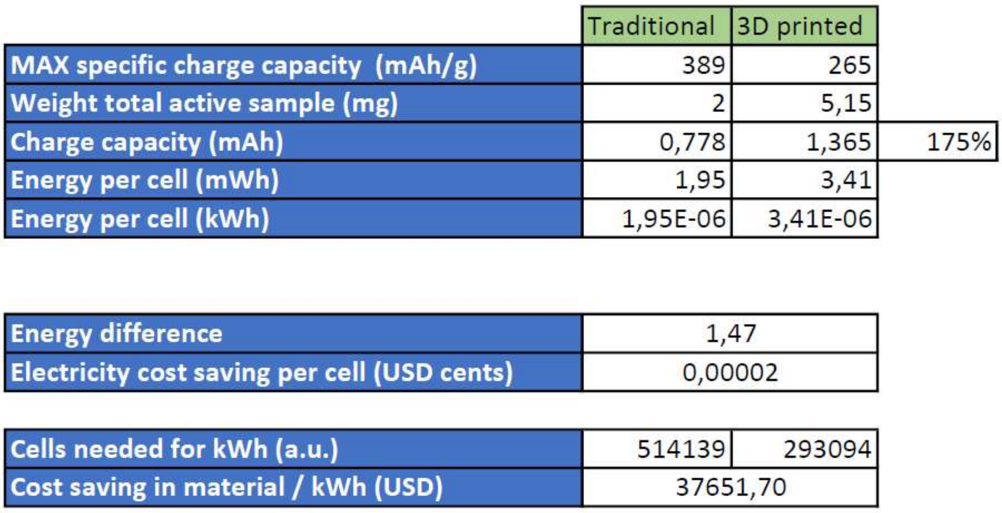

	Traditional	3D printed	
MAX specific charge capacity (mAh/g)	389	265	
Weight total active sample (mg)	2	5,15	
Charge capacity (mAh)	0,778	1,365	175%
Energy per cell (mWh)	1,95	3,41	
Energy per cell (kWh)	1,95E-06	3,41E-06	

Energy difference	1,47
Electricity cost saving per cell (USD cents)	0,00002

Cells needed for kWh (a.u.)	514139	293094
Cost saving in material / kWh (USD)	37651,70	

The total charge capacity of the 3D printed electrode is, as expected, 175%, higher than the traditional one. The energy per cell is proportional to the charge capacity, as seen above, but their difference is lower than the carbon graphite electrodes; in fact, even if the specific charge capacity is higher for this 3Dprinted electrode, the total charge capacity is less deviating from the traditional one. For this reason, the electricity saving per cell is 0.00002centsUSD.

Similarly, the material cost saving for kWh is about 37,651.70USD, which is not so high as the previous cell, but it is still a great saving.

Conclusion and Future Development

This thesis would prove the efficiency in manufacture siliconoxycarbide 3D-printed electrodes for energy storage devices, such as batteries, differentiating from the SiOC electrodes used nowadays, produced with additional procedures and wasting time.

The work has well demonstrated the feasibility of using direct ink writing (DIW), as a manufacturing technology, in producing the final ceramic matrix composite (CMC) shapes starting from preceramic polymer loaded with different types of carbon sources, which enhance the electrical conductivity in the final material. The rheology of the ink prepared with commercial H44 has been studied in order to pursue a proper solvent amount in future preparations. It has also been investigated the appropriate mixing of preceramic polymer and solvent (isopropanol), adding graphite powder, doing a research which may be also useful in other applications.

The pyrolysis conduced in nitrogen atmosphere, i.e. inert environment, at 1000°C has led to dense structures, except for the material loaded with carbon fibers as filler, which has shown cracks on the surface, due to the anisotropic thermal expansion.

The materials have been analysed chemically and physically (TGA, XRD, FTIR, RMN), proving the chemical microstructure described in the literature, at 1000°C of pyrolysis temperature : the ceramic material comprises a SiOC matrix, where there are embedded the graphitic phase of the filler (except for the carbon fibers, which are amorphous) and the turbostratic carbon, produced during the heat treatment, after that all the organic compounds ($-CH_3$ and $-C_6H_5$) present at the side of the silicon-oxide backbone have been removed.

The samples produced are also analysed with a SEM analysis proving the cracks on the material containing carbon fibers, as expected, and a dimensional analysis has been conduced to understand the variability of the shrinkage caused by the pyrolysis treatment: the most reliable structural shape is the one with a structural porosity of 80%, regardless of the filler used, even if with the carbon fibers the shape is expanded instead of shrinking, for the aforementioned reason. The carbon nanoplatelet filler has demonstrated to be the most reliable filler, showing a perfect shape retention considering the 80% porosity structure.

The samples are then used as electrodes for half-cells in order to analyse the electrochemical properties of the produced materials.

Coin half-cells have been assembled in order to produce future lithium-ion batteries and a Galvanostatic Charge Discharge (GCD) test has been performed at different current rates (with the same program for all the samples tested), giving results in term of charge capacity, efficiency of the charge-discharge cycle and cyclability.

The cells are firstly characterized on the base of the filler used (graphite, carbon fibers, nanoplatelets), showing since the beginning the high capacity achievable by adding graphite and carbon fibers, compared to the not loaded SiOC material. The highest values are achieved by adding carbon fibers (265.97mAh/g) thanks to the higher superficial area available, due to the cracks formed in the surface, allowing the intercalation of a higher quantity of lithium-ions in the electrode microstructure. Moreover, during the set program, this filler has shown a strong increase of capacity going back to the initial current rate of 50mA/g, demonstrating the opening of the material due to the intercalation/deintercalation process. This aspect should be studied deeply in future to understand if it is due to the degradation of the material or if it gains a stable condition over a certain amount of cycles, guaranteeing a stable shape for a long-term cycling. Carbon nanoplatelets have revealed to be useless in the SiOC matrix in terms of capacity, even if it could be related to an ineffective formation of a solid electrolyte interface (SEI): in this work it has been demonstrated how the time of pre-set of the electrodes, and so the SEI formation at the first cycle, is fundamental, being achievable only with low current rate for this material in this particular shape (especially with graphite).

The efficiency achieved for the graphite samples is the best, because of the stability shown during cycling.

The different structural shape of the electrodes and the different amount of fillers have not shown high diversity from each other to prove an evident correlation with these factors: in particular, in a stable regime (testing at 50mAh/g over the 20th cycle), the capacity achieved with a higher amount of filler seems inferior, probably because of the well-known higher capacity of SiOC compared to graphite and the related lower amount in the material.

The capacity values achieved are still low compared to the current graphite electrodes (370mAh/g) but are still higher compared to 3D printed electrodes recently produced and published in papers.

Anyway, the loss of performance is ascribable to a shorter pre-set time, combined with a low surface area, and not to the nature of the material, here demonstrated by testing the same material in traditional manufactured electrodes. In future, it should be interesting to evaluate the proper time of pre-set and study ways of increasing the structural porosity, in order to produce electrodes with higher surface area. For this purpose, in this research, an etching with ozone UV light and HF has been conduced, without improving the results already obtained, because of the non-existence of SiO_2, easily dissolvable in that acid attack. For this reason, a higher temperature of pyrolysis should be conduced, even if the probable SiC precipitation discourages the electrical conductivity, in any case favoured by the carbon fillers.

A basic economical statement has then been conduced to prove the saving achievable in terms of materials and energy consumption, compared to the traditional electrodes, promoting the research for future studies.

Acknowledgement

I had the opportunity to study a subject that has always excited me, to expand my knowledge and take part in this project; above all thanks to the support and sacrifices of my family, to whom I am very grateful.

I would like to thank my tutors Prof. Paolo Colombo, Dr. Gurpreet Singh and Dr. Giorgia Franchin for the opportunity they have given me to take part in this project, which has allowed me to grow not only scientifically, in a wonderful professional environment, but also personally. Furthermore, I would like to thank all the staff which has helped me during this experience in the laboratories and in particular Kai Huang, Shakir Bin Mujib and Hamada Elsayed.
I would also like to thank Kansas State University for hosting me and the National Science Foundation PIRE project #1743701 for supporting my research and conference travel in “Colorado University” during my stay in the USA.

My gratitude also goes to the professors who have brilliantly educated me during this master program, giving me the required skills to enter the labour market.

Finally, I would like to thank my friends, who have made these years more pleasant.

Bibliography

1. Colombo, P., Mera, G., Riedel, R. & Sorarù, G. D. Polymer-Derived Ceramics: 40 Years of Research and Innovation in Advanced Ceramics1). *Ceram. Sci. Technol. Appl.* 4, 245–320 (2013).
2. Colombo, P. & Motz, G. Applications of polymer derived ceramics. *Adv. Appl. Ceram.* 108, 453–453 (2009).
3. Parcianello, G. Advanced ceramics from preceramic polymers and fillers. 1–186 (2011).
4. Abe, Y. & Gunji, T. Oligo- and polysiloxanes. *Prog. Polym. Sci.* 29, 149–182 (2004).
5. Gunji, T. Encyclopedia of Polymeric Nanomaterials. *Encycl. Polym. Nanomater.* 1–5 (2021). doi:10.1007/978-3-642-36199-9
6. Synthesis of Linear Pol Ysiloxanes. 3–41 (2000). doi:10.1007/978-94-011-3939-7_1
7. Methods for Control in the Synthesis of Structured Siloxane Architectures.
8. Verdejo, R., Bernal, M. M., Romasanta, L. J. & Lopez-manchado, M. A. Graphene filled polymer nanocomposites †. 3301–3310 (2011). doi:10.1039/c0jm02708a
9. Franchin, G. *et al.* Optimization and characterization of preceramic inks for Direct Ink Writing of Ceramic Matrix Composite structures. *Materials (Basel).* 11, 1–14 (2018).
10. Franchin, G. Additive Manufacturing of Ceramics Printing Beyond the Binder. (2013).
11. Chen, Z. *et al.* Journal of the European Ceramic Society(3D printing of ceramics) : A review. 39, 661–687 (2019).
12. Corcione, C. E., Greco, A., Montagna, F., Licciulli, A. & Maffezzoli, A. Silica moulds built by stereolithography. *J. Mater. Sci.* 40, 4899–4904 (2005).
13. Scalera, F., Esposito Corcione, C., Montagna, F., Sannino, A. & Maffezzoli, A. Development and characterization of UV curable epoxy/hydroxyapatite suspensions for stereolithography applied to bone tissue engineering. *Ceram. Int.* 40, 15455–15462 (2014).
14. Perale, G. *et al.* A novel process for the manufacture of ceramic microelectrodes for biomedical applications. *Int. J. Appl. Ceram. Technol.* 5, 37–43 (2008).
15. Franchin, G. 3D-Printing of a preceramic polymer for biomedical applications. (2013).
16. Zanchetta, E. *et al.* Stereolithography of SiOC Ceramic Microcomponents. *Adv. Mater.* 28, 370–376 (2016).
17. Manapat, J. Z., Chen, Q., Ye, P. & Advincula, R. C. 3D Printing of Polymer Nanocomposites via Stereolithography. *Macromol. Mater. Eng.* 302, 1–13 (2017).
18. Cesarano, J. *et al.* Customization of load-bearing hydroxyapatite lattice scaffolds. *Int. J. Appl. Ceram. Technol.* 2, 212–220 (2005).

19. Lee, Y.-J. & Braun, P. V. Tunable Inverse Opal Hydrogel pH Sensors. *Adv. Mater.* 15, 563–566 (2003).

20. Fu, Q., Saiz, E. & Tomsia, A. P. Direct ink writing of highly porous and strong glass scaffolds for load-bearing bone defects repair and regeneration. *Acta Biomater.* 7, 3547–3554 (2011).

21. Li, Y. Y. *et al.* Polymer replicas of photonic porous silicon for sensing and drug delivery applications. *Science (80-.).* 299, 2045–2047 (2003).

22. Lewis, J. A., Smay, J. E., Stuecker, J. & Cesarano, J. Direct ink writing of three-dimensional ceramic structures. *J. Am. Ceram. Soc.* 89, 3599–3609 (2006).

23. Vakifahmetoglu, C. & Colombo, P. A direct method for the fabrication of macro-porous SiOC ceramics from preceramic polymers. *Adv. Eng. Mater.* 10, 256–259 (2008).

24. Dibandjo, P. & Soraru̇, G. D. Study of the nanostructure of SiCO glasses through HF acid attak The SiCO System and Properties SiCO. 1–38 (2007).

25. Pantano, C. G., Singh, A. K. & Zhang, H. Silicon Oxycarbide Glasses. 25, 7–25 (1999).

26. Kolář, F., Machovič, V., Svítilová, J. & Borecká, L. Structural characterization and thermal oxidation resistance of silicon oxycarbides produced by polysiloxane pyrolysis. *Mater. Chem. Phys.* 86, 88–98 (2004).

27. Wilson, A. M. *et al.* Pore Creation in Silicon Oxycarbides by Rinsing in Dilute Hydrofluoric Acid. *Chem. Mater.* 9, 2139–2144 (1997).

28. Mera, G., Navrotsky, A., Sen, S., Kleebe, H. J. & Riedel, R. Polymer-derived SiCN and SiOC ceramics-structure and energetics at the nanoscale. *J. Mater. Chem. A* 1, 3826–3836 (2013).

29. Hurwitz, F. I., Hyatt, L., Gorecki, J. & D'Amore, L. Silsesquioxanes as Precursors to Ceramic Composites. 732–743 (2008). doi:10.1002/9780470320402.ch29

30. Mahmood, N., Zhang, C., Yin, H. & Hou, Y. Graphene-based nanocomposites for energy storage and conversion in lithium batteries, supercapacitors and fuel cells. *J. Mater. Chem. A* 2, 15–32 (2014).

31. Winter, M. & Brodd, R. J. What are batteries, fuel cells, and supercapacitors? *Chem. Rev.* 104, 4245–4269 (2004).

32. Korthauer, R. *Lithium-ion batteries: Basics and applications*. *Lithium-Ion Batteries: Basics and Applications* (2018). doi:10.1007/978-3-662-53071-9

33. Lu, L., Han, X., Li, J., Hua, J. & Ouyang, M. A review on the key issues for lithium-ion battery management in electric vehicles. *J. Power Sources* 226, 272–288 (2013).

34. Nitta, N., Wu, F., Lee, J. T. & Yushin, G. Li-ion battery materials: Present and future. *Mater. Today* 18, 252–264 (2015).

35. Characterization of the pyrolytic conversion of polysilsesquioxanes to silicon oxycarbides. *J.*

Mater. Sci. 28, 6622–6630 (1993).

36. Iwase, Y. *et al.* Formation and Thermal Behaviors of Ternary Silicon Oxycarbides derived from Silsesquioxane Derivatives. *Materials (Basel).* 12, 1721 (2019).

37. Černý, M. *et al.* Changes in structure and in mechanical properties during the pyrolysis conversion of crosslinked polymethylsiloxane and polymethylphenylsiloxane resins to silicon oxycarbide glass. *Ceram. Int.* 41, 6237–6247 (2015).

38. Valle, M., Ferrari, S., Orlandi, M., Turani, S. & Pagani, M. Use of polysiloxane resins in friction materials. *Adv. Appl. Ceram.* 108, 461–467 (2009).

39. Jeon, E., Kim, H. & Yun, J. Preparation of silicon oxycarbide amorphous ceramics from polymer precursors and the characterization of their high temperature stability. *J. Ceram. Process. Res.* 13, 239–242 (2012).

40. Mahalingam, S., Pierin, G., Colombo, P. & Edirisinghe, M. Facile one-pot formation of ceramic fibres from preceramic polymers by pressurised gyration. *Ceram. Int.* 41, 6067–6073 (2015).

41. Ridge, O. Characterization of the pyrolytic conversion of polysilsesquioxanes to silicon oxycarbides. 28, 6622–6630 (1993).

42. Pivin, J. C. & Colombo, P. Ceramic coatings by ion irradiation of polycarbosilanes and polysiloxanes: Part II Hardness and thermochemical stability. *J. Mater. Sci.* 32, 6175–6182 (1997).

43. Du, W., Lu, J., Sun, P., Zhu, Y. & Jiang, X. Organic salt-assisted liquid-phase exfoliation of graphite to produce high-quality graphene. *Chem. Phys. Lett.* 568–569, 198–201 (2013).

44. Kaspar, J., Graczyk-Zajac, M. & Riedel, R. Carbon-rich SiOC anodes for lithium-ion batteries: Part II. Role of thermal cross-linking. *Solid State Ionics* 225, 527–531 (2012).

45. Renlund, G. M., Prochazka, S. & Doremus, R. H. Silicon oxycarbide glasses: Part II. Structure and properties. *J. Mater. Res.* 6, 2716–2722 (2011).

46. Tsang, D. K. L., Marsden, B. J., Fok, S. L. & Hall, G. Graphite thermal expansion relationship for different temperature ranges. *Carbon N. Y.* 43, 2902–2906 (2005).

47. Colombo, P., Schmidt, J., Franchin, G., Zocca, A. & Günster, J. Additive manufacturing techniques for fabricating complex ceramic components from preceramic polymers. *Am. Ceram. Soc. Bull.* 96, 16–23 (2017).

48. Franchin, G., Wahl, L. & Colombo, P. Direct ink writing of ceramic matrix composite structures. *J. Am. Ceram. Soc.* 100, 4397–4401 (2017).

49. Raccichini, R., Amores, M. & Hinds, G. Critical review of the use of reference electrodes in li-ion batteries: A diagnostic perspective. *Batteries* 5, 1–24 (2019).

50. Pradeep, V. W. S. Study of Silicon Oxycarbide (SiOC) as Anode Materials for Li-ion Batteries. 1–278 (2013).

51. Hamidah, N. L., Wang, F. M. & Nugroho, G. The understanding of solid electrolyte interface (SEI) formation and mechanism as the effect of flouro-o-phenylenedimaleimaide (F-MI) additive on lithium-ion battery. *Surf. Interface Anal.* 51, 345–352 (2019).

52. Schroder, K. W., Dylla, A. G., Harris, S. J., Webb, L. J. & Stevenson, K. J. Role of surface oxides in the formation of solid-electrolyte interphases at silicon electrodes for lithium-ion batteries. *ACS Appl. Mater. Interfaces* 6, 21510–21524 (2014).

53. Deshpande, R., Verbrugge, M., Cheng, Y. T., Wang, J. & Liu, P. Battery cycle life prediction with coupled chemical degradation and fatigue mechanics. *J. Electrochem. Soc.* 159, (2012).

54. David, L., Bhandavat, R., Barrera, U. & Singh, G. Silicon oxycarbide glass-graphene composite paper electrode for long-cycle lithium-ion batteries. *Nat. Commun.* 7, 1–10 (2016).

55. Reyes, C. *et al.* Three-Dimensional Printing of a Complete Lithium Ion Battery with Fused Filament Fabrication. *ACS Appl. Energy Mater.* 1, 5268–5279 (2018).

56. David, L., Bernard, S., Gervais, C., Miele, P. & Singh, G. Facile synthesis and high rate capability of silicon carbonitride/boron nitride composite with a sheet-like morphology. *J. Phys. Chem. C* 119, 2783–2791 (2015).

57. Bhandavat, R. & Singh, G. Stable and efficient li-ion battery anodes prepared from polymer-derived silicon oxycarbide-carbon nanotube shell/core composites. *J. Phys. Chem. C* 117, 11899–11905 (2013).

58. Swain, I. P., Pati, S. & Behera, S. K. A preceramic polymer derived nanoporous carbon hybrid for supercapacitors. *Chem. Commun.* 55, 8631–8634 (2019).